FOCUS-AFRICA

Full-value chain Optimised Climate User-centric Services for Southern Africa

Analysis of the predictability of seasonal and decadal forecasts over the SADC Region

Deliverable D3.2

Lead Beneficiary: Land Bank (South Africa), Local Farmer's Association (Malawi), Smallholder Farmers (Mozambique), Tanzania Agricultural Research Institute, COWI (Tanzania), TANESCO (Tanzania), TotalEnergies (Tanzania), EDF (Malawi), Water and Agriculture Local communities (Mauritius).

September 2021

Francois Englebrecht[1], Jonathan Padavatan[1], Piot Wolski[2], Christopher Jack[2], Lisa van Aardenne[2], Izidine Pinto[2], Andre F. Kamga[3], Asmerom F. Beraki[4,11], Nico Caltabiano[5], Sebastian Grey[5], Hamid Bastani[5], Matteo Dell'Acqua[6], Robel T. Miteku[6], Roberto Buizza[6], Llorenç L. Ponsati[7], Chihchung Chou[7], Nube González-Reviriego[7], Raul Marcos[7], Matteo Zampieri[8], Laura Trentini[9], Sara Dal Gesso[9], Marcello Petitta[9] , Nicolas Fournier[10]

[1] *Global Change Institute – University of the Witwatersrand (WITS), Johannesburg, South Africa*
[2] *Climate System Analysis Group, University of Cape Town (UCT), Cape Town, South Africa*
[3] *African Centre for Meteorological Applications for Development (ACMAD), Niamey, Niger*
[4] *CSIR-Smart Places, Pretoria, South Africa*
[5] *World meteorological organization (WMO), Geneva, Switzerland*
[6] *Institute of Life Sciences, Sant'Anna School of Advanced Studies, Pisa, Italy*
[7] *Barcelona Supercomputing Center (BSC), Barcelona, Spain*
[8] *European Commission Joint Research Centre (JRC), Ispra, Italy*
[9] *Amigo Climate, Roma, Italy*
[10] *Met Office (MO), Exeter, UK*
[11] *University of Pretoria, Department of Geography, Geoinformatics and Meteorology, Pretoria, South Africa*

This project has received funding from the European Commission's Horizon 2020 Research and Innovation Programme. The content in this presentation reflects only the author(s)'s views. The European Commission is not responsible for any use that may be made of the information it contains.

www.focus-africaproject.eu

Document Information

Grant Agreement:	869575
Project Title:	Full-value chain Optimised Climate User-centric Services for Southern Africa
Project Acronym:	Focus-Africa
Project Start Date:	1 September 2020
Related work package:	WP 3
Related task(s):	Task 3.2
Lead Organisation:	Global Change Institute – University of the Witwatersrand
Submission date:	25 April 2022
Dissemination Level:	1

History

Date	Submitted by	Reviewed by	Version (Notes)
25/04/2022	F. Englebrecht	WMO	V1

About FOCUS-Africa

FOCUS-Africa – Full-value chain Optimised Climate User-centric Services for Southern Africa – is developing sustainable tailored climate services in the Southern African Development Community (SADC) region for four sectors: agriculture and food security, water, energy and infrastructure.

It will pilot eight case studies in six countries involving a wide range of end-uses to illustrate how the application of new climate forecasts, projections, resources from Copernicus,

Coordinator Contact

Roberta Boscolo | Climate & Energy Scientific Officer

Applied Climate Services Division

Services Department

World Meteorological Organization (WMO)

CP 2300, 1211 Geneva SWITZERLAND

email: rboscolo@wmo.int

Table of Content

List of Acronyms

AMIP – Atmospheric Model Intercomparison Project

BAI – Baroclinic Amplitude Index

CCAM - Conformal-Cubic Atmospheric Model

CMIP5 - Coupled Model Inter-comparison Project Phase 5

CMIP6 - Coupled Model Inter-comparison Project Phase 6

CORDEX - Coordinated Regional climate Downscaling Experiment

CRU – Climatic Research Unit

DJF – December January February

ECMWF – European Centre for Medium-Range Weather Forecasts

ERA-Interim – ECMWF Re-Analysis Interim

ESAF - East Southern-Africa

GCM – Global Climate Model

GFCS - Global Framework for Climate Services

GHG – Green House Gas

ITCZ – Intertropical Convergence Zone

LLJs - Low-Level Jets

JJA – June July August

MAM – March April May

RCM – Regional Climate Model

RCP - Representative Concentration Pathway

SARCOF – Southern Africa Regional Climate Outlook Forum

SEAF – South-Eastern-Africa

SON – September October November

SADC – Southern African Development Community

SSP - Socio-economic Pathways

SR - Spearman Rank

SWIOCOF – South-West Indian Ocean Regional Climate Outlook Forum

TRB – Tropical Rain Band

WASF – West Southern-Africa

WP – Work Package

● Executive Summary

The SADC countries are particularly vulnerable to climate variability, change and extremes. Water resources, agriculture, hydropower generation, ecosystems and basic infrastructures are especially under stress because of increased frequency and intensity of floods, droughts, and landslides. The development of improved climate information and forecasts of decision-relevant parameters is essential to address these challenges

FOCUS-Africa's climate services will be developed by ensuring the full value chain is implemented, starting from close involvement of end-users to assess their climate-related challenges and risks

(WP2), understanding regional climate processes (WP3), developing methods and tools (WP4), creating prototypes of end-user tailored climate services (WP5), assessing their economic value, and exploiting results (WP6) and capacity building (WP7).

This will be demonstrated by piloting eight case studies in six countries involving a wide range of fellow-users. The case studies will illustrate how the use of WP3 climate science, forecasts and projections can maximize socio-economic benefits in the Southern Africa region and potentially in the whole of Africa.

Indeed, WP3 builds up the climate foundation of the project and focuses specifically on advancing the underpinning science required to provide robust climate services and development of climate-integrated applications for the energy, water, infrastructure, and food security sectors. To achieve this, WP3 explores the performances of the latest climate projections (Task 3.1, M12) and predictability at seasonal forecast time scales s (Task 3.2, M18) as well as analyse the extremes in the region (Task 3.3, M24).

In Task 3.2 described in this report, we built up some climate foundation of this project by analysing the main drivers of climate variability over the SADC region. This will allow the next task (i.e., Task 4.3) developing and adapting the most relevant seasonal forecasts to be used in the case studies for specific countries and climate parameters based on our findings.

We showed indeed that SARCOF and SWIOCOF are using a series of predictors over the region for seasonal forecasting with ENSO, IOD, SIOD, Benguela Nino demonstrating to drive rainfall variability across southern Africa. Current statistical tools have useful predictability usually limited to years with strong ENSO signal.

The evaluations of skill in the AMIP-simulations of inter-annual variability in the Southern Hemisphere showed that a pronounced seasonal cycle in predictive skill exists over the Southern Hemisphere continents in the subtropics, with peak skill in summer in association with ENSO forcing. However, the seasonal prediction of winter rainfall and underpinning circulation anomalies need to focus on improved systems of initialisation and data assimilation, rather on sources of predictability, since for these regions the latter is insignificant compared to the dominating role of internal variability.

We then investigated the observed interannual to multi-decadal variability and changes of droughts and other environmental conditions that directly affect rainfall, streamflow, and river discharges across the Orange River basin as it is the largest river system in southern Africa. This showed that this is largely explained by the natural variability throughout the 20th Century. However, the worsening of water stress due to loss from surface water, drainage systems, and other covers is likely associated with temperature amplification. We also demonstrated that the problems of seasonal forecasting in correctly predicting baroclinic activity may be directly related to the low skill values of precipitation predictions observed in the seasonal forecast. In addition, in a showcase for Lake Malawi, it was shown that low level moisture transport plays an important role in rainfall over the Lake Malawi catchment, and its dynamics are linked to seasonal and interannual rainfall variability.

Going further, we evaluated the prospects of improving seasonal predictions of ECVs in SADC by means of the characterization of teleconnection links with large scale patterns like El Niño Southern Oscillation (ENSO).It was shown that higher skills could be generated by using estimates from the teleconnection indices, especially for precipitation using linear regression models. Indeed, the seasonality of precipitation over most of Africa is arguable linked to the migration of the Tropical Rain Band that is closely linked to large scale processes such as the Hadley circulation through the ITCZ. The Copernicus seasonal forecast models show some potential in predicting the main features of

variability of this tropical rain band over Africa in key periods of the year well in advance. Finally, in another showcase, we characterized the influential large-scale climate drivers on crop production by showing that the rainfall season has been shortening and average temperature increasing significantly from 1981 to 2020. Interannual yield anomalies are often linked to variations in the large-scale systems that control the regional climate with quasi-periodic fluctuations. The results suggest that recent large-scale climate trends, attribute to human activity, have a negative impact on the countries yield progress.

Keywords

Seasonal forecast, Predictability, South Africa, Climate change and Variability

1 Introduction

Southern Africa epitomizes the link between climate and the water–energy–food nexus, as multiple challenges collide across a very diverse socioeconomic spectrum of countries (Mabhaudhi et al., 2021; Siderius et al., 2021). According to the World Bank Classification (see Table 1 below) of the countries that comprise SADC (Southern African Development Community); six are defined as low income including Malawi, Mozambique, and Tanzania which are the focus of 5 of our project's case studies.

Table 1 – Income group of the countries that comprise SADC

INCOME GROUP		SADC COUNTRY
LOW		Lesotho **Malawi** **Mozambique** **Tanzania** Zambia Zimbabwe
MIDDLE	LOWER	Angola Botswana Namibia Swaziland
	UPPER	**Mauritius** **South Africa**

Food security is the main sector of interest in our project and agriculture's contribution to regional Gross Domestic Product (GDP) is 17% for the whole SADC region, and up to 28% for the low-income countries. At the same time, ca. 75% of the land in SADC is either arid or semi-arid, and agriculture is estimated to consume 70% of the renewable water resources of the region (Nhemachena et al., 2020). Major water scarcity issues are expected in the SADC because of ongoing exploitation and degradation, coupled with increased demand and climate change (IPCC, 2021). With 27 million food

insecure people, the 2015/16 El Niño-induced drought provides an example of how increased water demand for agriculture can aggravate water, energy, and food insecurity (Nhemachena et al., 2020; Kolusu et al., 2019).

Climate change is expected to impact infrastructures, renewable energy, and agricultural production in SADC in multiple ways. Indeed, approximately 30% of the region is critically exposed to a variety of climate hazards such as drought, flood, climate variability and high temperatures (Ramirez-Villegas et al., 2021). The SADC countries are particularly vulnerable to climate variability, change and extremes: particularly water resources, agriculture, hydropower generation, ecosystems and basic infrastructures are especially under stress because of increased frequency and intensity of floods, droughts, and landslides. The 2015/16 drought, one of the most severe on record, contributed to over 40 million people to be food insecure, and dam water levels to be reduced, leading to intermittent power outages in most countries in the region (Conway et al., 2017). Climate change is also projected to reduce the amount of suitable land for cropping and crop, pasture, livestock productivity (Pequeno et al., 2021, Ekine-Dzivenu et al., 2020) as well as to double the risk of drought such as the 2015/16 event occurring (Kolusu et al., 2019). Decreased suitable land for cropping and reduced crop and livestock productivity would exacerbate water scarcity and insecurity, and decrease national self-sufficiency ratios, and impact food availability locally, with devastating effects on food insecurity in the region. Water, energy, and food are thus inextricably linked across multiple scales in SADC and are heavily interdependent.

Therefore, addressing these existing and emerging infrastructure-water-energy-food issues requires a better understanding and characterization of the predictability of available seasonal and decadal forecasts. This is the objective of Task 3.2 described in this report. We are building up the climate foundation of this project by analysing the most recent climate data available to investigate the main drivers of climate variability over the SADC region. This will then enable in the next task (i.e., Task 4.3) to develop and adapt the most relevant seasonal forecasts to be used in the case studies for specific countries and climate parameters.

In this report, Section 2 describes the status of decadal forecasting in SADC. Section 3 provides an overview of the current predictors used in operational seasonal forecasting in the region. Section 4 investigates the main drivers of climate variability across the region with a showcase for Malawi. Finally, Section 5 explores the main large-scale processes linked with rainfall onset, crop yield variations and other variables across the region with another illustrative showcase for Mozambique.

FOCUS-AFRICA

2 Review of the status of decadal forecasting

Climate variability at a decadal or longer time scale is a key issue for the society to mitigate climate-related risks and establish long-term adaptation plans for sectors such as agriculture, fisheries, water management and city design (Morioka et al., 2015). To develop such plans, better understanding of the drivers of natural variability and the sources of predictability at these timescales are essential. Merryfield et al. (2020) synthesized the current understanding of these drivers and sources of predictability, with a focus on the seasonal to decadal (S2D) time scales and timescales interactions. Lüdecke et al. (2021) assessed six potential climatic drivers of rainfall natural variability in the African

continent linked to teleconnections in the Atlantic, Pacific and Indian oceans. As rainfall in African shows strong inter-annual fluctuations, with recurring wet and dry periods (Dieppois et al., 2016), it is essential analysis of its variability is better understood for better planning in relation to droughts and floods. Looking at different climate scenarios, (Lim Kam Sian et al., 2021) shows that precipitation in the wet and dry seasons shows an initial increase during the near future (2015–2044) over western and eastern Southern Africa, followed by a reduction in precipitation during the far future.

With the deployment of operational centres around the globe and continued advances in climate modelling, in combination with user demand for climate services, predictions of the near-term climate have become more robust (O'Kane et a., 2022). Decadal prediction systems have shown levels of skill that are comparable to predictions in operational seasonal forecasting (Kushnir et al., 2019), particularly for surface air temperature and to precipitation (Doblas-Reyes et al., 2013; Smith et al., 2019). In addition to these, predictions at this timescale also provide skilful information for the frequency of extreme events such as heatwaves and tropical storms (Caron et al., 2018; Eade et al., 2012). Of course, the main difference between the seasonal and decadal predictions is in the temporal resolution which would influence the applicability of such products depending on the needs of different sectors. As the skill levels of near-term climate predictions indicate, there is considerable potential for several sectors to benefit from such predictions.

The agricultural sector is largely affected by climate variability and particularly by climate extremes (e.g., droughts, flooding and heatwaves). Chatzopoulos et al. (2020) shows that regional climate extremes may have significant economic impacts on agricultural commodity markets. Skilful and reliable predictions are essential for planning given that unfavourable conditions such as heat or water stress affect both grain yield and quality, with large impacts on food security in many regions of the world. Landman et al. (2017) developed a procedure that can provide some guidance to policy makers responsible for action plans to mitigate and adapt to the impacts of increasing temperatures on dry land maize yield. Solaraju-Murali et al. (2021) showed that predictions on multi-annual timescales support decision making in the wheat sector have improved but efforts are still needed to convert those available climate predictions into information that can be understood and used by stakeholders involved in that sector. The interaction of climate scientists with users and policy makers to understand the needs of information and some existing obstacles in law and regulations is essential.

To effectively leverage the utility of decadal forecasts, there is the crucial task of communicating prediction and uncertainty information in an appropriate form to meet the needs of the end user. One issue, to keep in mind, is that the information that can be extracted from forecasts and predictions can offer a range of benefits. However, these are not all equally distributed or weighted. As with seasonal forecasts, some of the information may be detrimental or disadvantageous to some groups and providers should consider the ethical aspects of forecast delivery (Hobday et al., 2019). For example, multi-year drought prediction may increase insurance costs to individual farmers (disadvantage) while reducing losses to insurance providers (advantage).

Kushnir et al. (2019) also point out that as the climate changes, there is great need for updated information, particularly in relation to the risk of extreme and unprecedented events and their impacts

on several economic sectors. Annual–decadal climate predictions can offer early warning of where the risk of extreme events, due to both climate change and natural variability, is higher. Decadal prediction is an essential component of the Global Framework for Climate Services (GFCS) as this timeframe of up to 10 years is a key for decision makers to develop plans, particularly for infrastructure. There will be an increase in demand for decadal predictions, particularly with further co-development of specific products based on user feedback. Outputs of operational decadal climate prediction systems are now routinely available, with multiple centres now producing operational near-term climate predictions and making it available via the WMO Lead Centre for Annual-to-Decadal Climate Prediction (www.wmolc-adcp.org) and since 2020, an annual synthesis has been provided via the WMO Global Annual to Decadal Climate Update. Hermanson et al. (2022) shows the results of the latest annual synthesis for the period 2021-2025. The ensemble mean predictions of precipitation captured the correct sign of anomalies in several regions including wetter conditions across the Sahel, India and East Africa, and drier conditions in South America and southern Africa.

3 Review of the current SARCOF and SWIOCOF predictors

Background

Reliable seasonal climate forecasting, particularly for the rainy season for Southern Africa has the potential to be of great benefit to users. The 2015/16 drought impacts included up to 40% inflation in agriculture commodity markets and some southern Africa countries loosing up to 50% of their normal hydropower capacity. Anticipated knowledge of temperature and rainfall variability can assist planning, management, and mitigation decisions for users from many sectors of the economy (Johnston et al. 2004). However, useful seasonal forecast, would require ease of interpretation, acceptable accuracy as well as efficient dissemination. Southern Africa is a relatively dry area and depends on rainfall for farming and hydropower. Prior knowledge of precipitation patterns can lead to improvement in food security, more profits for farmers, assistance with planning of planting, fertilisation, and harvesting. Reduction in agriculture losses, increase in crop productivity and profitability are expected outcomes of reliable seasonal forecasts interpretation, communication, and use. Thus, we focus in this section on the predictors used in operational seasonal forecasting for southern Africa.

The Southern Africa region had been using the Nino Sea Surface Temperatures (SSTs) as the main predictor for several years until the evolution of tools such as ClimLab2000, Climate Predictability Tool (CPT), SWIOFORDS, GeoCOF and currently the Climate Forecasting Tool (CFT) which has been upgraded into a Climate Forecasting Toolbox (CFTx) with the inclusion of a clustering module in January 2022. The evolution of tools enhanced the ingestion of a multiple array of predictors including Mean Sea Level Pressure (MSLP), lower and middle troposphere Geopotential height, SSTs, and related indices such as Equatorial Indian Ocean Dipole (IOD) and Sub tropical Indian Ocean dipole (SIOD). Horizontal winds are also included in the SWIOFORDS tool but not extensively explored yet in the Southern Africa Regional Climate Outlook Forum (SARCOF) processes.

Figure 1 provides the key SST areas (SSTAs) known to influence African climate including SADC regions' precipitation variability at seasonal to interannual and decadal timescales. Known SSTAs patterns of interest that have well known and often direct influence on the SADC region rainfall performance are Nino 3.4, SWIO (South-West Indian Ocean), Benguela Nino (BN), Subtropical Indian Ocean Dipole Mode (SIOD) and Indian Ocean Dipole (IOD) basins.

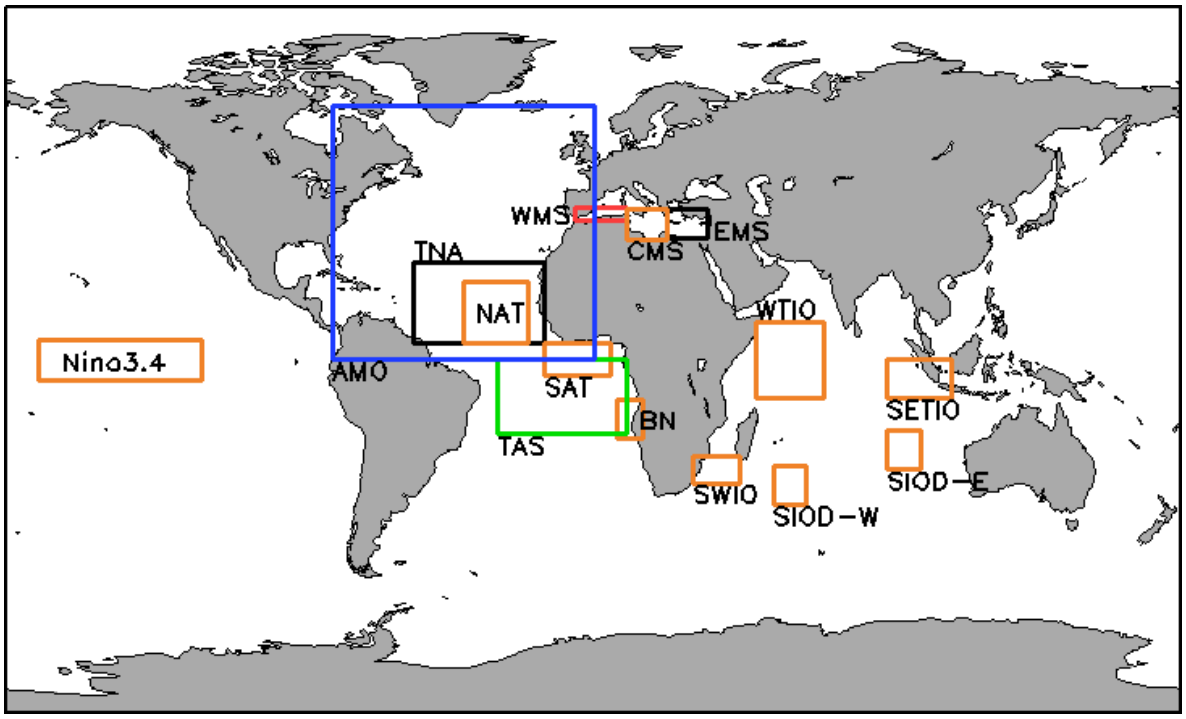

Figure 1: Major Ocean basins that influence the African continental rainfall. BN, SWIO, SIOD, IOD, TAS, AMO and NINO are key SST areas influencing rainfall variability in southern Africa

3.1 El Nino Southern Oscillation

ENSO is characterized by positive (El Nino) and negative (La Nina) Sea Surface Temperature Anomalies (SSTAs) in the equatorial pacific. This phenomenon influences the global climate with a frequency between 2 and 7 years. El Niño-Southern Oscillation phases have a regionally unique, although generally predictable influence on weather. El Niño-Southern Oscillation phases influence the number of typical summer weather systems and where they form. That in turn influences rainfall and temperature patterns over the globe including the Southern Africa region. Wetter and cooler conditions occur during La Niña phases because tropical temperate troughs, large rain-producing cloud bands form more frequently and move eastward over the sub-continent. Tropical lows form more frequently and are located further south. Conversely, high-pressure systems which promote hot, dry conditions are reduced in intensity and are located further south. The opposite occurs during El Niño phases. La Nina conditions have persisted since June 2020 leading to enhanced rainfall activity in the sub-continent as can be evidenced on the November-December 2020-January 2021 observed rainfall tercile map (Figure 2).

Reduced precipitation over most of the Southern Africa sub-continent is associated with El Niño events (i.e. 2015/16 southern summer), with warm SST across the east and central Pacific Ocean and warmer than average SST over the Indian Ocean. These regional precipitation reductions are forced primarily by large-scale mid-tropospheric subsidence associated with anticyclonic circulation in the upper troposphere during the first half of the rainy season over southern Africa.

La Niña events, with cool SST anomalies over the central Pacific and warm SST over the west Pacific and adjacent Indian Ocean, are associated with precipitation increases over Southern Africa during the first half of the rainy season. The regional precipitation increases are forced primarily by lower

tropospheric cyclonic circulation, resulting in mid-tropospheric ascent and an increased flux of moisture into the region.

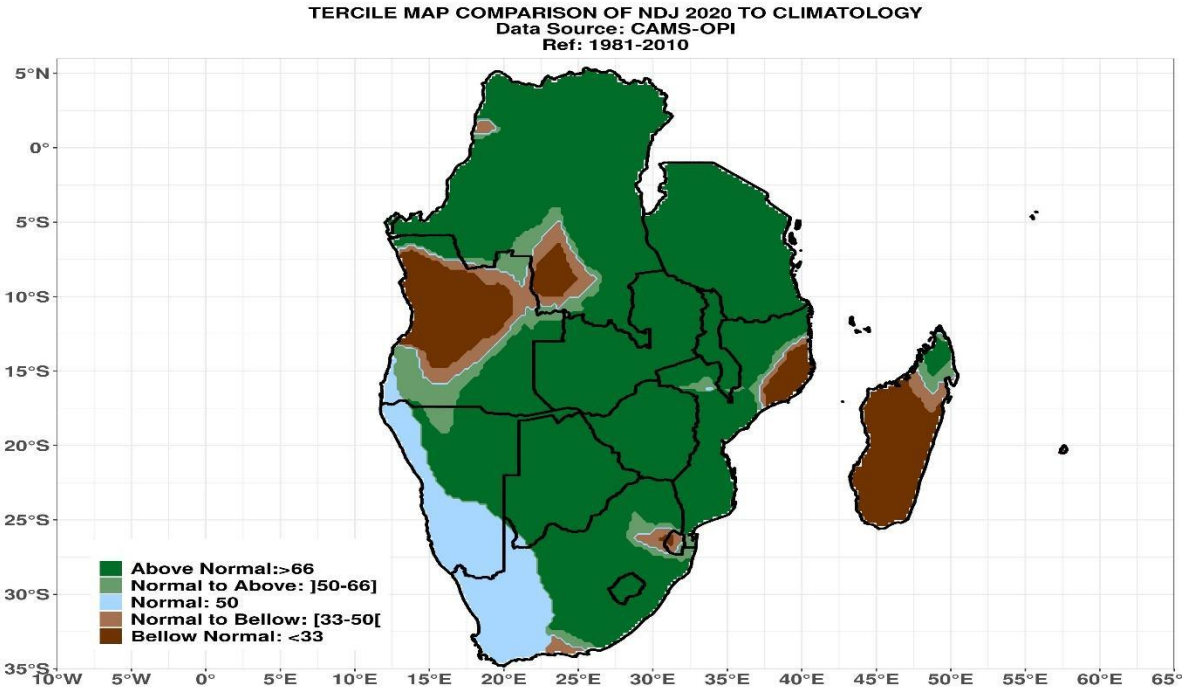

Figure 2: Observed rainfall tercile map for November-December 2020 to January 2021 (NDJ) during a La Nina phase

3.2 Indian Ocean Dipole

The IOD is an irregular oscillation of sea surface temperatures and related atmospheric circulation in the Indian Ocean. The IOD has positive and negative phases, which are defined by opposing sea surface temperature anomalies in the western and eastern tropical Indian Ocean (Figure 3 and Figure 4). Key characteristics of IOD events include:

- Events occur irregularly and vary in strength and duration,
- Positive and negative IOD events often coincide with El Niño and La Niña events, respectively, but sometimes occur independently,
- Simultaneous positive IOD and El Niño, and negative IOD and La Niña, events may enhance precipitation deficits or excess respectively.

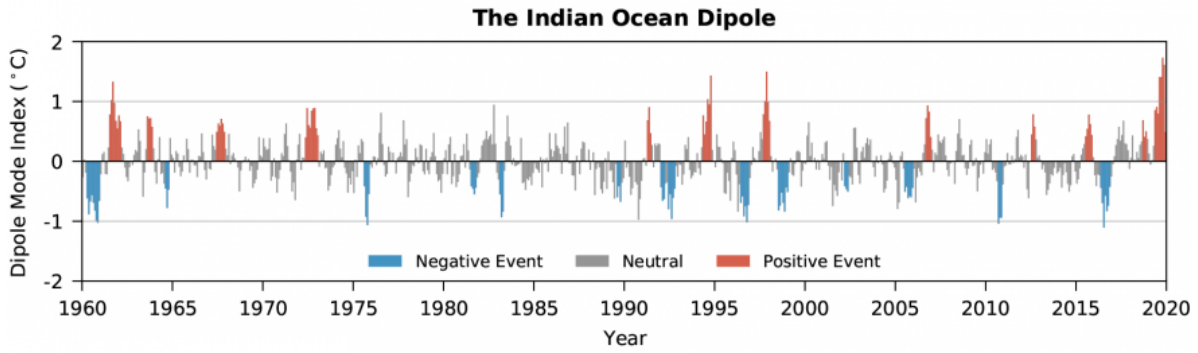

Figure 3: Indian Ocean Dipole years since 1960 (source: Bureau of Meteorology-Australia)

Figure 4: Indian dipole years since 1960 (source: BoM)

The IOD is related to changes in atmospheric and oceanic circulation in and around the Indian Ocean basin. While precipitation outcomes differ from one IOD event to the next, consistent patterns across past events provide a baseline for prediction. Corresponding to the seasonality of events, the IOD is related to wet and dry conditions over Africa during October-December. Over the African continent, the IOD is related to wet and dry conditions (depending on the phase) along the Indian Ocean Rim, extending from Somalia to Mozambique, during September-December.

3.3 Subtropical Indian Ocean Dipole Mode

The SIOD is featured by the oscillation of SST in which the southwest Indian Ocean i.e. south of Madagascar is warmer/cooler and the opposite cooler/warmer in the eastern part i.e. off Australia (Figure 5). It was first identified in the studies of the relationship between the SST anomaly and the south-central Africa rainfall anomaly; the existence of such a dipole was identified from both observational studies and model simulations. SIOD usually influences precipitation mostly during the second half of southern Africa and IOC regions rainfall season (December to April). The evolution process of the SIOD event is highly affected by the position of the subtropical high of the Mascarenes.

Positive phase of SIOD is characterized by warmer-than-normal sea surface temperature in the south-western part, south of Madagascar, and colder-than-normal sea surface temperature off Australia, causing above-than-normal precipitation in many regions over south and central Africa. The negative phase of the SIOD is featured by the opposite conditions, with warmer SSTs in the eastern part, and cooler SSTs over the south-western part. Positive events tend to be associated with reduced TC activity. Positive events are generally associated with dry mid troposphere conditions and cooler than usual SST over the central southern Indian Ocean. When SST is warm to the south of Madagascar and cool off Western Australia, increases southern summer rains occur over large parts of southern Africa. Models results suggest that this SST pattern leads to increases rainfall via enhanced moisture convergence or the region (Reason C.J.C , 2001).

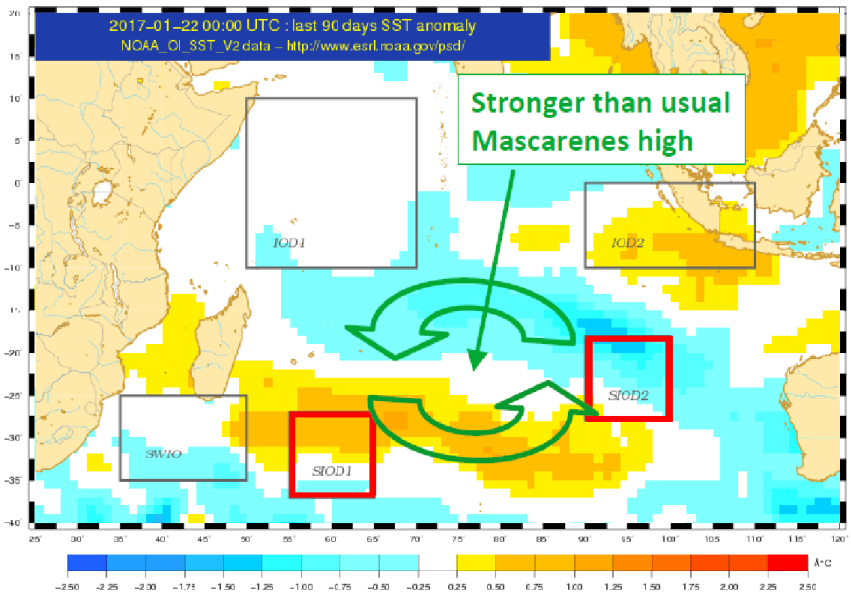

Figure 5: SST anomalies pattern during the strong positive SIOD event in 2016/17. A positive (negative event is associated with warmer(cooler) waters south of the Mascarenes islands and cooler (warmer) near Australia and the aster subtropical southern Indian ocean.

3.4 Benguela Nino

The south-eastern tropical Atlantic Ocean hosts the Angola Benguela upwelling system which is one of the most productive marine ecosystems in the world (Chavez and Messié, 2009; Jarre et al., 2015) fuelled by the upwelling of nutrient-rich waters (see Figure 1, BN box).

Benguela Ninos warm SSTs off the coasts of Angola and Namibia are off associated with above average precipitation and floods in these countries with strongly enhanced rainfall in the Namib desert. Moisture flux and rainfall anomalies over southern Africa that have occurred during strong warm SST events off the coast of Angola since 1950 typically occur during February-April (FMA), the main rainy season for Angola/northern Namibia (Figure 6). Eleven of these events have occurred in the 60-year period since 1950 and each experiences increased rainfall somewhere in coastal Angola, and in 10 cases, somewhere in northern Namibia. Droughts are associated with Benguela Nina.

The upwelling system is marked by the presence of a sharp meridional temperature gradient called the Angola Benguela front (ABF) located in the region between 15°S and 18°S which separates the warm tropical waters in the north to the cold upwelled waters in the south. The region exhibits high sea surface temperature (SST) variability at a wide range of frequencies varying from sub-monthly to decadal timescales. Inter-annual timescale are marked by the occurrence of extreme warm events of the so-called Benguela Niños and their cold counterparts, the Benguela Niñas (Florenchie et al., 2004; Koseki and Imbol Koungue, 2020). Those interannual warm and cold events usually peak in boreal spring when the SSTs are climatologically high, and the intertropical convergence zone (ITCZ) reaches its southernmost position. During a Benguela Niño (Niña) event, the SSTs can be up to 3°C higher (lower) than the climatology in the Angola Benguela area (ABA, 8°E – coast; 10–20°S).

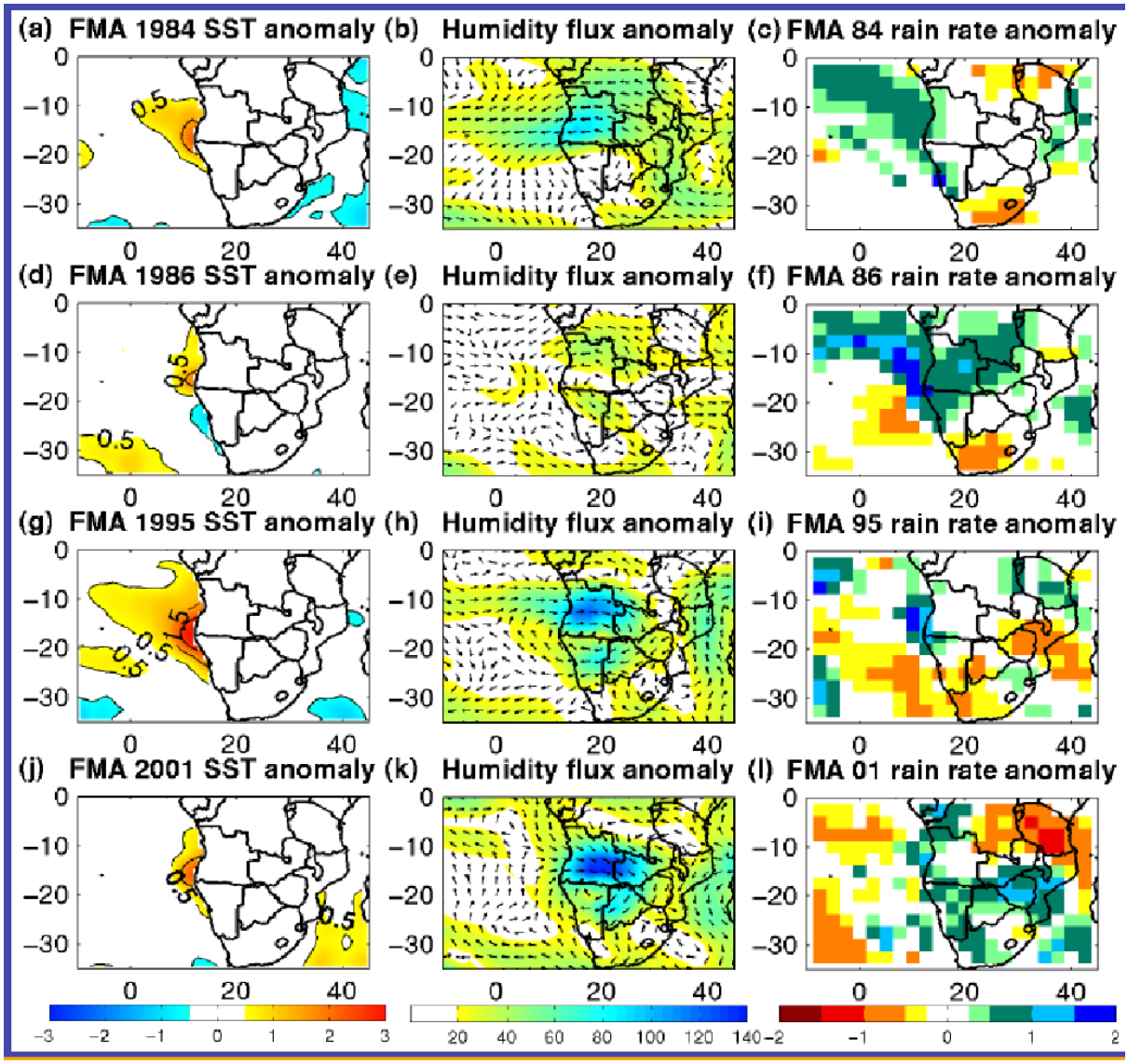

Figure 6: Left: mean February to April SSTAs for 1984 (a); 1988(b); 1995(g); and 2001(j) isocontour at 0.5°C , 1.5°cC and 2.5°C. Middle: mean February to April integrated moisture flux anomalies from surface to 300hPafor the same years in g/kg./s. Right: mean February to April rain rate normalized for the same years.

3.5 Predictors

The SADC RCOF uses similar predictors as the SWIO region including Mean Sea Level Pressure (MSLP) and Sea Surface Temperatures (SSTs) related to ENSO, IOD, SIOD, but in addition to these two common predictors the SADC-RCOF uses geopotential data at 850 and 500hpa, with zonal wind fields at 850, 500 and 200 hPa. Because of teleconnections linking SSTs on the ENSO, IOD and IOD boxes and regional circulations patterns, it is likely that some circulation patterns related predictors are correlated with SSTs and therefore provide little additional information on the forecast performance. Upcoming efforts may assess predictability of statistical tools built with these predictors and filter out those with limited added value.

As shown in Table 2, these predictors are mostly available from the International Research Institute (IRI) an initiative initially established as a cooperative agreement between NOAA's Climate Program

Office and Columbia University. For the Southern Africa Regional Climate Outlook Forum (SARCOF) forecast generation process, IRI is the main source of observed and forecasted predictor dataset for both the CPT and CFT tools. While the SWIOCOF process uses mostly forecasted predictors obtained from three Global Producing Centres (GPCs) namely, the Meteo France S8 model outputs, ECMWF and NCEP. The climate predictability tool (CPT) has three modes by which climate forecast is produced, namely, Canonical Correlation Analysis (CCA), Principal Component Regression (PCR) and Multiple Linear Regression (MLR).

Table 2: SADC RCOF predictor data and sources

	Predictor	Source	Months	Statistical Forecasting Tool(s)
1	Extended Reconstructed Sea Surface Temperatures (ERSSTs)	NOAA NCDC ERSST version5 sst through IRI	July (main COF) and December (Update COF)	CFT and CPT
2	Mean Sea Level Pressure (MSLP)	NOAA NCEP-NCAR CDAS-1 MONTHLY Intrinsic MSL pressure through IRI	July (main COF) and December (Update COF)	CFT and CPT
3	Geopotential Heights Re-analysis at 850hpa	NOAA NCEP-NCAR CDAS-1 MONTHLY Intrinsic Pressure Level phi through IRI	July (main COF) and December (Update COF)	CFT and CPT
4	Geopotential Heights Re-analysis at 500hpa	NOAA NCEP-NCAR CDAS-1 MONTHLY Intrinsic Pressure Level phi through IRI	July (main COF) and December (Update COF)	CFT and CPT
5	Geopotential Heights Re-analysis at 200hpa	NOAA NCEP-NCAR CDAS-1 MONTHLY Intrinsic Pressure Level phi through IRI	July (main COF) and December (Update COF)	CFT and CPT
6	Zonal (U) Winds Re-analysis at 850hpa	NOAA NCEP-NCAR CDAS-1 MONTHLY Intrinsic Pressure Level u through IRI	July (main COF) and December (Update COF)	CFT and CPT
7	Zonal (U) Winds Re-analysis at 500hpa	NOAA NCEP-NCAR CDAS-1 MONTHLY Intrinsic Pressure Level u through IRI	July (main COF) and December (Update COF)	CFT and CPT
8	Zonal (U) Winds Re-analysis at 200hpa	NOAA NCEP-NCAR CDAS-1 MONTHLY Intrinsic Pressure Level u through IRI	July (main COF) and December (Update COF)	CFT and CPT
9	Meridional (V) Winds Re-analysis at 850hpa	NOAA NCEP-NCAR CDAS-1 MONTHLY Intrinsic Pressure Level v through IRI	July (main COF) and December (Update COF)	CFT and CPT
10	Meridional (V) Winds Re-analysis at 500hpa	NOAA NCEP-NCAR CDAS-1 MONTHLY Intrinsic Pressure Level v through IRI	July (main COF) and December (Update COF)	CFT and CPT
11	Meridional (V) Winds Re-analysis at 200hpa	NOAA NCEP-NCAR CDAS-1 MONTHLY Intrinsic Pressure Level v through IRI	July (main COF) and December (Update COF)	CFT and CPT
12	ENSO Indices	Indices nino EXTENDED NINO34 through IRI and from Tokyo Climate Center (TCC)	July (main COF) and December (Update COF)	CFT

13	IOD Indices	Tokyo Climate Center (TCC)	July (main COF) and December (Update COF)	CFT

Summary

A series of predictors have been tried over the region for seasonal forecasting. Over the years, ENSO, IOD, SIOD, Benguela Nino have been demonstrated to drive rainfall variability across southern Africa. Current statistical tools have useful predictability usually limited to years with strong ENSO signal. Statistical tools available carry quite well the ENSO signal and perform better in the ENSO years.

4 Analysis of the drivers of climate variability across SADC

Changes in climate patterns may alter the world's terrestrial hydrological systems, strongly influencing water resources availability. They may directly impact natural ecosystems along with critical socioeconomic sectors such as water supply, energy, crop production, animal raising, and fishery (Dore, 2005). Managing water resources at local and regional scales under changing climate is a major challenge faced by societies today. Although the trajectory of human-related aspects of future atmospheric greenhouse gas emissions and the climate projections' uncertainty remains high, finding a beneficial solution to the interrelated problems of population growth and global warming is one of the great challenges of the 21st century (von Storch et al., 2012; O'Neill et al., 2017). An understanding of the extent of weather and climate variability-related extreme events on the one hand, and the risks associated with the projection of future climate, are key in informing all national development plans and priorities towards a climate change resilient state (Niang et al., 2014).

Climate change is a complex and cross-cutting problem that needs an integrated and transformative systems approach to respond to the challenge (Mpandeli et al., 2018). In the context of the water-energy-food nexus, the climate system forms the cornerstone of the full value-chain of climate services (Sanders, 2015). The latest Intergovernmental Panel on Climate Change (IPCC) report (IPCC, 2018) specifies Southern Africa as one of the global climate-change-induced *hotspots* that occur through interactions across the physical climate system, ecosystems, and livelihoods. Along with the other such defined global hotspots, the region focuses the report on the extent to which risks can be avoided or reduced by achieving the 1.5°C global warming goal, as opposed to the 2°C goals of IPCC's 5th Assessment Report (AR5). Also, subtropical Southern Africa is projected to be a climate change hotspot both in terms of heat extremes and drying with rapidly rising temperatures at approximately twice the global rate (e.g., Engelbrecht et al., 2015).

Furthermore, in southern Africa, seasonal prediction is most skilful in the austral summer, with predictability largely attributed to the ENSO teleconnection to southern Africa (Cook, 2001). El Niño events are associated with below-normal rainfall over southern Africa in summer, with East Africa typically experiencing above-normal rainfall during the same time. La Niña events typically bring above normal rainfall to southern Africa and below normal rainfall to East Africa during summer (Indeje et al., 2020). Investigations of the relatively high levels of skill in forecasting summer rainfall anomalies over southern Africa have revealed the highest skill levels for seasons of La Niña forcing; skill is also high for seasons with El Niño forcing, but only marginal when conditions in the Pacific Ocean are neutral (Landman and Beraki, 2012). Forecast still is substantially lower for spring, autumn and winter. One reason for this apparent 'seasonal cycle' in predictability is that the ENSO signal is strongest in

summer, and often absent or weak during the austral winter. There is also evidence of the Southern Annular Mode (SAM) impacting on inter-annual rainfall over southern Africa. The positive mode of SAM is associated with above-normal summer rainfall over southern Africa in summer (Gillett et al., 2006), as well as to the more frequent landfall of tropical cyclones over Mozambique and northeastern South Africa (Malherbe et al., 2014).

An open question in southern African climate science is whether the relatively low skill in predicting seasonal rainfall anomalies in winter and the transition seasons can be improved. Such improvements may follow from model development, including improved initialisation and assimilation systems that better incorporate information of the ocean state, or long and planetary waves, which can translate to forecast skill at seasonal time scales. Also important is exploring whether there are forms of external forcing, not sufficiently represented in climate models, that if included can substantially improve forecast skill. Antarctic stratospheric ozone is a primary example in this regard. The importance of its concentrations for climate variability in the Southern Hemisphere troposphere is a relevant recent discovery (Thompson et al., 2011), and its implications to southern African inter-annual variability remains largely unexplored (Engelbrecht et al., 2015).

4.1 AMIP simulations analysis

Background

A relatively unexplored data set that forms part of the larger Coupled Model Intercomparison Project Phase Six (CMIP6) archive, and that may help to explore this open question, is that of the Atmospheric Model Intercomparison Project (AMIP). These simulations are constructed using global atmospheric models forced at their lower boundaries with observed sea-surface temperature and sea-ice reconstructions. Radiative forcing is in the form of observed greenhouse gas and ozone concentrations, as well as aerosol emissions, for the period 1979-2014 (the same forcings used in the 'historical' simulations of CMIP6). To the extent that atmospheric inter-annual variability is the response to lower-boundary and radiative forcing, AMIP simulations may be regarded as an important measure of seasonal or inter-annual predictability. To some extent, since the boundary forcing (e.g. ENSO forcing and anomalous Antarctic stratospheric ozone) in AMIP simulations is 'perfect', the representation of inter-annual variability in the simulations may be regarded as an upper boundary for seasonal forecast skill. That is, AMIP simulations include all the potentials 'sources of predictability' that may translate to seasonal forecast skill over southern Africa (or globally, for that matter). However, AMIP simulations are initialised only once, at the beginning of 1979, rather than for each season of every year at different lead-times (as in an operational seasonal forecast system or when generating seasonal hindcasts). This implies that AMIP simulations do not utilize knowledge of the initial state of planetary scale atmospheric flow (long waves) that may provide seasonal forecast skill, at least for the first 30 - 40 days of a seasonal forecast (Engelbrecht et al., 2021).

In this section, the predictive skill of a multi-model ensemble of AMIP simulations is analysed in the context of inter-annual variability in the Southern Hemisphere. The purpose of the analysis is to obtain a measure of the upper boundary of predictive skill, that is of the fundamental predictability that exists in the region as a consequence of all available sources of predictability that exist in the form of lower boundary and radiative forcing.

Methodology and data

The CMIP6 AMIP simulations make use of the same set of radiative forcings used to drive the more widely used set of 'historical' simulations in CMIP6. These include the historically observed or reconstructed greenhouse gas (including CO_2 and methane) and ozone (tropospheric and stratospheric) concentrations, aerosol emissions, and solar radiation. Whereas the CMIP6 simulations

span the period 1850-2014 and rely on the use of coupled global climate models (CGCMs), the AMIP simulations were designed to span the period 1979-2014 and rely on the use of atmospheric global circulation models (AGCMs). This is towards making use of the satellite era to provide to the AMIP experimental design the most realistic set of lower boundary conditions in the form of observed monthly sea-surface temperatures (SSTs) and sea-ice concentrations (SICs) (Xiang et al., 2017). The CMIP6 'historical' simulations, on the other hand, are constructed using 'free-running' CGCMs, without any lower-boundary forcing being applied.

In the analysis that follows, we make use mainly of a multi-model ensemble of AMIP simulations, constructed by using a single ensemble member of 41 AGCMs that participated in the AMIP experiment of CMIP6. A minority of participating models also contributed large initial-condition (IC) based ensembles to AMIP, and we also analyse one of these, namely an 18-member IC-ensemble generated by the GISS-E2-G-1 model. We finally, for comparison purposes, make use of a single ensemble member of the GISS-E2-G1 ensemble, to place in perspective the performance of the individual ensemble member in representing inter-annual variability as compared to that of the IC-based ensemble average. In combination the three sets of simulations analysed provide insight into the predictability that may be derived purely from 'perfect' boundary forcing, that is, from including all possible sources of predictability in the simulations. The IC-based ensemble additionally explores the role of model internal-variability on predictive skill. The predictive skill analysis is undertaken for the variables of 850 hPa height, representing low-level circulation. By considering model performance for this fundamental variable, we avoid the further uncertainties that result in simulating rainfall, for example, from the parameterisation of cumulus convection. As a verification data set, we make use of NOAA-CIRES-DOE reanalysis v3 (Slivinski et al., 2019), as a representation of the historical inter-annual variability in low-level circulation over the period 1979-2014.

The analysis is undertaken separately for the seasons DJF, MAM, JJA and SON. The Spearman Rank Correlation Coefficient (SR) is used to calculate correspondence between the various simulations and the reanalysis, to determine the degree of correspondence between the 'observed' and 'simulated' inter-annual variability. For DJF, 35 'cases' have been simulated over the 1979-2015 period, which yields that an SR of 0.283 or higher as statistically significant at the 95% level. For the remaining seasons there are 36 simulation years to consider, yielding a SR of 0.279 or higher as statistical significant at the 95% level. All data sets were interpolated onto a 1° latitude-longitude grid in order for the calculation of the SR at the grid-point level across the Southern Hemisphere.

Analysis

The spatial variation of the SR across the SH in terms of representing inter-annual variability in summer low-level circulation is shown in Figure 7. High correlation coefficients occur in the central and eastern parts of the tropical Pacific Ocean, which is indicative of the strong atmospheric response to the SST anomalies associated with ENSO. Correlations are also high across the tropical and subtropical Atlantic Ocean, as well as over the eastern tropical Indian Oceans. Correlations are relatively low, but still statistically significant, over the tropical western Pacific and western Indian Oceans. Across southern Africa, correlation coefficients are high and statistically significant for DJF. This suggests that strong control is exerted over the inter-annual variability in low-level circulation by the combination of lower-boundary and radiative forcing. Previous research (Landman and Beraki, 2012) have indicated that this forcing first and foremost derives from El Niño and La Niña events in the Pacific Ocean. There is an east-west gradient in the strength of the correlation across southern Africa (relatively low coefficients in the east, and relatively high coefficients in the west). To the south of southern Africa, and across the Southern Ocean, correlation coefficients are relatively low over the Southern Ocean. This includes regions within the westerly wind regime where the coefficients are not statistically significant, and in some cases are negative. This is a staggering and potentially highly significant result: there are portions of the westerly wind regime in the Southern Hemisphere where the inter-annual variability in low-level circulation is not responsive to either lower boundary or radiative forcing. These

regions of 'unpredictability' reach as far north as the southern tip of South America and south-eastern Australia in summer.

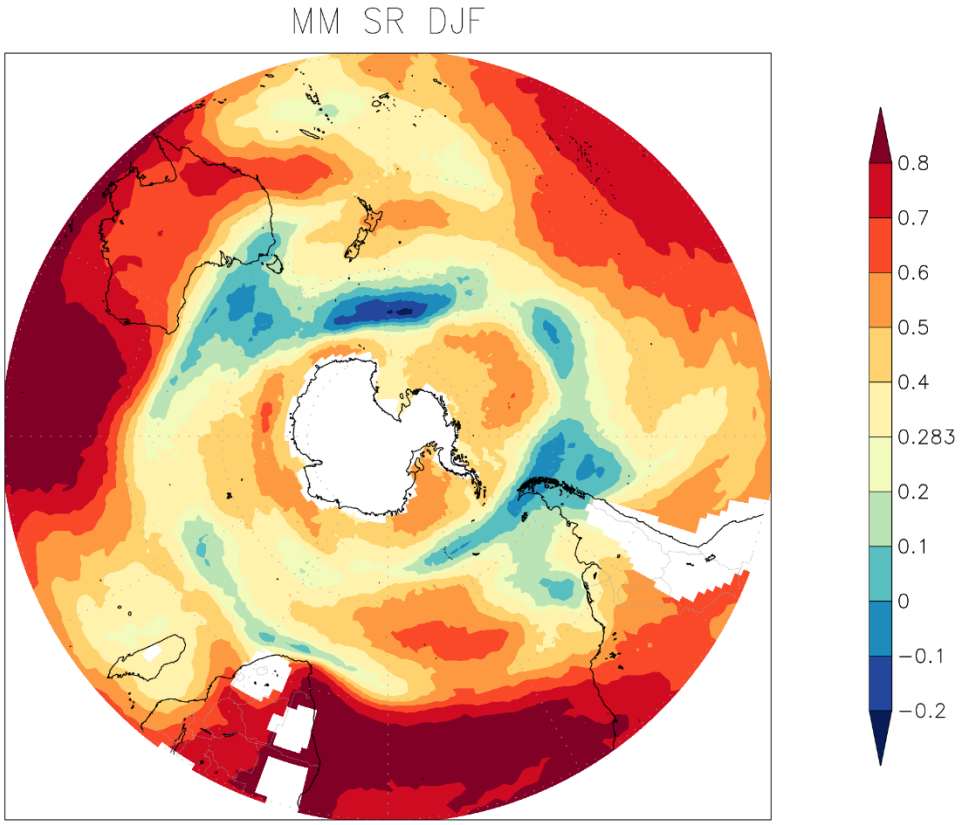

Figure 7: Spearman Rank Correlation Coefficients for summer (DJF) for 1979/80 to 2013/14 depicting the ability of the AMIP multi-model ensemble average to represent inter-annual variability in low-level circulation (850 hPa) in the Southern Hemisphere. Correlation coefficients of 0.283 or larger (yellow to red shaded) are statistically significant (α=0.05).

The SR values depicting the ability of the AMIP simulations to depict inter-annual variability in March are shown in Figure 8. The same pattern of high correlation coefficients over the tropical oceans found for summer persists in autumn, and as in summer, extend to the tropical continental areas. Over southern Africa the SR values are substantially lower than for summer, but still statistically significant. Over the Southern Ocean, the area of negative correlations are substantially larger and displaced northwards, likely in response to the more intense and northward displaced westerlies in autumn. The negative correlations reach as far north as the southern tip of South America, south-eastern Australia and the southwestern Cape and Cape south coast regions of South Africa. These findings suggest that even in the presence of perfect lower boundary and radiative forcing, autumn inter-annual variability in low-level circulation is fundamentally not predictable over vast regions of the Southern Ocean and the southern extremities of the Southern Hemisphere continents, at least not in the context of AMIP simulations.

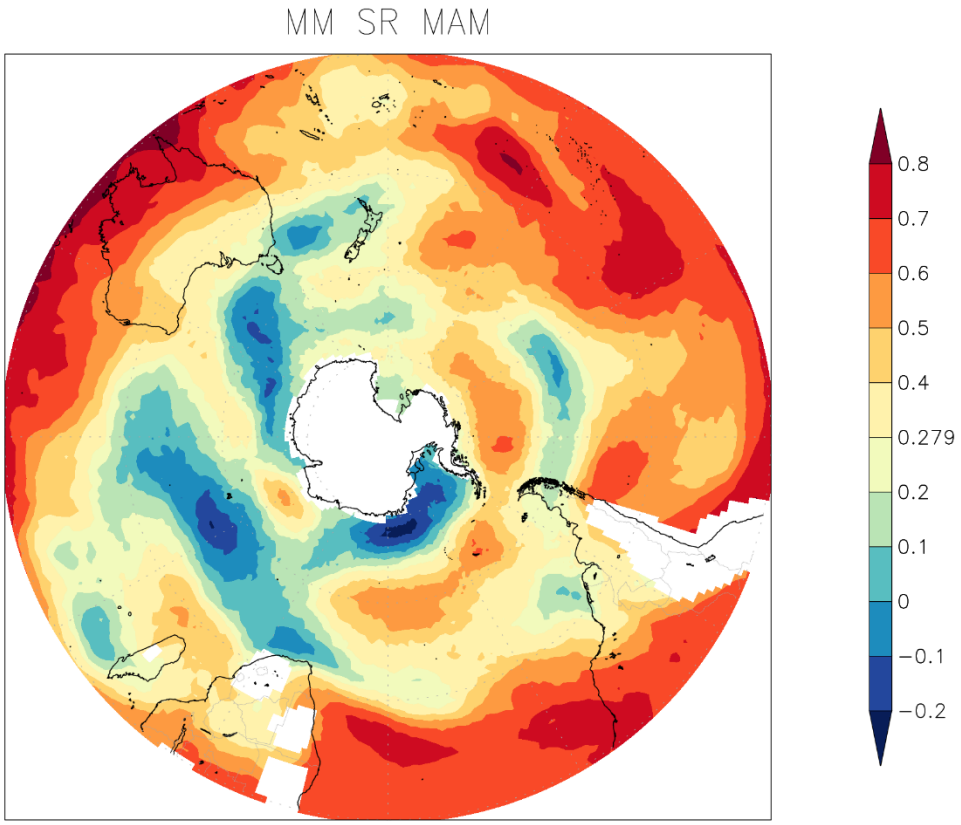

Figure 8: Spearman Rank Correlation Coefficients for autumn (MAM) for 1979 to 2014 depicting the ability of the AMIP multi-model ensemble average to represent inter-annual variability in low-level circulation (850 hPa) in the Southern Hemisphere. Correlation coefficients of 0.279 or larger (yellow to red shaded) are statistically significant (α=0.05).

During winter there is a further northward displacement of areas exhibiting statistically insignificant correlations across southern Africa, as the westerlies assume their most equatorward location (Figure 9). This result puts in doubt whether inter-annual low-level circulation (and thus rainfall) is at a fundamental level predictable over southern Africa in winter. That is, even in the presence of all known sources of predictability, observed inter-annual variability is not represented in the simulations. The results implies that the best prospects for skilful predictions of winter rainfall in southern Africa is in large IC-ensembles initialised using information of the planetary-scale flow. Across the Southern Hemisphere tropics, the SR values are high and statistically significant in winter. Over the tropical western Indian Ocean, and tropical western Pacific Ocean, correlations are substantially higher in winter compared to summer and autumn.

During autumn, SR values remain statistically insignificant over the southwestern Cape of South Africa, south-eastern Australia, and the southern tip of South America (Figure 10). Correlations are statistically significant across the Southern Hemisphere subtropics, but with relatively low values over the western Indian Ocean, and the western Pacific Ocean, like in spring and summer.

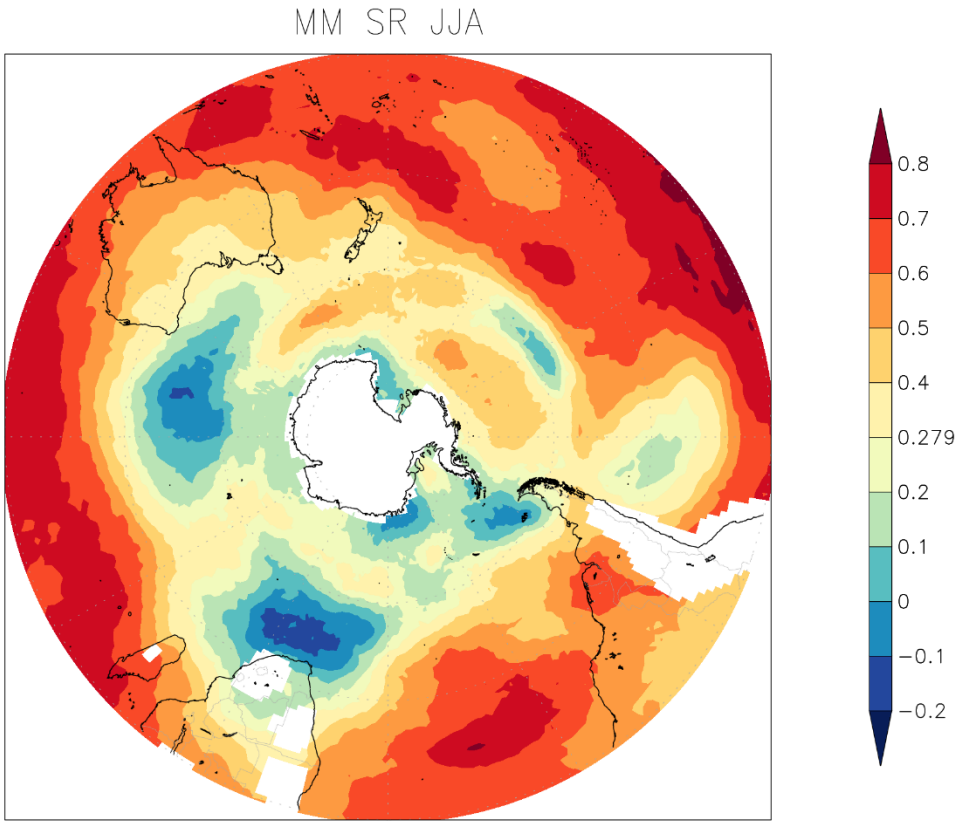

Figure 9: Spearman Rank Correlation Coefficients for winter (JJA) for 1979 to 2014 depicting the ability of the AMIP multi-model ensemble average to represent inter-annual variability in low-level circulation (850 hPa) in the Southern Hemisphere. Correlation coefficients of 0.283 or larger (yellow to red shaded) are statistically significant (α=0.05).

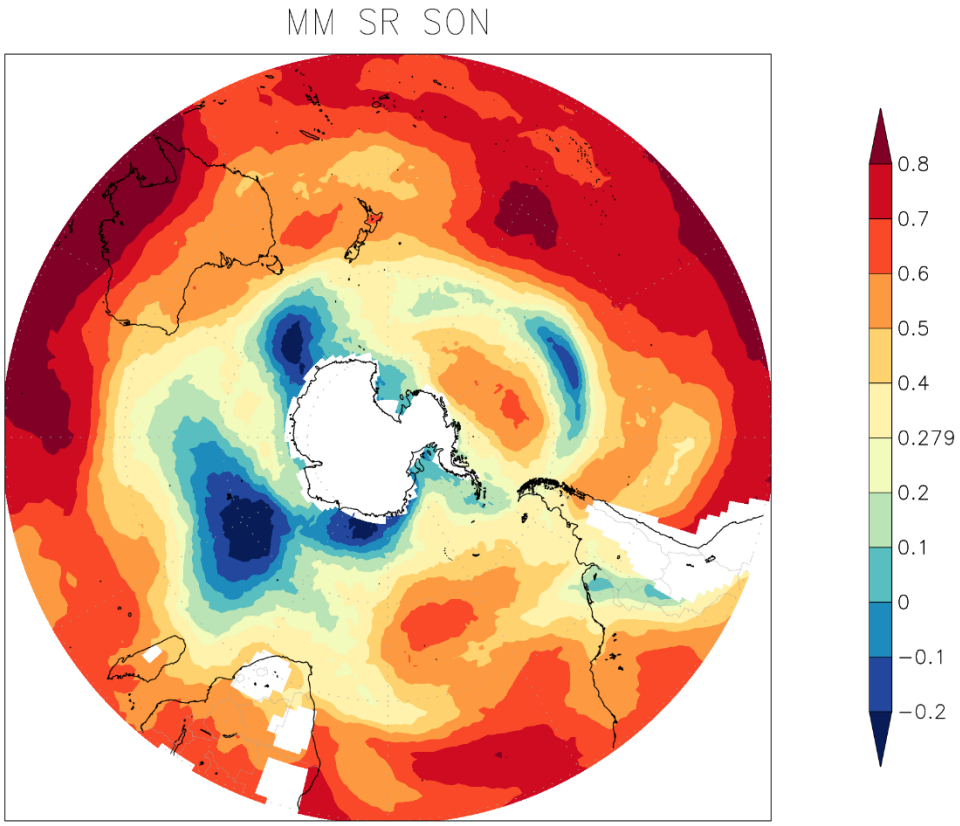

Figure 10: Spearman Rank Correlation Coefficients for spring (SON) for 1979 to 2014 depicting the ability of the AMIP multi-model ensemble average to represent inter-annual variability in low-level circulation (850 hPa) in the Southern Hemisphere. Correlation coefficients of 0.283 or larger (yellow to red shaded) are statistically significant (α=0.05).

For summer, the skill of an IC-based ensemble average of simulations is very similar to that of the multi-model ensemble, in terms of representing observed inter-annual variability (Figure 11). A single ensemble member still provides a skilful result, which in facts implies that the control of lower-boundary and radiative forcing over low-level circulation over southern Africa is so strong that it is in fact deterministically predictable. The lower SR values for the case of a single ensemble member, relative to that of the corresponding IC-ensemble average does point, nevertheless, to the role of internal-variability in the model simulations, and the need to use an ensemble average for the dominant boundary forcing signal to be captured.

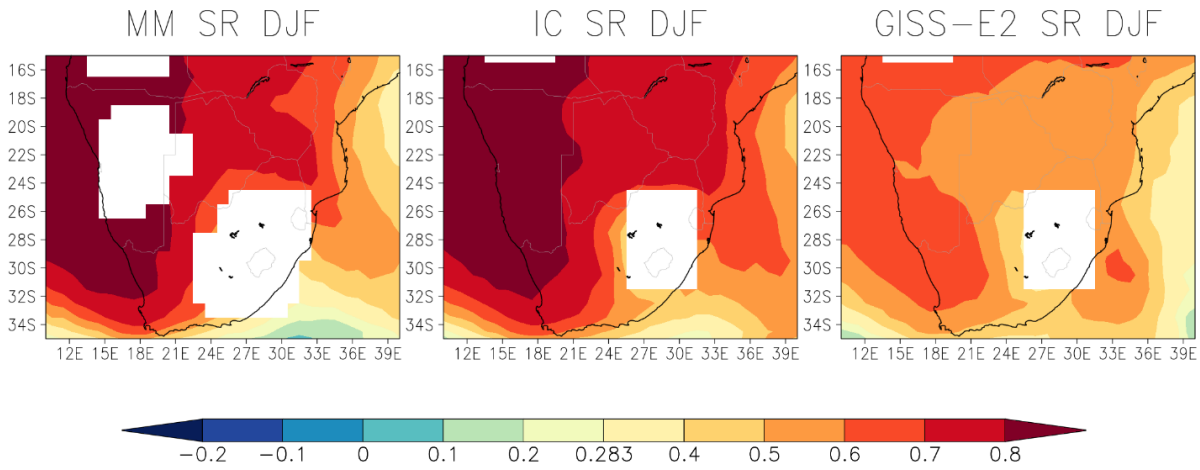

Figure 11: Spearman Rank Correlation Coefficients for summer (DJF) for 1979/80 to 2013/14 over southern Africa depicting the representation of inter-annual variability in low-level circulation for the a) 41- model ensemble average; b) 18-member initial condition ensemble of the GISS-E2-G-1 model and c) a single ensemble member from the GISS-E2-G-1 ensemble. Correlation coefficients of 0.283 or larger (yellow to red shaded) are statistically significant (α=0.05).

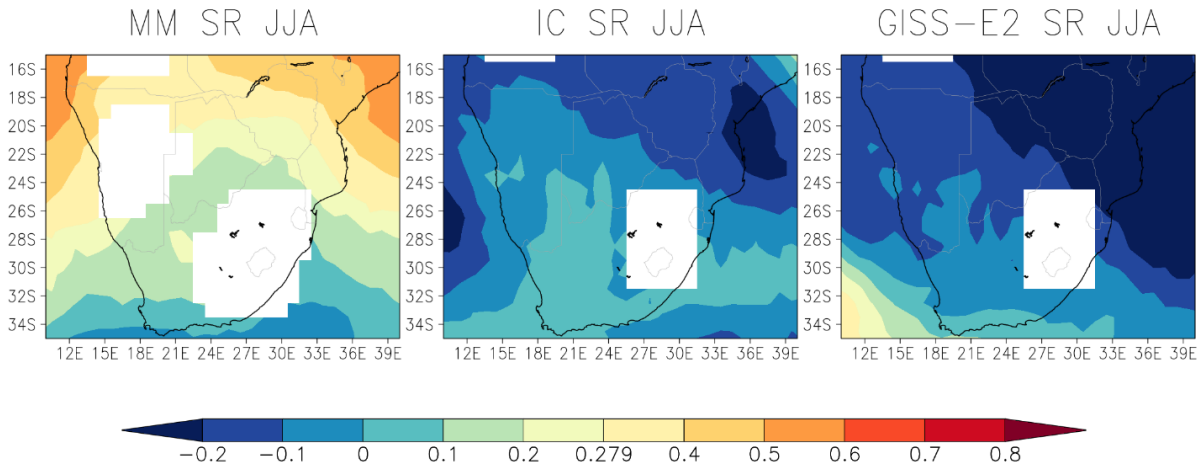

Figure 12: Spearman Rank Correlation Coefficients for winter (JJA) for 1979 to 2014 over southern Africa depicting the representation of inter-annual variability in low-level circulation for the a) 41-model ensemble average; b) 18-member initial condition ensemble of the GISS-E2-G-1 model and c) a single ensemble member from the GISS-E2-G-1 ensemble. Correlation coefficients of 0.279 or larger (yellow to red shaded) are statistically significant (α=0.05).

For the case of winter (Figure 12), behaviour is rather different. The IC-ensemble produces substantially lower SR values than the multi-model ensemble, suggesting the importance of the response of different models to the lower boundary and radiative forcing in terms of representing inter-annual variability of winter circulation, as opposed to hat of a single model (or at least the specific model used here). The single ensemble member verified, like the IC-based ensemble average, produces statistically insignificant and/or negative correlations across southern Africa, clearly indicating the inability of the simulations to represent winter inter-annual variability over southern Africa. For the multi-model ensemble, however, such skill does exist over the northern parts of the domain.

We finally consider the zonally averaged SR values across the Southern Hemisphere, for the cases of summer (black dots) and winter (green dots; Figure 13). Consistent with the spatial maps of SR values in Figure 7 and Figure 8, correlations are generally higher for summer as opposed to winter across the Southern Hemisphere. Moreover, correlations are highest in the tropics and decrease towards the mid-latitudes. Over the high-latitudes towards Antarctica, correlations are relatively high for summer as opposed to winter, suggesting a signal from radiative and lower-boundary forcing in this region in summer.

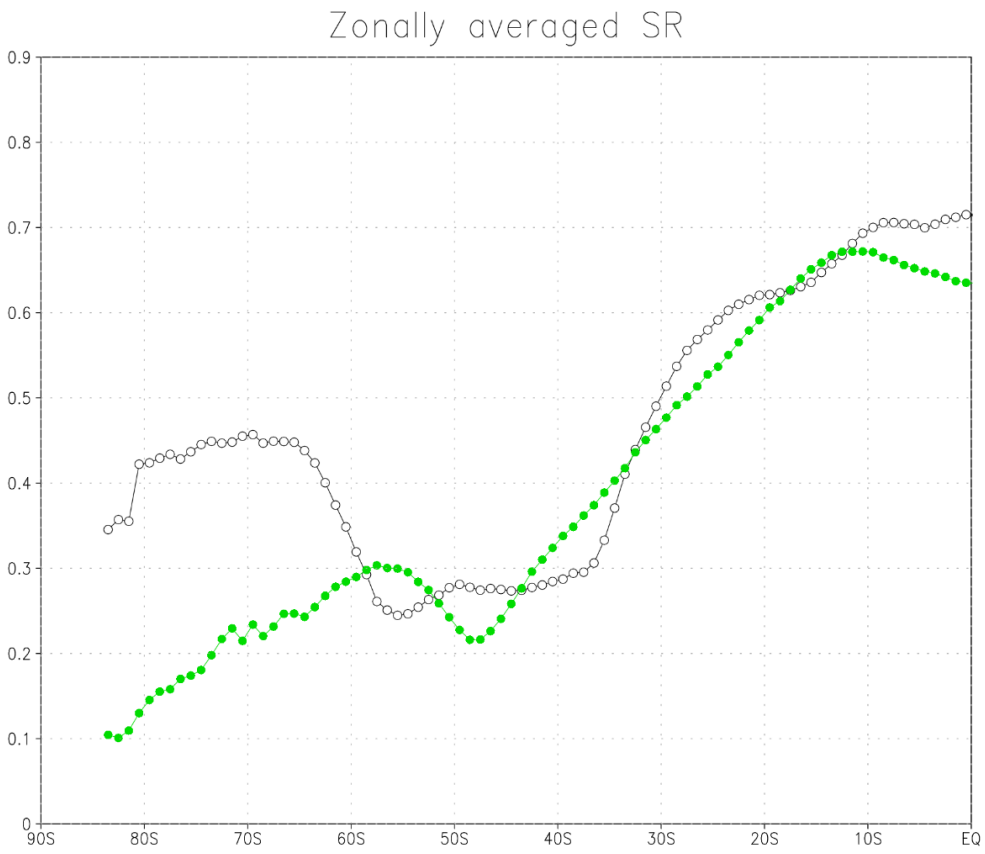

Figure 13: Zonally averaged Spearman Rank Correlation Coefficients in representing summer (DJF; black dots) and winter (JJA, green dots) inter-annual variability in the AMIP multi-model ensemble average of low-level circulation.

Summary

The resulting evaluations of skill in the AMIP-simulations of inter-annual variability in the Southern Hemisphere confirm the results from operational seasonal forecasting, namely that a pronounced

seasonal cycle in predictive skill exists over the Southern Hemisphere continents in the subtropics, with peak skill in summer in association with ENSO forcing. However, in spring and autumn and particularly in winter, circulation patterns of lower predictability originating from the Southern Ocean impact on atmospheric variability over the subtropical landmasses. Since these circulation patterns seem to be relatively unconstrained by lower boundary and atmospheric radiative forcing, it implies that predictability in the subtropics may be constrained in winter and the transition seasons by the relatively less predictable mid- and high-latitude circulation regimes of the Southern Hemisphere. This is a finding with pronounced implications for the seasonal prediction of winter rainfall in southern Africa, effectively suggesting that there are no known sources of predictability (in terms of lower boundary forcing and radiative forcing) for this region. Over the tropics, predictive skill is the highest in the AMIP simulations, likely as a direct response of atmospheric circulation to SST forcing. However, this skill is relatively low over the western Indian Ocean and western Pacific Ocean, indicating a relatively larger role of internal variability for these regions. This finding has implications for the seasonal prediction of landfalling tropical cyclones over southern Africa, and eastern Australia. Operational seasonal forecasting needs to predict the slow-changing lower-boundary and radiative forcing conditions, which places it in a disadvantaged position compared to AMIP-simulations. However, operational forecasting can draw information of the slowly changing planetary waves from the latest set of atmospheric initial conditions, and their incorporation in the operational prediction system through data assimilation. The findings presented here suggest that for the most southern parts of the Southern Hemisphere continents, including the southwestern Cape of South Africa, south-eastern Australia and the southern tip of South America, the seasonal prediction of winter rainfall and underpinning circulation anomalies need to focus on improved systems of initialisation and data assimilation, rather on sources of predictability, since for these regions the latter is insignificant compared to the dominating role of internal variability.

4.2 Multi-year droughts analysis

Background

Drought is a multi-faceted phenomenon that occurs across a range of temporal and spatial scales and is experienced across a range of societal sectors that are dependent on climate and water resources (Wilhite, 2000). It is a consequence of climate anomalies and human water use practices, but many impacts on society are more directly related to hydrologic conditions resulting from these two factors. Despite various type of droughts, hydrological and socio-economic droughts limit use of water for industrial and domestic consumptions, and negatively affects production and wider economy (FAO, 2004). We focus here on the assessment of the regional interannual to multi-decadal variability and changes of droughts and other related environmental conditions. This ongoing study has furthermore endeavoured to understating the driving mechanisms that presumably shape these variability and changes.

Methodology and data

The analysis uses model simulations emanated from the CSIR seamless forecasting system (SFS). The SFS uses the conformal-cubic atmospheric model (CCAM; McGregor and Dix 2008). The model is developed by the Commonwealth Scientific and Industrial Research Organisation (CSIRO) of Austria. The SFS has applied over range of timescales (i.e., weather forecast to climate change projections). The system can also be applied globally with a quasi-uniform horizontal resolution or stretched grid mode, which yields a variable horizontal resolution with regional or local details needed over a region of interest. In our case, the model interactively couples a sophisticated biosphere model, referred to as Atmosphere Biosphere Land Exchange (CABLE; Kowalczyk et al. 2013). In addition, it includes a

prognostic aerosol scheme due to Mitchell et al. (1995) which can be applied consistently with the emission inventories and radiative forcing specifications of the Coupled Model Intercomparison Project Phase Five/Six (CMIP5/6; Taylor et al., 2012). The model also incorporates biogeochemical knowledge and elements of the terrestrial carbon cycle.

The simulations comprise 50km horizontal resolution of present-day (baseline) climate and projections of future climate simulations over Africa. It covers the period from 1971 to 2099, which comprises the downscaling of 6 model outputs from the CMIP5. The simulations were made for two Representative Characteristic Pathways (RCPs) scenarios: RCP4.5 (mitigation scenario; Thomson et al., 2011) and RCP8.5 (uncheck scenario; Riahi et al., 2011). These simulations were extensively applied and fairly explained in previous studies (e.g., Muthige et al., 2018; Beraki 2019). Nonetheless, results for the latter presented in this report.

Analysis

Historical observed interannual and multi-decadal variability

The historical analysis is based on the Climate Research Unit (CRU TS v. 4.04; Harris et al., 2020). The data has a range of climate variables including rainfall and potential evapotranspiration (PET) and is suitable for calculating both the SPI (Standardized Precipitation Index; McKee et al., 1993, 1995) and SPEI (Standardized Precipitation-Evapotranspiration Index; Vicente-Serrano et al., 2010). The CRU is presumably the most reliable available high-resolution (50km) global observed dataset particularly in places where reliable in situ observations are not readily available mostly in Africa.

We investigate the observed interannual to multi-decadal variability and changes of droughts and other environmental conditions that directly affect rainfall, streamflow, and river discharges across major River Basins of over Africa. We present herein the Orange River basin (excluding the northern transboundary contributions from Namibia, Zimbabwe, and Botswana). The Orange is the largest river system in Africa south of the Zambezi and forming the western border of Lesotho, and the Vaal and flows west to the Atlantic Ocean (Cambray et al., 1986).

Figure 14 presents how the 20th Century and the last two decades observed interannual and multi-decadal variability and changes of drought and other environmental conditions affect moisture budget and streamflow extents over the Orange River Basin.

The SPEI during the historical period, which spans a period of over 120 years (1901 to 2019), suggests that the succession between droughts and floods was likely the consequence of natural rainfall variability. Furthermore, it is also apparent although the response of the SPEI is delayed to the observed steady increase of temperatures since the 1980s (as a drought develops slowly), the last two decades have seen a faster amplification of SPEI severity than its SPI counterpart. This could be due to moisture loss through evaporation (PET) from the drainage systems since 2000s as the global average temperature has increased by 1.2°C in 2020 relative to the pre-industrial era (WMO, 2020).

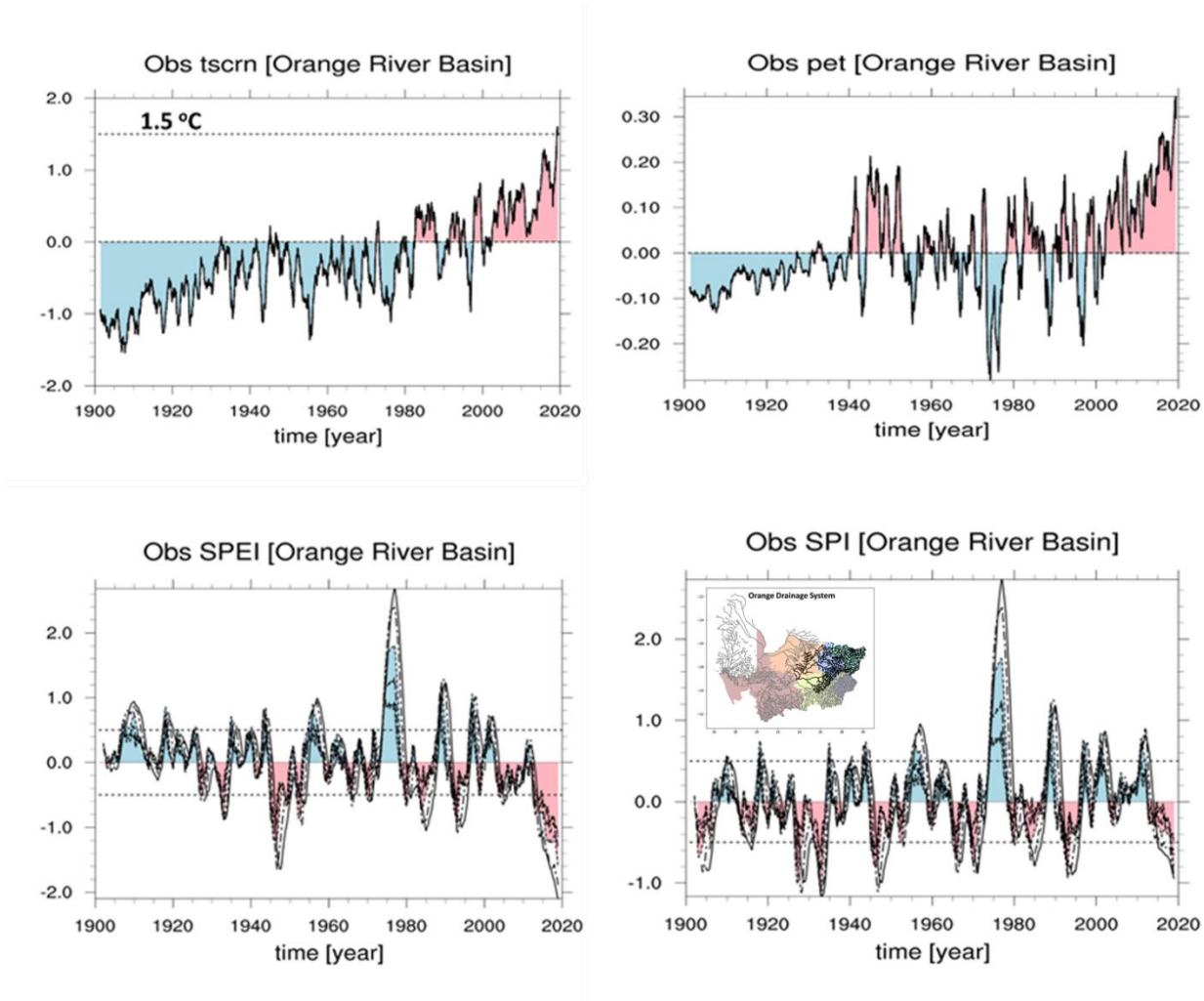

Figure 14: Observed time-series near-surface air temperatures (tscrn), moisture loss due to potential evaporation (pet), and droughts (SPEI and SPI) conditions over the Orange River Basin (catchment within South Africa). The assessment, which shows basin-wide interannual to multi-decadal variability and changes during the last 120yrs (1901 to 2019) based on the CRU climate data. The drought graphs also depict the 3, 6 12, 24, 36 months' scale. Furthermore, all of them also subject to 24 months running mean (smoothing) to detect the slowly evolving signal. The severity and scale tend to increase proportionally, where ≤the 12-month scale is shaded with light blue and light pink for the tendency of wetness and dryness respectively. Graphs produced with NCAR Command Language (NCL, 2017)

Future projected interannual and multi-decadal variability

To achieve this analysis, we have revisited the drought work done for the CSIR Greenbook (Beraki 2019). The work comprises at range of spatial details including at the catchment level and Continental Africa. Figure 15 shows the state of drought under global warming of 3°C and RCP8.5 worst-case scenario using the SPI and SPEI indices. Also shown is the multi-decadal observed (CRU) and modelled SPI multi-decadal variability and trends, which spans a period of over two centuries (1901 to 2099). The analysis suggests that although the historical period is largely explained by natural variability, the region may be heading towards future climate system characterized with intense and more frequent droughts under global warming of 3°C and with the current emission trajectory leading towards the end of 21st century. Besides, those regional may seem to benefit from the change including the greening of the Sahara Desert (Figure 15(a)). Notwithstanding, when the moisture loss is accounted, the continent may be exposed to a perpetual water stress without exception (Figure 15(b)).

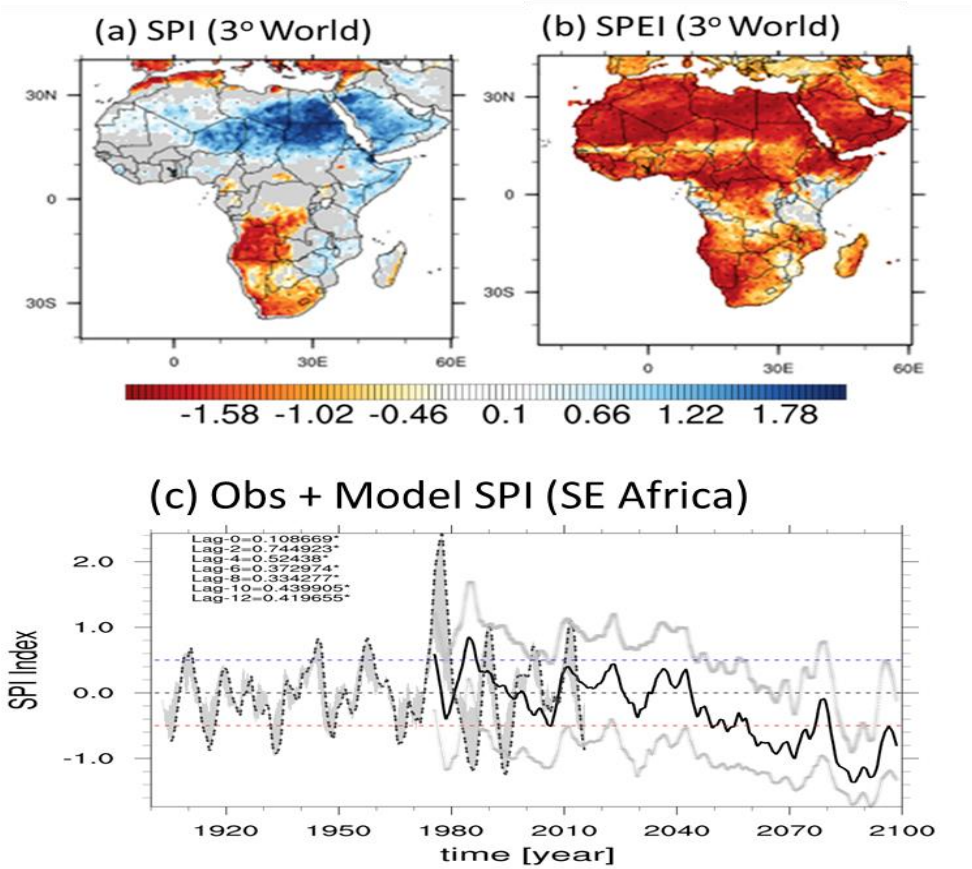

Figure 15: The state of drought under 3°C and above global temperature goals and RCP8.5 scenario using two indices of drought (a, b) and multi-decadal observed and modelled drought (SPI) variability and trend (c).

Summary

The interannual and multi-decadal drought variability over the Orange River basins is largely explained by the natural variability throughout the 20th Century. The difference between the SPI and SPEI during this period was barely noticeable further suggests that the succession between droughts and floods was likely the consequence of rainfall variability. The response of the SPEI delayed to the observed steady increase of temperatures since the 1980s presumably because droughts develop slowly. However, the last two decades have seen the amplification of SPEI severity faster than its SPI counterpart. The worsening of water stress due to loss from surface water, drainage systems, and other covers is likely associated with temperature amplification. The impact of drastically rising temperatures on the future moisture budget and surface water resources may arise from the continental scale loss of water due to potential evapotranspiration (PET), as suggested by the markedly worse drought conditions depicted in Fig. 15b (SPEI) compared to Fig. 15a (SPI) for a future world where global warming has reached the level of 3 °C. This is consistent with the increasing impact of rising temperatures on the historical variability in drought over the last two decades (Fig.14). However, the impact of climate change on rainfall is complex and nonlinear in nature and its signature is likely felt with a drastic shift on rainfall bearing systems. This gradual shift may be due to the northward migration of the tropical temperate cloud bands associated with the Inter-Tropical Convergence Zone (ITCZ) during austral summer and the poleward displacement of the frontal system associated with the westerlies during austral winter as investigated in section 5.2.

4.3 Baroclinic instability analysis

Background

This section focuses on the analysis of the ability of seasonal forecasts to describe energy transfer in the atmosphere, applying spectral analysis to study the winter atmospheric variability at the mid-latitudes of the Southern Hemisphere from 1993 to 2020. We estimate the power content of the atmospheric phenomena typical of mid-latitudes, such as baroclinic perturbations. This is done by comparing the results of the ERA5 climate reanalyzes with those of the long-range forecasting system SEAS5, both provided by the European Centre for Medium-Range Weather Forecasts (ECMWF) and the seasonal forecasts operated by the Deutscher Wetterdienst (DWD) and Meteo France. The reference dataset consists of the geopotential height fields of 500 hPa belonging to the ERA5 reanalysis and the seasonal forecast (SF) provided by ECMWF (SEAS5, 25 ensemble members), and the ones operated by the Deutscher Wetterdienst (DWD, 30 ensemble members) and Meteo France (25 ensemble members).

The ability of climate models to correctly predict the intensity of baroclinic instability is a very important requirement, as this phenomenon is a significant component of the climate system, associated with the meridional transport of a large amount of energy and momentum. Moreover, baroclinic instability is related to precipitation activity and its intensity. For this reason, an analysis of the ability of seasonal forecasting to correctly predict baroclinic activity can contribute to the understanding of the skill of precipitation prediction. We perform a space-time spectral analysis to quantify the power content of the atmospheric phenomena, computing the Hayashi spectra of the 500-hPa geopotential height field, which are named after the first who formulated a method for decomposing waves through spectral analysis (Hayashi, 1971). Subsequently, Pratt (1976) and Fraedrich and Bottger (1978) reinterpreted the method for calculating the power spectra of space-time series. The analyses made by Dell'Aquila et al. (2005, 2007), which we used as a starting point, were partly based on these studies. In addition, following the procedure described by Dell'Aquila et al. (2006), we evaluate the Baroclinic Amplitude Index (BAI), an indicator that allows quantifying the intensity of the baroclinic activity.

Methodology

Since the purpose is to analyses the Southern Hemisphere winter atmospheric variability, the months June, July, and August (JJA) have been selected for both the reanalysis and the SF. The three months have lead times equal to 1, 2, and 3 respectively since we set May as the issue month. For both the reanalysis and the seasonal forecast datasets, we select the latitude band between 30°S and 75°S, to capture the bulk of the baroclinic activity and low-frequency planetary waves (Dell'Aquila et al., 2005). Subsequently, we perform the weighted average of the geopotential field on this latitudinal belt, obtaining a one-dimensional longitudinal field representative of the atmospheric variability at mid-latitudes. Therefore, the geopotential height field, which originally varied both zonally and meridionally, has a spatial dependence only on the longitude after it has been averaged over the latitudinal direction. Before performing all the subsequent calculations, we have reduced the spatial resolution of ERA5, bringing it from 0.25° to 1°, to ensure that the reanalysis dataset and the seasonal forecast datasets are consistent with each other. To do this, we applied a nearest-neighbor interpolation to the time-longitude-dependent geopotential height field. Afterward, we applied the Fourier space-time decomposition, to obtain a geopotential height field in the domain of frequencies and wavenumbers, instead of time and longitude. We used the Hayashi technique, with reference to Hayashi (1971) and Pratt (1976), to create the power spectra and distinguish the standing and traveling wave patterns. The variability of the geopotential height field in terms of periods and zonal wavenumbers can be described by the spatio-temporal Fourier decomposition introduced by Hayashi

(1971, 1979). Hayashi's technique allows the creation of power spectra of space-time series as a function of the frequencies *ω* and the wavenumbers *k*. According to Hayashi's treatment, for a periodic series in space *x* and infinitely extended in time *t*, the power spectra can be divided into standing and traveling components, the sum of which constitutes the total signal. It is important to underline that the decomposition of the original signal into standing and traveling parts is based on the fact that these waves are generated by different mechanisms and therefore attributable to different physical phenomena.

Baroclinic Amplitude Index

Baroclinic activity is quantified by calculating the Baroclinic Amplitude Index (BAI). The Baroclinic Amplitude Index is useful for getting an idea of baroclinic intensity and understanding how much energy is being released from the atmosphere in the form of rain and heat fluxes on Earth. The higher the BAI, the stronger the baroclinic activity. Before this metric can be calculated, a high-pass filter must first be applied to the daily geopotential field to obtain only the modes with a period of less than 10 days (Dell'Aquila et al., 2006). For this purpose, the Fourier transform is applied to the 500-hPa geopotential to express it in the temporal frequency domain. Then all geopotential heights corresponding to a period of more than 10 days are set to zero, while the others remain unchanged. The period is then calculated as the inverse of the frequency. Subsequently, we apply the inverse Fourier transform to return to the time domain. We then take the weighted average of the geopotential field on the latitudinal belt bounded by 30 °S and 75 °S. For each day in the winter period (JJA), the 500-hPa geopotential height is decomposed along the longitudinal direction using the Fourier transform. Finally, we calculate the index by applying the integral of the obtained Fourier coefficients between zonal wavenumbers 4 and 7, which comprise the region where baroclinic activity is strongest. The BAI is then calculated with the following formula:

$$Z_{4-7}(t) = (\sum_{k=4}^{7} 2|Z_k|^2)^{\frac{1}{2}}$$

Hayashi spectra of ERA5 reanalysis

Figure 16 shows the Hayashi spectra of the 500-hPa geopotential height averaged over the 28 winters of 1993-2020, calculated from the ERA5 reanalysis dataset. In particular, the four components of the spectra are displayed: total, stationary, travelling eastward and travelling westward.

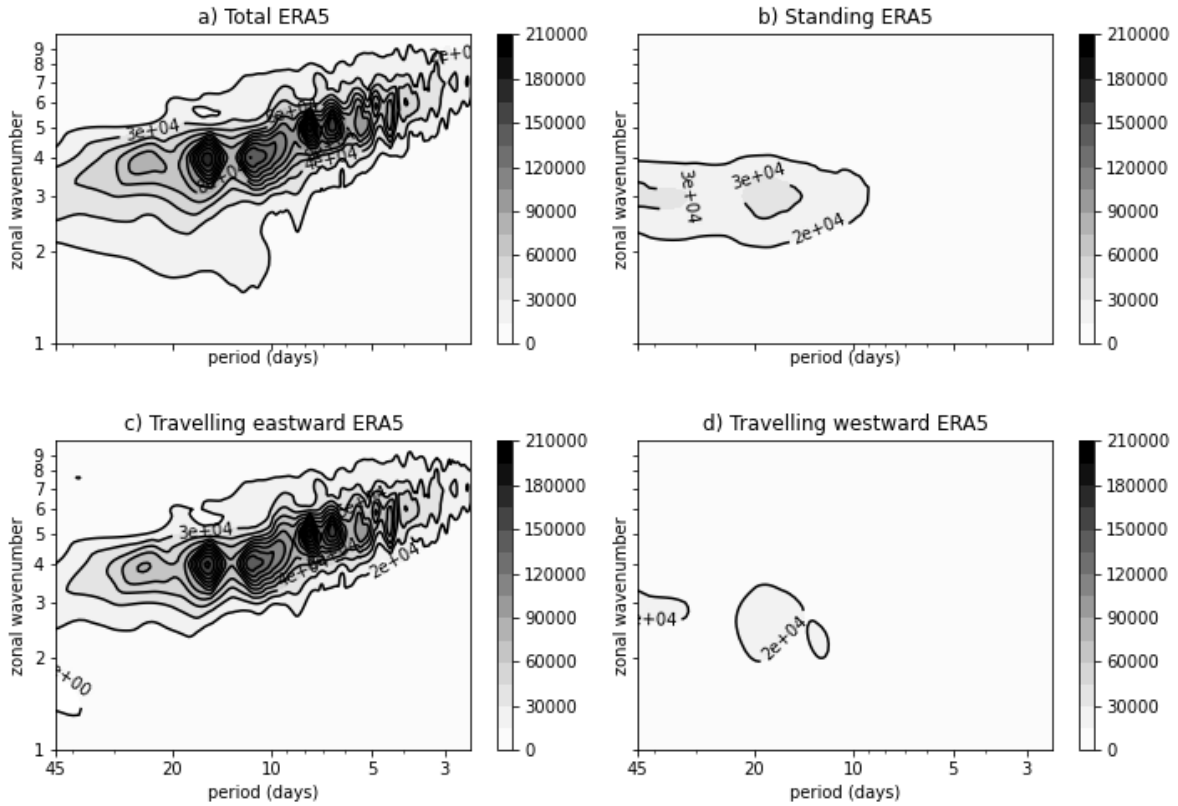

Figure 16: Hayashi spectra for 500-hPa geopotential height from ERA5 averaged over the 28 winters (1993-2020) in the Southern Hemisphere (30-75°S)

The spectra express the power density of the wave field in terms of frequency and zonal wavenumber. If we look at the total power spectrum (a), we can see from the darker colors that a large fraction of the total power is concentrated in periods between 4 and 16 days and in wavenumbers between 3 and 7. In this region we can identify the baroclinic disturbances, travelling waves with a period of the order of 2-7 days, wave numbers around 4-7 m^{-1} and a spatial scale of several thousand kilometers. This domain is related to the eastward propagating waves (c) and includes the synoptic phenomena associated with the release of available energy driven by conventional baroclinic conversion (Blackmon, 1976). They are thus involved in energy transfer in the Southern Hemisphere at mid-latitudes, leading to atmospheric stability or instability. Although the overall variability is mainly explained by the eastward propagation component, we can see that it also extends to planetary scales, with k = 3-4 and a period of about 16 days.

Standing waves (b) are characterized by low frequencies (long periods) and low wavenumbers. These types of waves allow us to get an idea of the average atmospheric situation. As Dell'Aquila et al. (2005) has shown, their contribution in the northern hemisphere has been considerable, mainly due to the Rocky Mountains. In the Southern Hemisphere, they have a peak in wave number around 3 m^{-1}, which could be associated with blocking episodes due to the presence of the Andes. However, they play a smaller role, as the Andes do not appear to make a significant contribution to the amplification of planetary waves (Adana and Colucci, 2005). Moreover, the westward propagating components are particularly weak, as expected in a region where the effects of large-scale topography are small.

Hayashi spectra of SEAS5 seasonal forecast

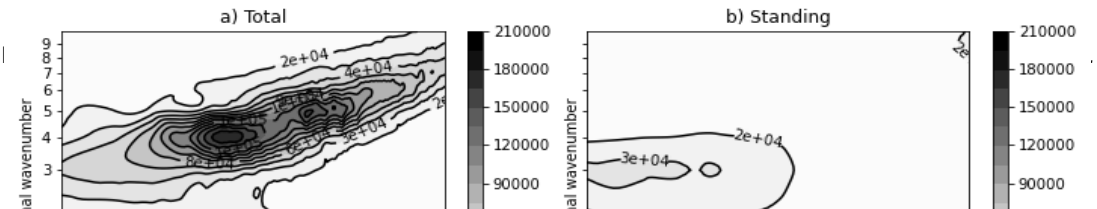

Figure 17: Hayashi spectra for 500-hPa geopotential height of SEAS5 in the Southern Hemisphere (30-75°S) averaged over the 28 winters and over the ensemble members.

We show the averaged Hayashi spectra across the members of the SEAS5 ensemble in Figure 17.

These plots were created by calculating the Hayashi spectra for each individual member and then averaging over the entire ensemble. This process naturally smooths out the peaks, which are not as noticeable as when looking at each individual element. However, we felt that calculating a representative average spectrum of the entire ensemble was more informative than analyzing the individual members separately, as these were generated with random perturbations to the initial conditions. Nevertheless, we can deduct from Figure 17 that also for the seasonal forecasts, the overall variability of the power spectrum of the 500-hPa geopotential height is mainly explained by the eastward propagating component, which also extends to the planetary scales (k = 3-4 and period around 15 days or more). Figure 18 shows the standard deviation of the SEAS5 ensemble. Using this metric, we can understand where the greatest variability exists among all the spectra of the ensemble members.

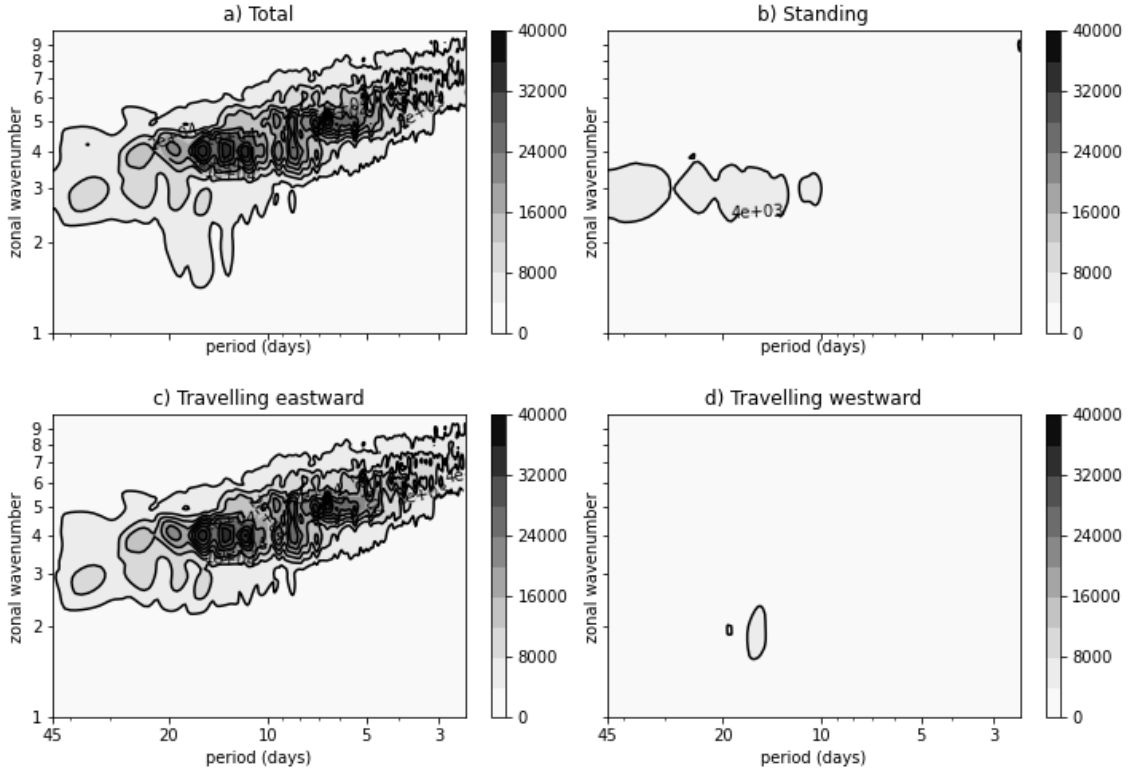

Figure 18: Standard deviation between ERA5 and SEAS5 Hayashi spectra for the 500-hPa geopotential height, averaged over the 24 winters.

We can see that there are some peaks for wavenumber k=4 aligned along a horizontal line, which means that the seasonal predictions for wavenumber 4 divide the spectrum into 3 distinct days. A similar pattern, but smoother, is also visible for wavenumbers around 5. In contrast, for a period of 8 days, there are some vertically aligned peaks corresponding to different wave numbers. This graph shows us that the peaks are not aligned along a sloping line as in ERA5, but that there is a problem in the partition of energy both in space (for a period of 8 days) and in time (for wavenumber 4). This suggests difficulties in accurately representing the structure of the baroclinic instability by the different elements of the seasonal forecast ensemble, as each of them attempts to represent the wave dynamics differently.

Difference between seasonal forecasts and ERA5

Figure 19 shows the mean of the differences between ERA5 and SEAS5 Hayashi spectra, averaged over the entire ensemble.

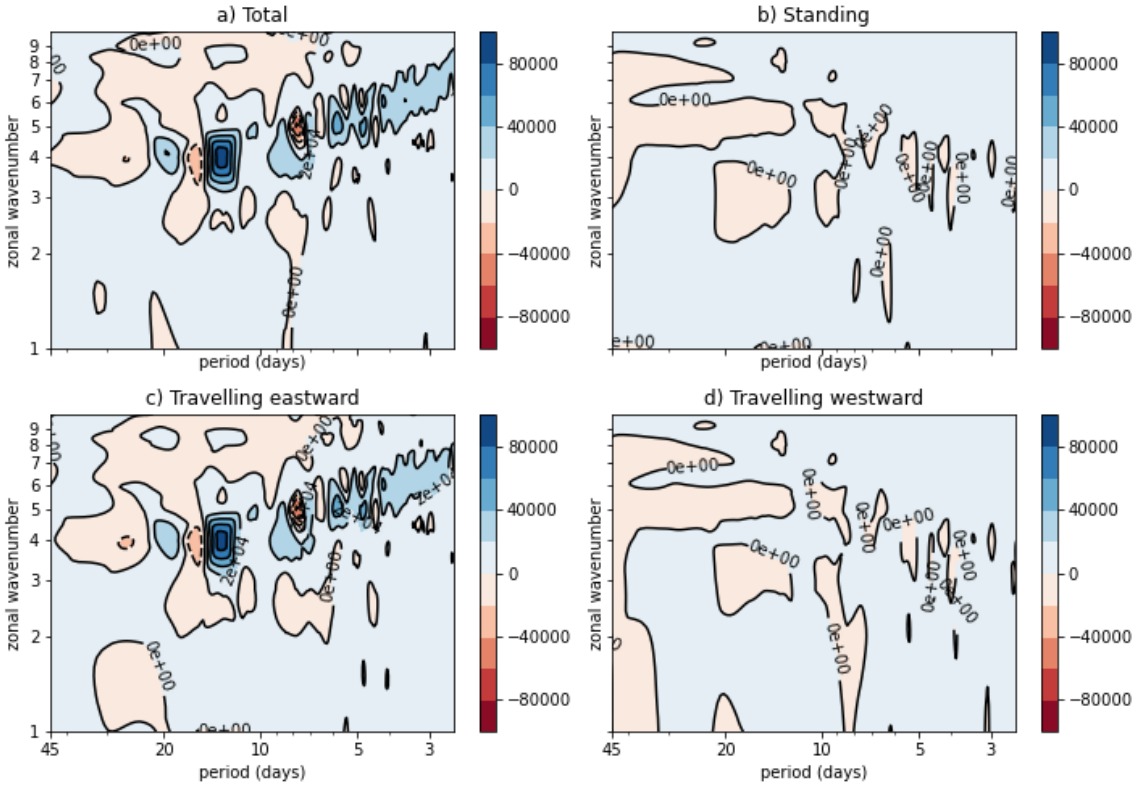

Figure 19: Difference between SEAS5 and ERA5 Hayashi spectra for 500-hPa geopotential height averaged over the 28 winters and over the ensemble.

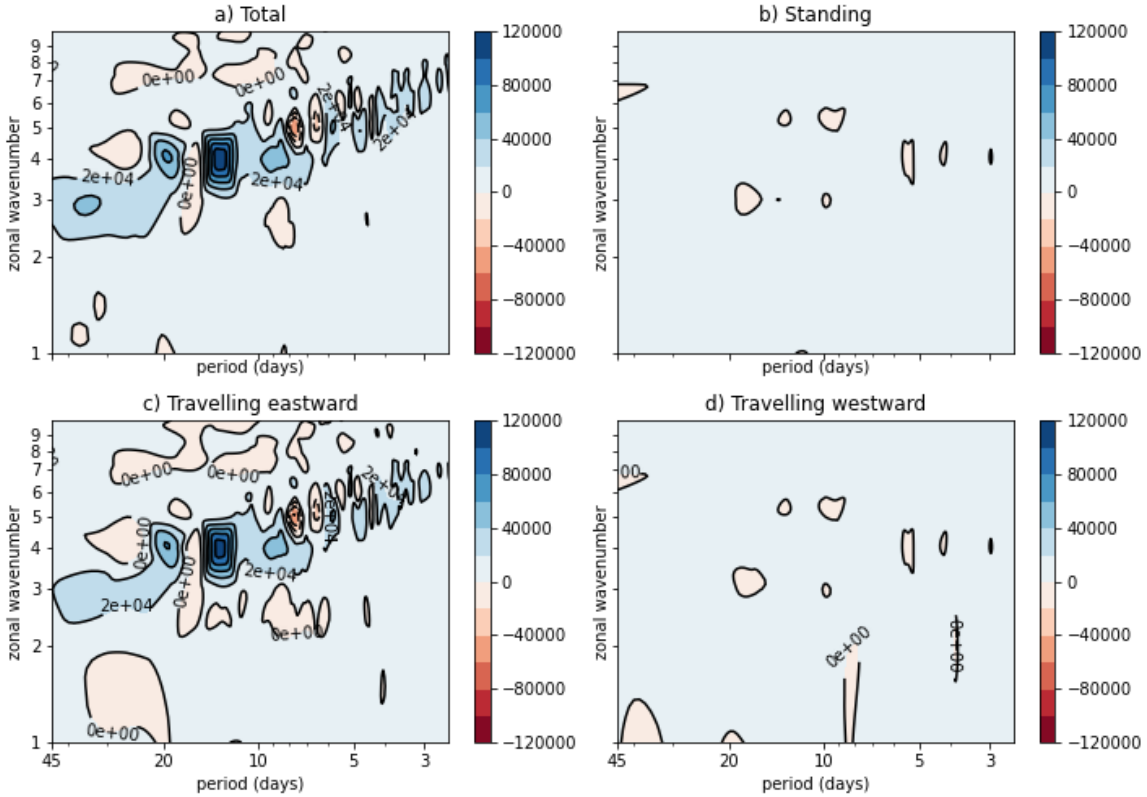

Figure 20: Difference between DWD seasonal forecasting system and ERA5 Hayashi spectra for 500-hPa geopotential height averaged over the 28 winters and over the ensemble.

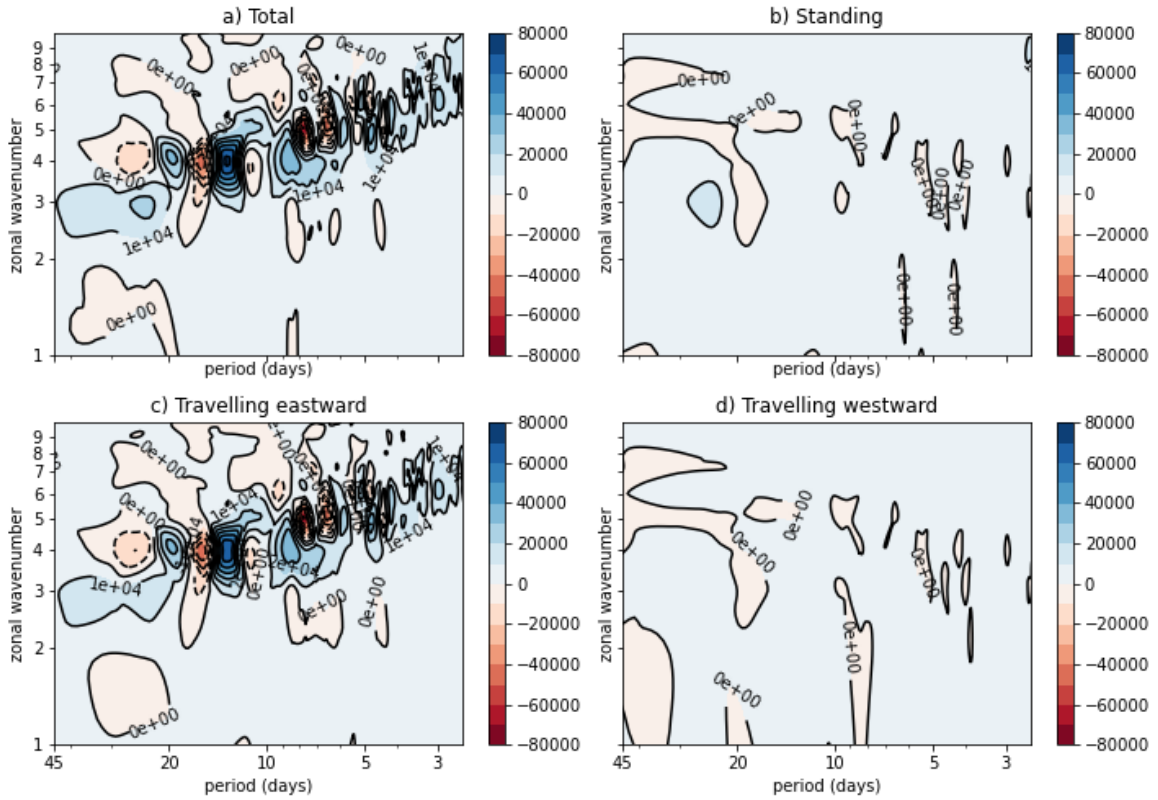

Figure 21: Difference between Meteo France seasonal forecasting system and ERA5 Hayashi spectra for 500-hPa geopotential height averaged over the 28 winters and over the ensemble.

It can be seen that in all three cases the differences are very small for standing and westward waves (Figure 19b-d, Figure 20b-d, Figure 21b-d), while the largest discrepancies occur for eastward waves (Figure 19c, Figure 20c, Figure 21c). The large peak of positive power (in blue) observed for periods of about 12 days and wavenumber 4 shows that in this spectral region the variability detected by the seasonal forecasts is much larger than that of ERA5. This overestimation occurs in all three seasonal forecasts but is less evident in Meteo France (Figure 21a-c). The blue peak around wavenumber 4 and 12-15 days is partially offset by the negative peaks (light red) around 15-17 days. There is also greater variability between 4 and 7 days, as can be inferred from the alternation of red and blue peaks in this region.

The Baroclinic Amplitude Index is calculated for each day of the time series. Through this analysis it is possible, on the one hand, to observe the change in the index over the years and, on the other hand, to understand whether the seasonal forecasts can calculate it correctly in comparison with the reanalyzes.

To show how the BAI is distributed in the ensemble, we use a box plot (Figure 22, Figure 23, Figure 24). The center line in the box represents the median of the data, which indicates that half of the data is above this value, the other half below. The mean is shown as a green triangle. If the data are symmetrical, both the median and the mean are in the middle of the box.

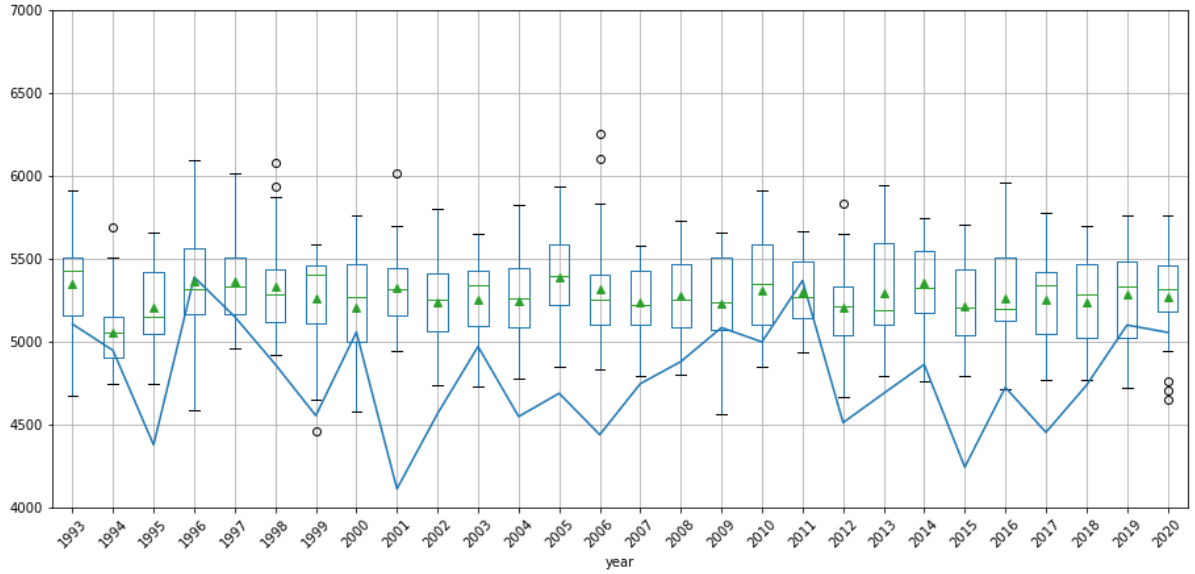

Figure 22: BAI of the ensemble members for SEAS5 (boxplot) and yearly averaged BAI for ERA5 (blue line). The integration is computed between k=4 and k=7.

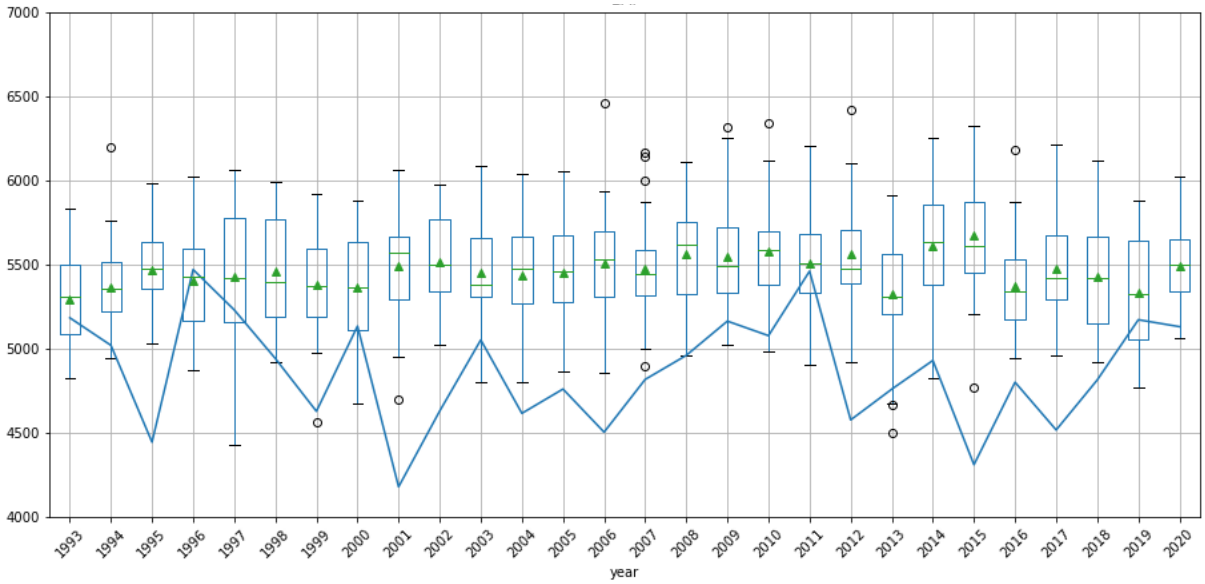

Figure 23: BAI of the ensemble members for DWD (boxplot) and yearly averaged BAI for ERA5 (blue line). The integration is computed between k=4 and k=7.

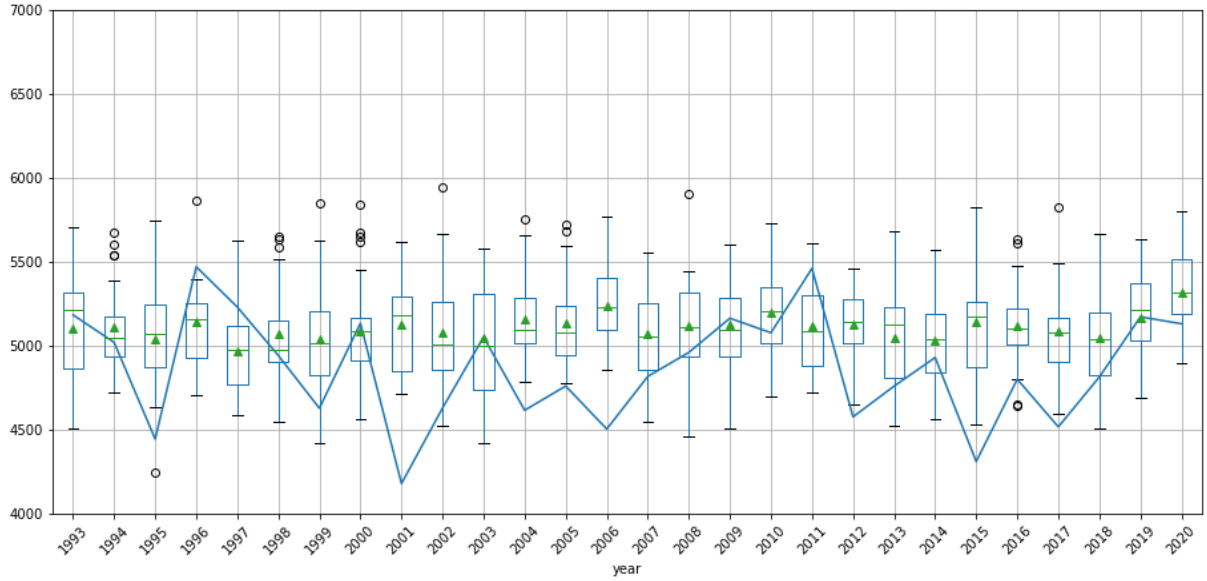

Figure 24: BAI of the ensemble members for Meteo France (boxplot) and yearly averaged BAI for ERA5 (blue line). The integration is computed between k=4 and k=7.

If we look at the boxplots, we see that the average annual BAI, calculated based on the reanalysis data and represented by the blue line, has a strong annual variability. The seasonal forecasts, on the other hand, show this variability only to a limited extent, as the signal remains relatively constant over the years. Moreover, BAI is overestimated by the seasonal forecasts, which becomes even more obvious when looking at the DWD forecast models (Figure 8). In this sense, the result of the seasonal forecasts of Meteo France is better, as there is no such overestimation. This is consistent with the graphs shown in Figure 21, where the difference between forecast and reanalysis is an alternation of peaks. But even in this case, the annual variability of BAI is not well captured.

Summary

The spectral analysis carried out showed that the winter variability in the southern hemisphere can be explained mainly by the eastward propagation component. In addition, it is shown that:

- The Hayashi technique can be considered a valid tool for identifying the waves that develop in the atmosphere because of various processes, especially baroclinic waves
- The spectral analysis carried out reveals, as expected, a series of peaks and structures that can be attributed to the phenomenology of baroclinic waves propagating towards the east
- Looking at the BAI boxplot, we see that the seasonal predictions do not always capture the annual variability, but a signal that remains constant over the years and instead becomes evident in the reanalysis
- The problems of seasonal forecasting in correctly predicting baroclinic activity may be directly related to the low skill values of precipitation predictions observed in the seasonal forecast

Therefore, this demonstrates the importance of baroclinic activity in understanding the role of rainfall and temperature variability in seasonal forecast data. FOCUS-Africa case studies can thus directly benefit from the application of this approach to better understand how seasonal forecast precipitation and temperature fields can be corrected to account for observed variability.

4.4 A show case for Malawi

Background

Lake Malawi region experiences a mild tropical climate with a monomodal austral summer rainy season October-April) and dry winter (May to September). The rainfall over Malawi is shaped by the interaction of the ITCZ, the sub-tropical high-pressure belt in the south, and the topography (Jury & Mwafulirwa, 2002). The ITCZ marks the convergence of the north-easterly monsoon and south-easterly trade winds, and during the rainy season it oscillates over the country, often connecting with troughs in the Mozambique Channel. Malawi is also affected by the northwest monsoon, which brings the recurved tropical Atlantic air that reaches Malawi through the Congo basin. This system brings well-distributed rainfall over the country (Jury & Mwafulirwa, 2002). The country is also affected by tropical cyclones from the west Indian Ocean. Depending on their position, cyclones may result in either dry or wet spells over Malawi.

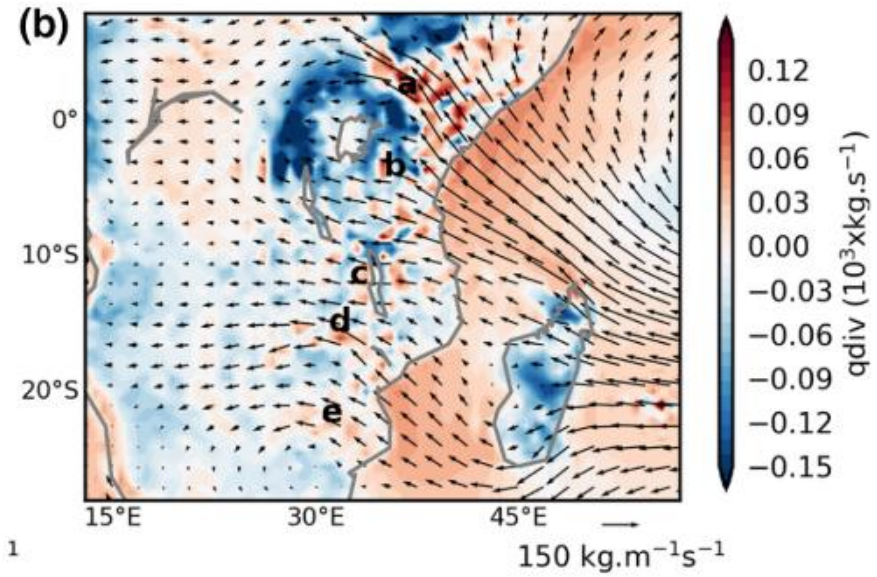

Figure 25: Integrated Vertical moisture transport in surface-700mb, mean annual flux (vectors), moisture divergence (colour map). Letters mark location of cores of Low-Level Jets (a - Turkana, b - Rufiji, c - Malawi, d - Zambezi, e- Limpopo). Figure reproduced verbatim from Munday et al. (2021).

New insights into the drivers of rainfall variability in the southern Africa region recently emerged from work focused on Low-Level Jets (LLJs), which form in the valleys punctuating the East African rift system (Figure 25). Barimalala et al. (2021) show that the LLJs transport most of the water vapor to central Africa from the Indian Ocean and those flows modulate regional sub-continental scale phenomena such as Angola Low and ridging high over south-eastern Africa and penetration of the tropical Atlantic air masses into the mainland. Munday et al. (2021) reveal that the enhanced easterly winds from the subtropical Indian Ocean led to an increase in low-level divergence in water vapor export, and consequently to drought in eastern and southern Africa, including the Lake Malawi region. Notably, they identify one of the jet "passages" to be in the vicinity of Lake Malawi.

Here we investigate the linkage between low level jets or low-level moisture fluxes in general, and rainfall variability over the Lake Malawi catchment (or upper Shire basin), towards potential implications to rainfall predictability at seasonal time scales as well as improvement of climate projections through better understanding of regional dynamics underlying rainfall delivery over Lake Malawi catchment.

Methodology and data

We use ERA5 wind and humidity (u, v, q) reanalyses data integrated over surface to 700 mb, and for maintaining consistency between moisture fluxes and rainfall, also the ERA5 rainfall. We calculate moisture fluxes over the African domain (40N-40S, 25W-55E) in all levels between 1000mb and 700mb, filtering out levels below the pressure at surface, individually for each day in the period of 1979-01-01 and 2021-12-31. We schematize the Lake Malawi catchment as a "box' spanning 33E to 35.5E, and 14.50S to 9.25S (Figure 26). In the analyses, we define two low level moisture flow regimes - westerly flow and easterly flow and schematize them as occurring on days when the net zonal flow across the western boundary of the Malawi "box", i.e. across the "window" spanning 14.50S to 9.25S along the 33E meridian is westerly and easterly respectively.

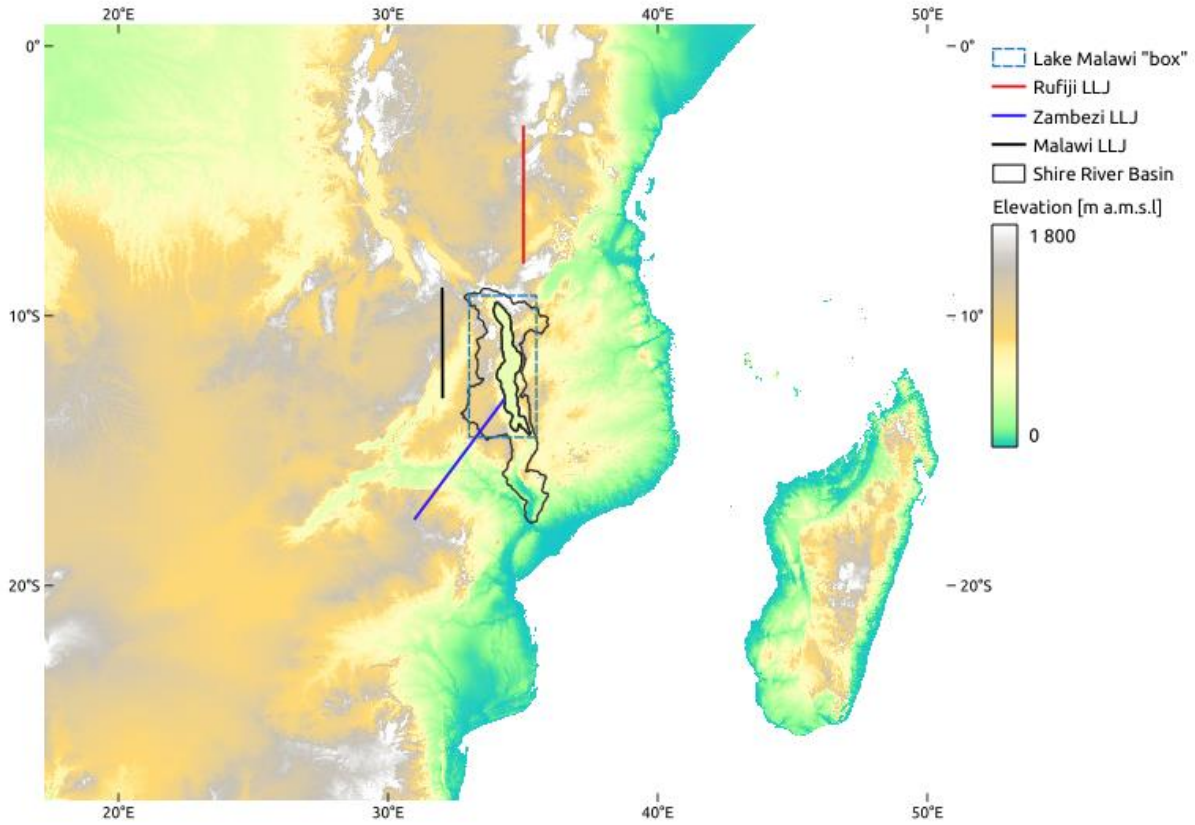

Figure 26: Location of Lake Malawi "box" and location of the three Low Level Jets identified by Munday et al. 2021.

Analysis

Mean annual low level (surface to 700mb) moisture flux in the Lake Malawi region is illustrated in Figure 27. It is dominated by south easterly flow, and while the Zambezi and Turkana Jets of Munday et al. (2021) are relatively well articulated, the Malawi one appears not to be strongly evident. The Zambezi LLJ clearly recurves the south easterly flow of moisture from over the southern Indian Ocean, south of the Madagascar into easterly to north-easterly fluxes in the interior. The flows in the vicinity of Lake Malawi are clearly easterly.

A clearer picture emerges when the mean monthly moisture fluxes are visualized (Figure 28). The Zambezi LLJ remains active throughout the year, recurving south-easterly flow into the interior of the sub-continent. In Oct-Dec period, this LLJ appears to also receive moist tropical air through transport from north-east across Lake Malawi region.

Moisture fluxes in the Lake Malawi region in the core winter period (May-Aug) are dominated by dry south-easterly flows, with an increase of moisture fluxes and an increase in easterly flows in Sep-Oct. Early rainy season (Nov-Dec) is characterized by strong moisture transport into the Lake Malawi catchment and further toward the interior from the tropical Indian Ocean by north-easterly winds. The period of Jan-Feb appears to be characterized by minimal moisture fluxes across the Lake Malawi "box". This is surprising, as these two months are in fact the wettest months of the year, and this is explored further below.

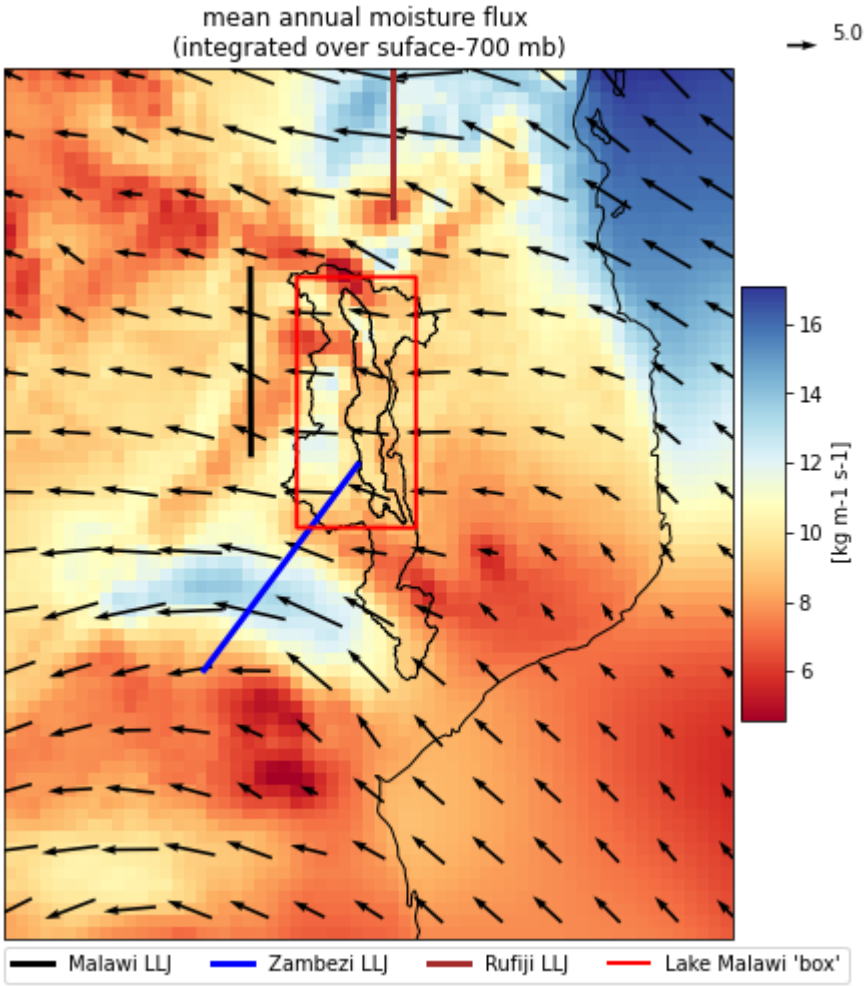

Figure 27: Mean annual low level moisture flux in Lake Malawi region. Lines mark LLJ core regions identified by Munday et al. 2021, red rectangle marks Lake Malawi "box", as in Figure 26

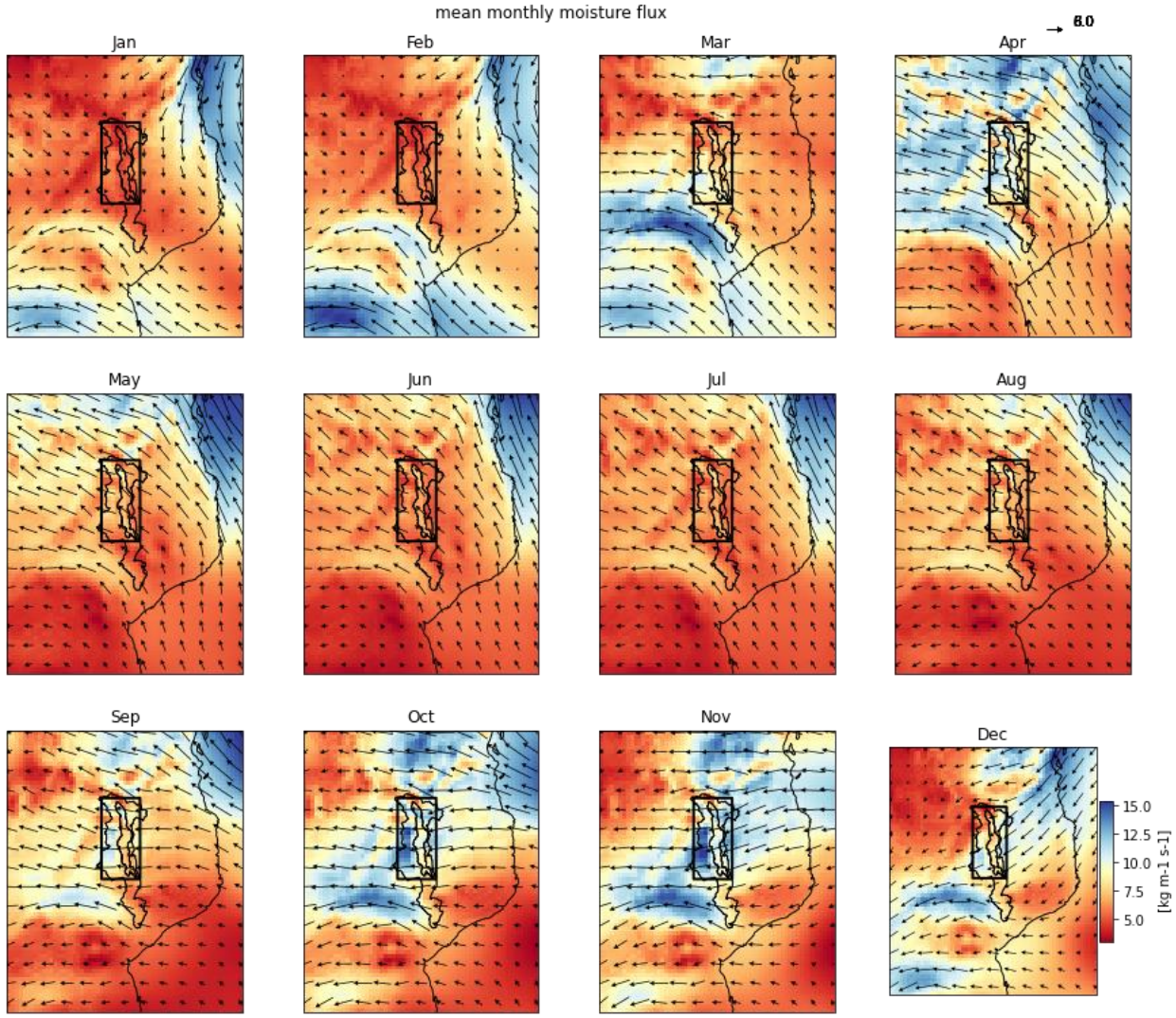

Figure 28: Mean monthly low level moisture flux in Lake Malawi region. Red rectangle marks Lake Malawi "box" as per Figure 26.

Climatology of moisture fluxes across Malawi "box" boundaries (Figure 29a) reflects a setting of "throughflow" - with zonal influx and outflux compensating each other, with similar pattern, although to a lesser extent, present in meridional fluxes. The seasonal pattern of the net flux (calculated by summing inflow and outflows across the boundaries) corresponds to the seasonal pattern or rainfall (Figure 29b), although there are relative differences between the early (Oct-Dec) and late (Jan-Apr) rainy season. There is a net moisture outflow from the Malawi region during the wintertime (May-Sep), which likely reflects the impact of evaporation from Lake Malawi on air moisture content.

The disparity between the overall magnitude of zonal moisture fluxes between Jan-Feb and other months is striking (order of magnitude difference in Figure 29a), although that difference has no impact on the net flux. This disparity is like the effect visible in monthly maps (Figure 28) and will be addressed explicitly later.

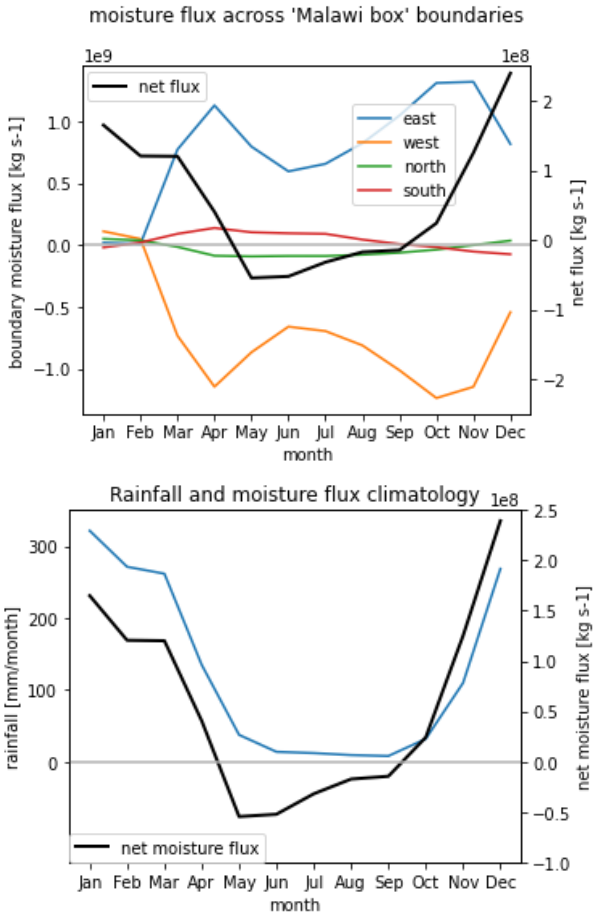

Figure 29: Low level moisture fluxes across the boundaries of the Malawi Box (a) and comparison of seasonality of net moisture flux and rainfall (b). Moisture flux taken as monthly zonal for east and west boundaries, and monthly meridional for north and south boundary. We adopted a convention where the positive value of moisture flux denotes inflow into the "box".

The correlations between boundary fluxes as well as the net box flux and rainfall calculated on a monthly basis over the period of 1979-2021 are illustrated in Figure 30 and are supported by time series plots in Figure 31, Figure 32 and Figure 33. Important effects that emerge are as follows:

- There is a negative correlation between Lake Malawi "box" rainfall in the core of the rainy season (Nov-Mar) and the magnitude of the moisture flux across the eastern boundary, implying that the stronger the LLJ, the less rain falls over the Lake Malawi catchment
- There is positive, although weaker correlations between "box" rainfall and moisture inflow across the northern and southern boundaries
- The correlations between "box" rainfall and the net low level moisture flux are high for Nov-Dec and Mar-May parts of the rainy season (0.65-0.75) but are very weak for Jan-Feb (<0.25). The correspondence of the low-level net moisture flux and rainfall in Nov-Dec (Figure 33) is particularly remarkable.

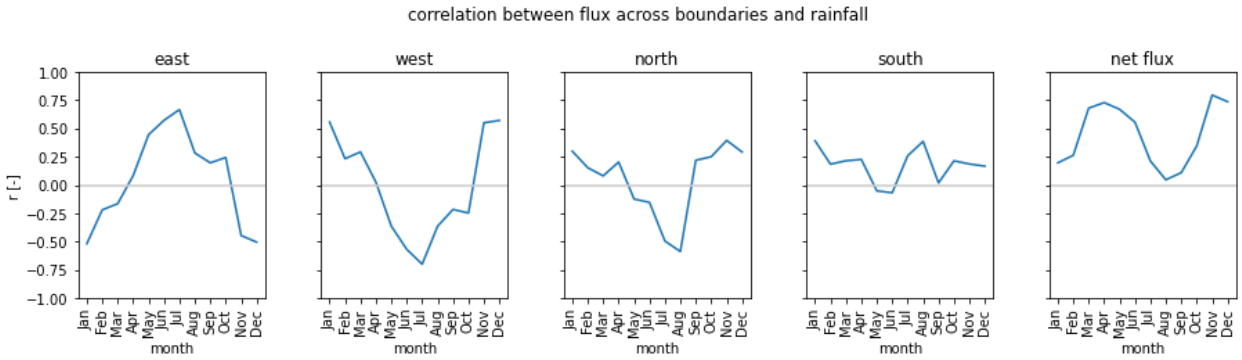

Figure 30*: Correlation between boundary monthly low-level moisture flux and rainfall in Lake Malawi region. Flux direction convention as in Fig. 5.*

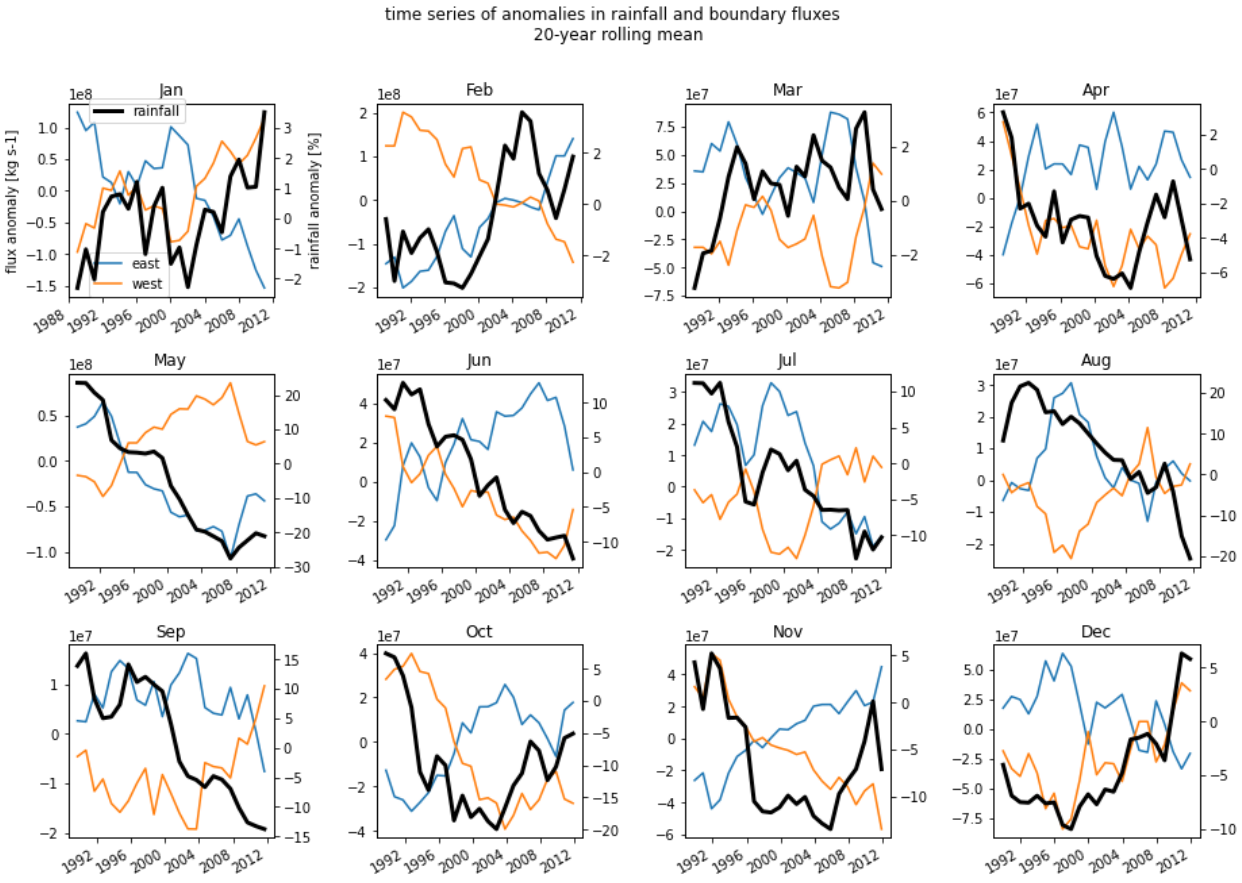

Figure 31*: Time series of monthly low level zonal moisture flux anomalies and monthly rainfall anomalies in the Lake Malawi "box". Flux direction convention as in* Figure 29*, correlations summarized in* Figure 30*.*

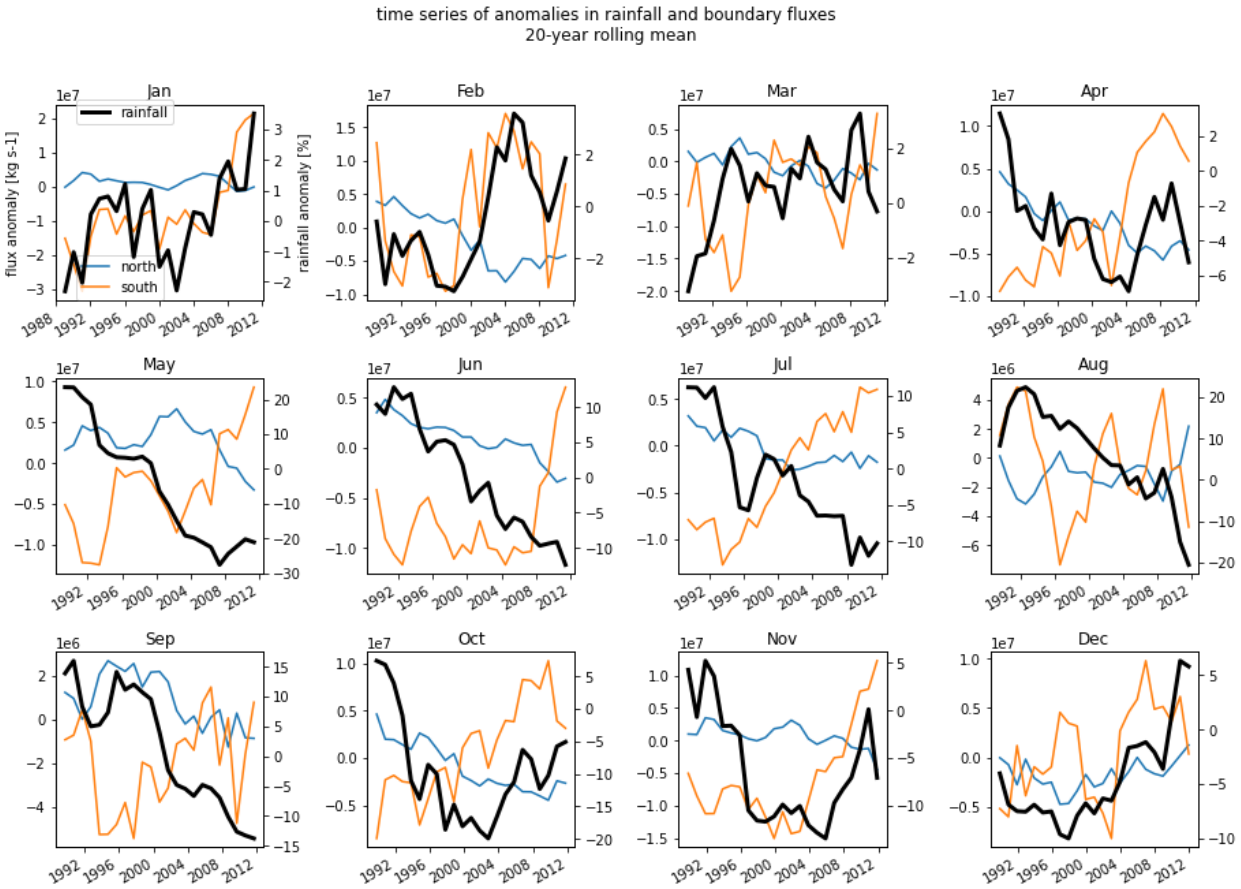

Figure 32*: Time series of monthly low level zonal moisture flux anomalies and monthly rainfall anomalies in the Lake Malawi "box". Flux direction convention as in* Figure 29*, correlations summarized in* Figure 30.

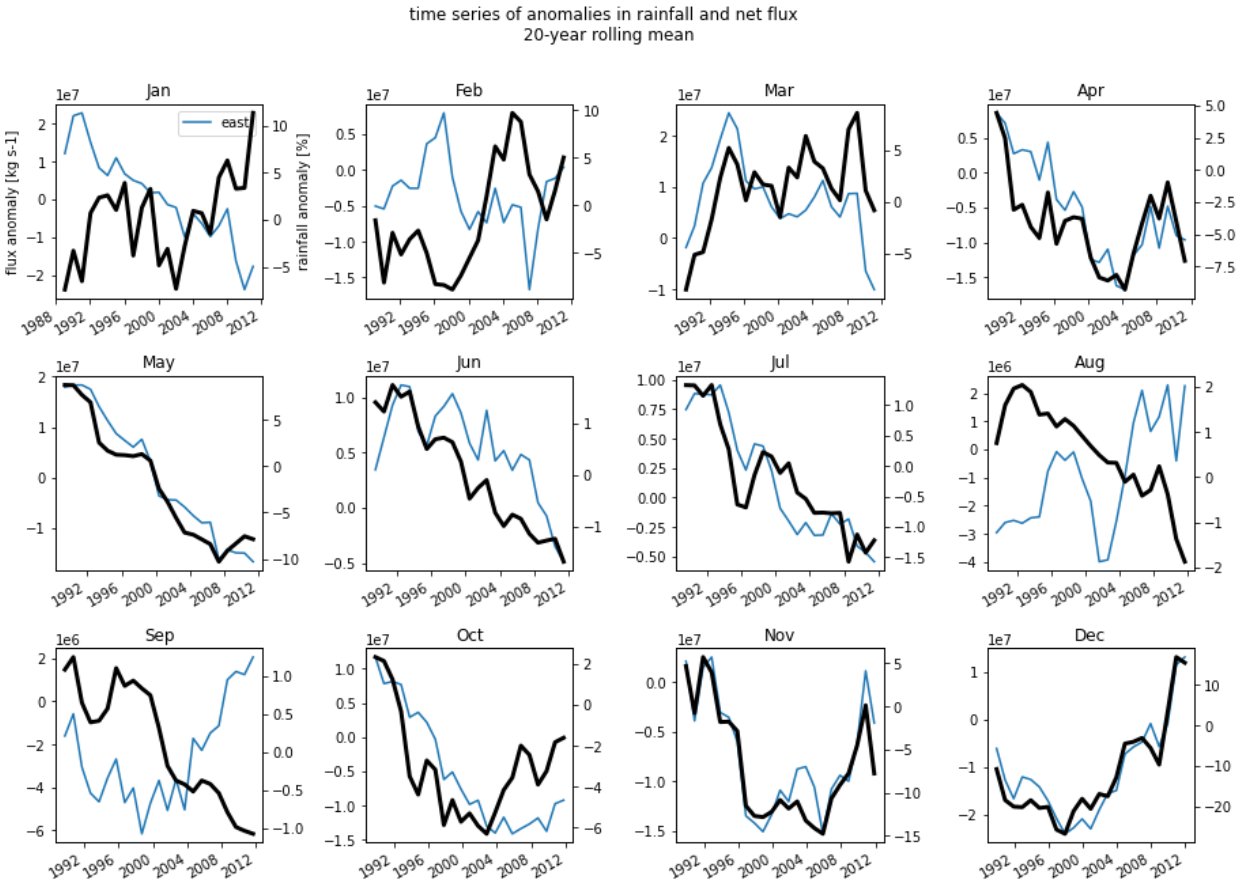

Figure 33*: Time series of net low level moisture flux anomalies and monthly rainfall anomalies in the Lake Malawi "box". Correlations summarized in* Figure 30.

To fully understand the anomalous patterns in moisture fluxes and rainfall during Jan-Feb period, manifested in Figure 28 and Figure 29 and in net flux correlation pane in Figure 30, one has to consider the following elements:

- The analyses are performed on monthly means of moisture fluxes. That is appropriate if shorter term (daily) fluxes maintain consistency in direction during the month. The monthly averaging becomes, however, inadequate if during a given month conditions occur that manifest through fluxes in opposite directions
- One of the sources of Malawi rainfall in the northwest monsoon, which brings the recurved tropical Atlantic air that reaches Malawi through the Congo basin (Jury & Mwafulirwa, 2002). That mechanism implies westerly moisture transport, and there are signatures of such in Jan-Feb maps in Figure 27. It is likely that the monthly aggregate analyses conceal moisture flow patterns underlying that mechanism.

To explore the role of north-west monsoon and westerly moisture flows from the Congo region that are likely associated with that, we disaggregate the daily moisture flux datasets into two subsets:

- Easterly flow across the Malawi domain, capturing days when integrated flux across the western boundary of the Malawi "box" is easterly
- Westerly flow across Malawi domain, capturing days when integrated flux across the western boundary of the Malawi "box" is westerly.

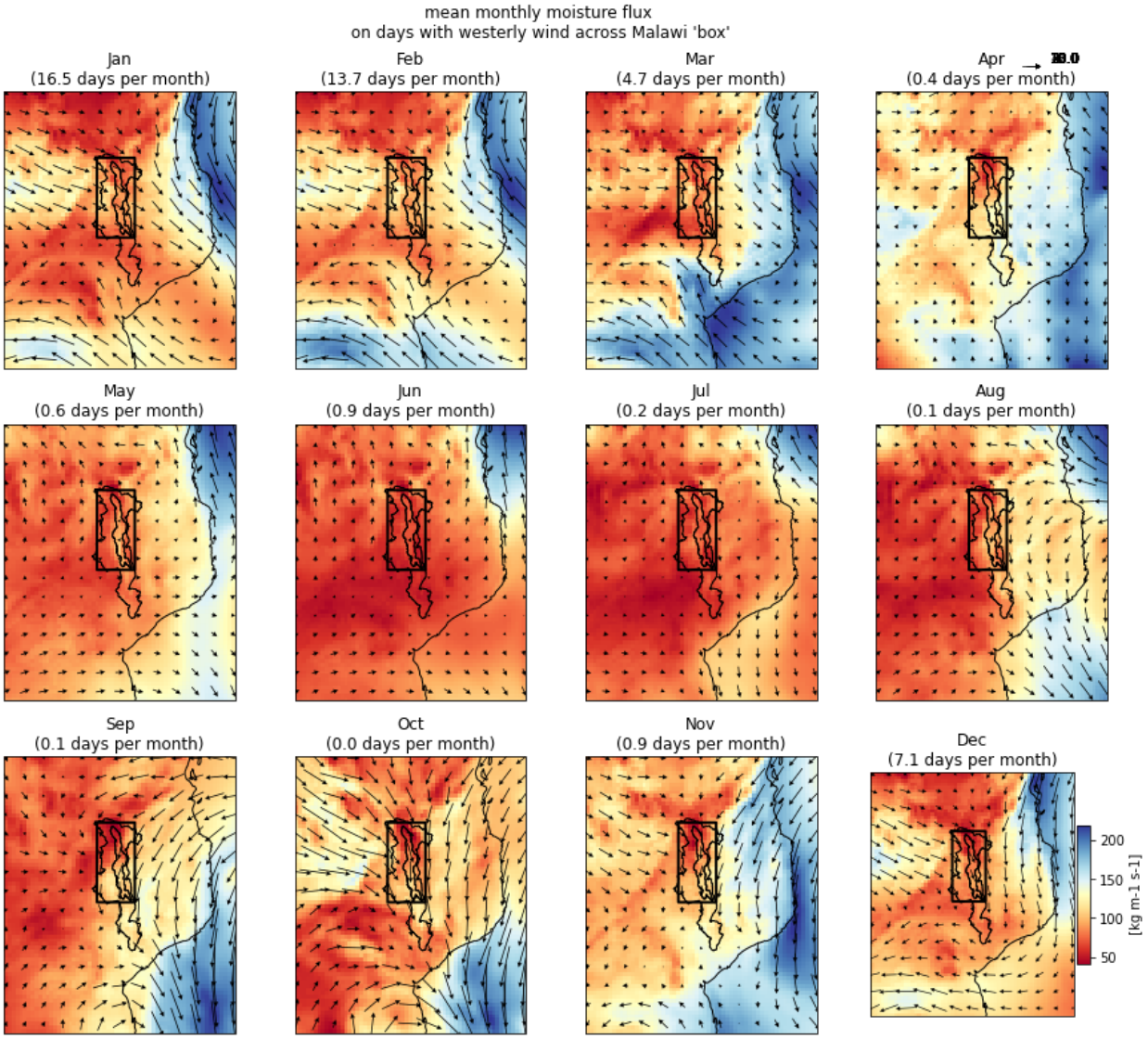

Figure 34: Mean monthly low level moisture flux in Lake Malawi region on days with westerly flow. Red rectangle marks Lake Malawi "box" as per Figure 26.

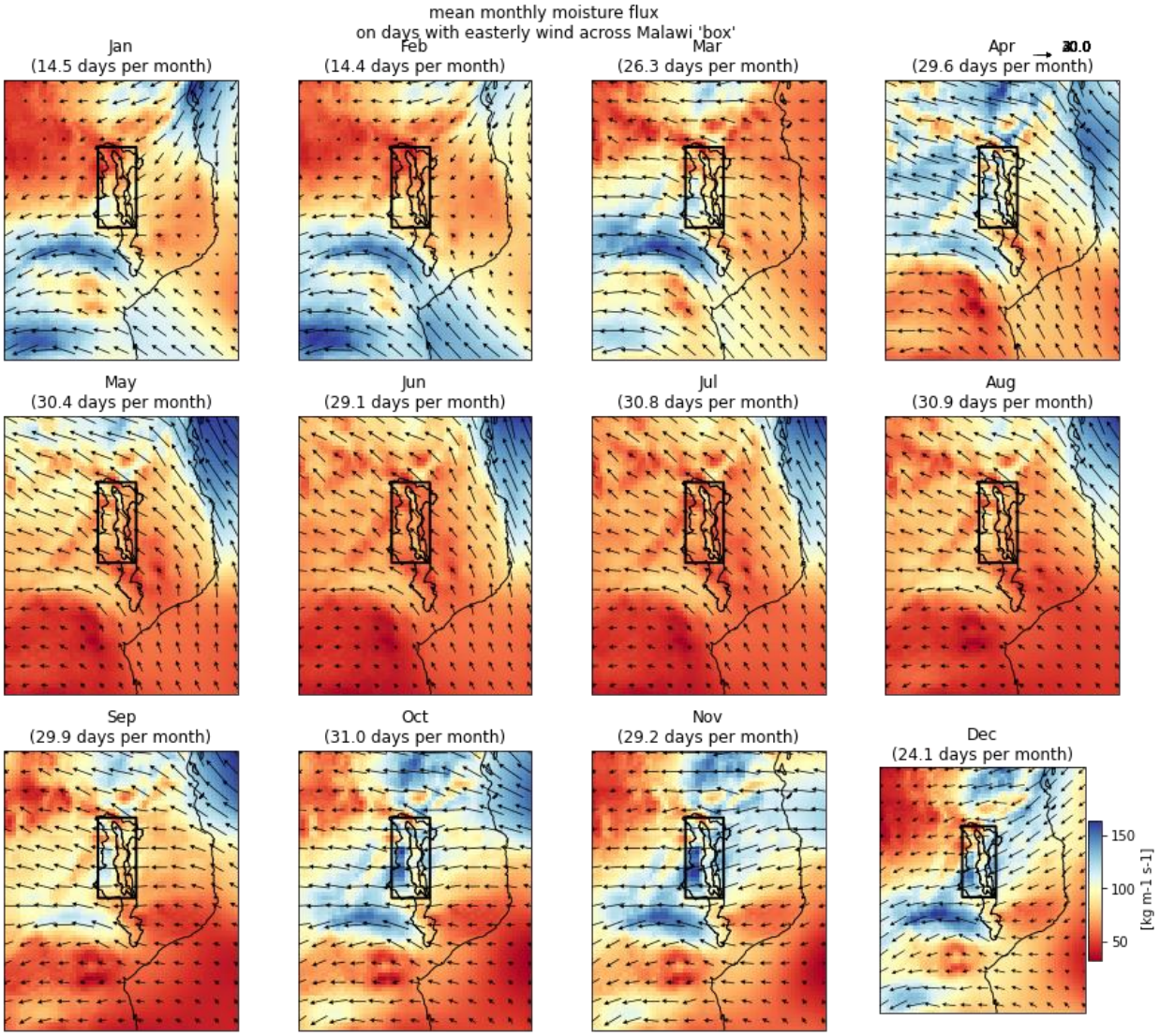

Figure 35: Mean monthly low level moisture flux in Lake Malawi region on days with easterly flow. Red rectangle marks Lake Malawi "box" as per Figure 26.

Figure 34 and Figure 35 illustrate monthly aggregate low level moisture fluxes for days with westerly and easterly flow respectively. Days with westerly flow occur 13-16 days per month in Jan and Feb, 5-7 days per month in March and Dec, and less than one day a month in other months. The westerly moisture flux from the interior of the continent into the Lake Malawi domain is very clear in the Dec-Mar, and perhaps in November, but in other months it seems to be an artifact of windless, stable conditions across the large part of the continent. Comparison of Lake Malawi "box" rainfall associated with the easterly and westerly flow (Figure 36, Figure 37, Figure 38) reveals the following:

- Region-average daily rainfall when brought by the westerly flow is larger than that brought by the easterly flow (~10mm/day vs. ~5mm/day). Highest widespread rainfall events (more than 30mm across the entire domain) is associated with the westerly flow
- Overall, approx. 33% of rainfall over the Malawi domain is delivered during the westerly flow events
- There is an indirect relationship between the amount of rainfall delivered during days with the easterly and westerly flow, and a direct relationship between total annual rainfall delivered during such days and number of such days in a year. This suggests "competing" dynamical drivers of the two sources of moisture

- On the monthly time scale, Jan-Feb rainfall during days with westerly moisture flux exceeds that from days with westerly fluxes, but Dec and March, the proportion of rainfall delivered under the westerly flow regime is lower, about 30% of total, and during the remaining months of the year - it is insignificant.

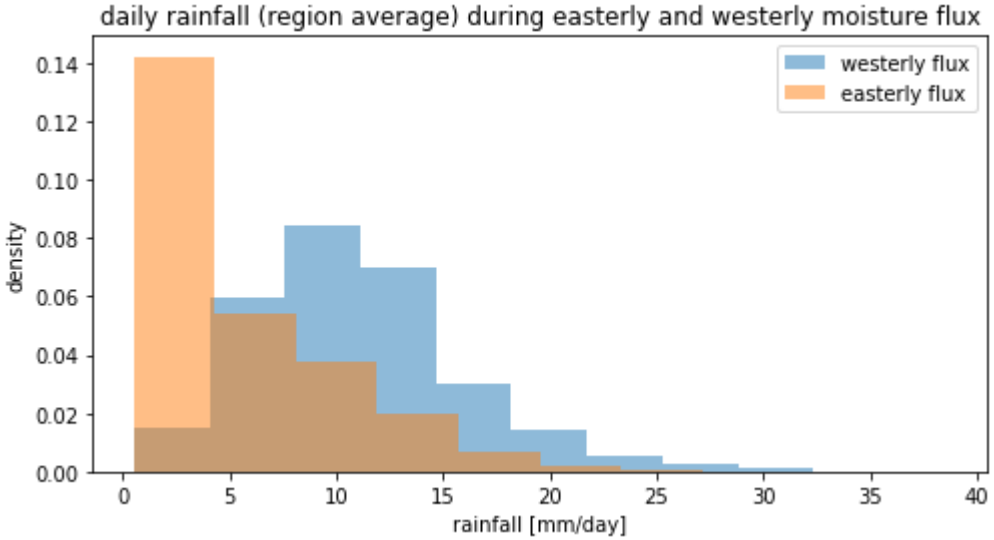

Figure 36: Histogram of region-average rainfall on days with easterly and westerly low level moisture flow.

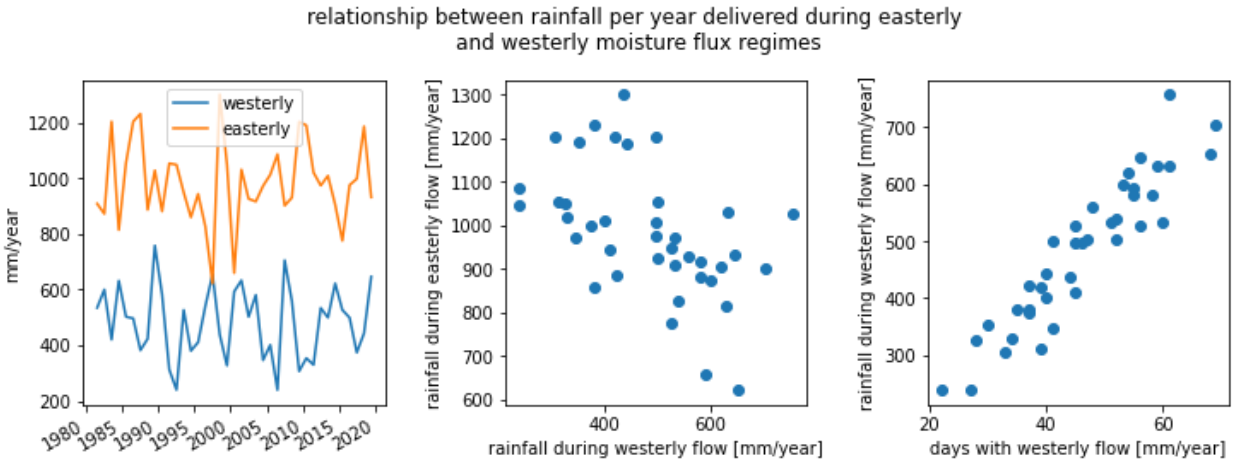

Figure 37: Contribution of rainfall under easterly and westerly flow regimes to total annual rainfall.

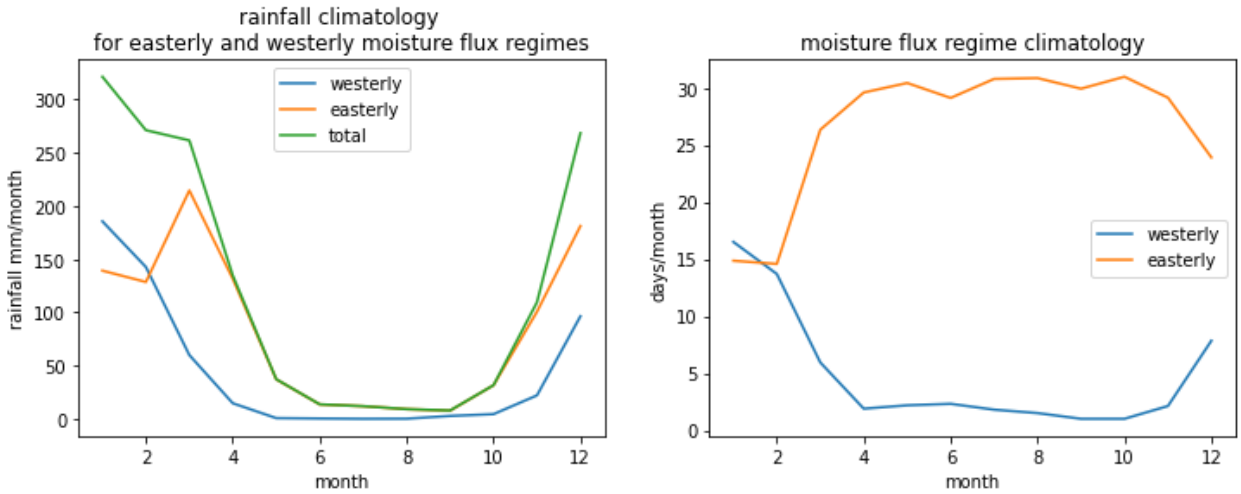

Figure 38*:* Contribution of rainfall under easterly and westerly flow regimes to total monthly rainfall.

Summary

The analyses indicate that low level moisture transport plays an important role in rainfall over the Lake Malawi catchment, and its dynamics are linked to seasonal and interannual rainfall variability. The strength of the Malawi Low Level Jet is, however, inversely proportional to rainfall over the Lake Malawi catchment during the core of the rainy season (Nov-Mar), i.e. stronger LLJ is associated with negative rainfall anomalies, but the relationship is inverse during the rest of the year, i.e. during shoulder season rains, and during winter. Rainfall during the shoulder rainy seasons (Nov-Dec and Feb-Apr) is clearly associated with net low level moisture flux over the Lake Malawi domain. The relationships between rainfall and LLJ flux are obscured in analyses of monthly aggregates, particularly during the Jan-Feb, due to competing influences of two air masses - easterly flow mostly from tropical Indian Ocean, and westerly flow from interior of the continent originating from tropical Atlantic. When disaggregated by the zonal moisture transport direction over the Lake Malawi domain, rainfall associated with the westerly flow contributes ~30% or total annual rainfall, over 50% or Dec and Jan rainfall and ~20-25% to November and March rainfall. Importantly, rainfall associated with westerly moisture flow appears to have a larger regional average than that associated with the easterly flow.

These relationships clearly indicate the importance of the dynamics of the low-level moisture fluxes, and, of the interactions between conditions facilitating westerly and easterly moisture flux, on the rainfall dynamics over the Lake Malawi catchment.

5 Analysis of large-scale climate processes across SADC

Large scale changes are predicted by using weather and climate models more skilfully than local extremes, so understanding the link between the two is crucial to understanding and characterizing the impacts of extremes such as drought. Understanding climatic situations where concurrent and recurrent extremes events are more likely to happen represents one important facet of disaster risk management. By understanding the teleconnections and their associated hazards, it becomes possible to develop risk management methods optimizing productivity in the energy, agriculture and other sectors of economy and society. El Niño–Southern Oscillation (ENSO), the Indian Ocean and the South West Indian Ocean Dipole (IOD, SIOD) modes and the Southern Annular Mode (SAM) are here considered. In the past, the long-range forecasts of the Southern Africa precipitation had been a challenge for climate modelling. Although its skill is still far from satisfactory, recent progress of climate modelling is making it possible to produce useful predictions up to several months ahead particularly when teleconnections are active. Better understanding of dominant variability modes and

processes enables us to understand the predictable variability of precipitation over the region. This requires the investigation of teleconnections and predictability at seasonal and decadal scales useful for the regional case studies i.e. rainfall timing, onset and extent, and accumulated amount as well as wind power. Therefore, we investigate some of the main observed ENSO, IOD, SIOD, SAM teleconnections and their link with different variability and extremes of weather in southern Africa. Rainfall deficit, extreme precipitation events, heatwaves, occurring in critical phenological phases, can considerably reduce crop yields, even if annual and seasonal mean climate conditions are at or near normal.

5.1 El Niño Teleconnection characterisation

Background

We investigate here the prospects of improving seasonal predictions of Essential Climate Variables (ECVs: precipitation, mean, maximum and minimum temperature) in SADC by means of the characterization of teleconnection links with large scale patterns like El Niño Southern Oscillation (ENSO). Originally, the planning involved the study of the North Atlantic Oscillation (NAO) and Niño3.4, but authors such as Lüdecke et al. (2021) showed the influence of the NAO is constrained to northern Africa. Consequently, in this work, NAO has been replaced by another index, the Atlantic Niño (ATL3), which has shown some potential in the tropical African countries (Foltz et al., 2019). As for ENSO, a negative (positive) correlation with the austral summer (winter) precipitation in Southern Africa has been already reported (Philippon et al., 2012, Funk et al., 2018). The following sections include a selection of results for precipitation and mean temperature to illustrate their relevance for the SADC area. Nevertheless, the analysis has been conducted for all the seasons and ECVs and, thus, the results are fully available to all the project partners.

Methodology and data

The reference dataset used in this study is the monthly ERA5 reanalysis from 1981 to 2016 (Hersbach et al., 2018). The selected variables include Sea Surface Temperature (SST) for computing the teleconnection indices; and four ECVs (i.e., precipitation, mean, maximum and minimum temperatures). The seasonal forecast used as a predictability benchmark is the ECMWF System 5 data set (SEAS5, Johnson et al., 2019). The same variables were downloaded from the Copernicus Data Store (CDS) for the same period. The domains of the two teleconnection indices are: 5ºN - 5ºS, 170ºW - 120ºW, for the Niño3.4 (Trenberth, 1997; Trenberth and Stepaniak, 2001); and 3ºN - 3ºS, 20ºW - 0ºW, for the ATL3 (Hounsou-Gbo et al., 2020). These regions are depicted in Figure 39.

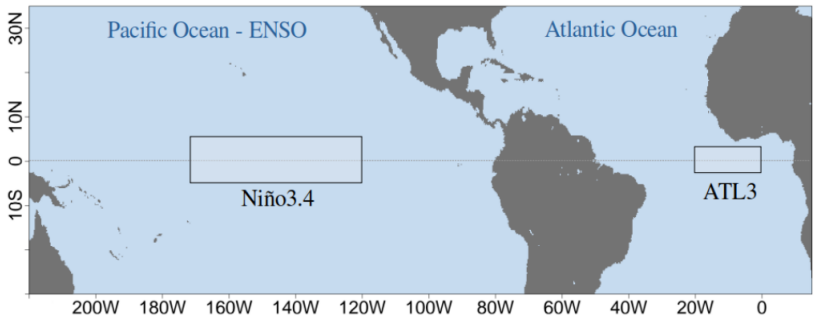

Figure 39: The locations of the teleconnection indices: Niño3.4 (5ºN - 5ºS, 170ºW - 120ºW) and ATL3 (3ºN - 3ºS, 20ºW - 0ºW).

The first step has been to compute the time series for the teleconnection indices (i.e., Niño3.4 and ATL3) from the ERA5 monthly SST data covering the period 1981-2016. This computation has been

carried out in two ways: for every single month and for three-month aggregations. After that, the link between these indices and the corresponding ECVs (also from ERA5) has been assessed up to one year into the past. By relating the ECVs' anomalies for each month (three-month season) with the teleconnection anomalies from the same paired month (three-month season) and, subsequently, with the teleconnection anomalies from the preceding months up to twelve months (three-month seasons) into the past. This association process has been performed by computing the Pearson correlation coefficient for each grid point over the SADC region.

The second step set up a linear regression model for each grid-point, time-lag, and teleconnection index, by using Niño3.4 and ATL3 as predictors for the calculation of the ECVs (in a leave-one-out approach). Turning to the SEAS5, the intrinsic biases have been reduced by applying a variance inflation bias correction (von Storch and Zwiers, 2001; Doblas-Reyes et al., 2005). To understand whether the linear regression approach could outperform the bias corrected SEAS5 seasonal predictions, the Pearson (ensemble-mean) correlation coefficient and the fair Ranked Probability Skill Score (FRPSS, Fricker et al., 2013; Ferro, 2014) have been applied to obtain their respective deterministic and probabilistic skills.

Niño3.4 teleconnection with ECVs

Figure 40 (Figure 41) shows the correlation of DJF precipitation (temperature) with the Niño3.4 index from 12 lagged months over the SADC region for the 1981-2016 period. Overall, precipitation manifests a mixture of positive and negative correlations while a positive correlation is predominant for temperature. Turning to the other seasons, precipitation in DJF and SON generally demonstrates a stronger signal than in MAM and JJA (Philippon et al., 2012; Funk et al., 2018), whereas DJF and MAM seasons attain higher correlation values for temperature. In terms of the seasonal temperature maximum and minimum, their features are basically consistent with the mean temperature as shown in Figure 41: MAM with the strongest signal remains and it is followed by DJF.

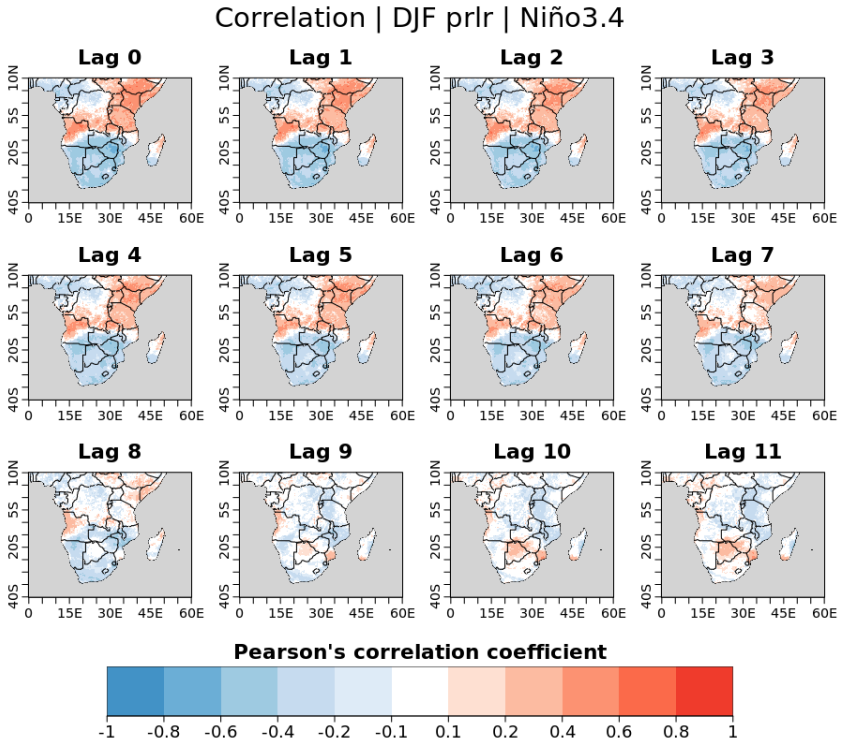

Figure 40: Pearson correlation between DJF precipitation and the Niño3.4 index over the SADC region for the 1981-2016 period. The 12 maps represent 12 lag months (from zero to eleven) between December and the first month of the used Niño3.4. For example, "Lag 0" means DJF precipitation and DJF Niño3.4; "Lag 1" represents DJF precipitation and NDJ Niño3.4 and the last "Lag 11" refers to DJF precipitation

and JFM Niño3.4. Correlations between ±0.1 are shaded white for better visualisation of those above (below) 0.1 (-0.1).

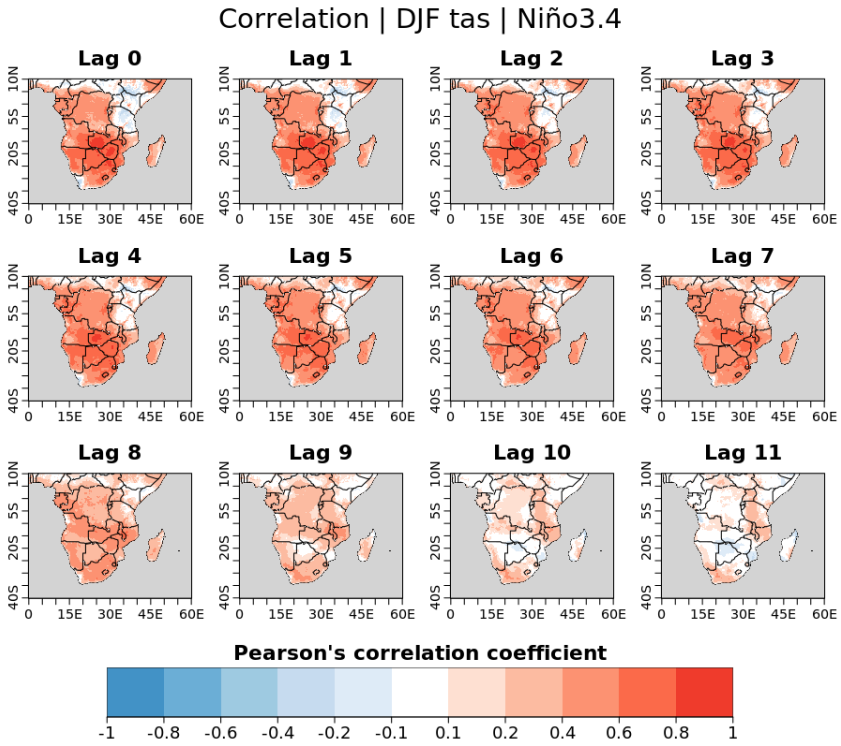

Figure 41: Same as Figure 40 but for DJF mean temperature

As for the spatial patterns of correlation for precipitation, when looking at the lag-zero maps, negative (positive) correlations are seen over the regions south (north) to 15ºS (especially in DJF and SON). JJA, on the other hand, displays an opposite behaviour. Regarding mean temperature, a widespread positive relationship can be found across the SADC region in all four seasons. The spatial distributions of temperature maximum and minimum are analogous to the mean temperature except for the north-eastern SADC region where the temperature maximum shows a negative correlation. Figure 40 and Figure 41 also show the effects of lag progression. For instance, the correlation for DJF precipitation progressively decreases with the lag month. Moreover, a switch of the direction of correlation (e.g., from positive to negative) seems to appear at 4- or 5- lag months in the JJA and SON seasons while the relationship remains more stable in DJF (and MAM). It is worth noting that a strong (and positive) correlation can be found across the SADC region for DJF (up to the lag-8 month) and MAM (throughout the 12 lag months) mean temperature maps.

ATL3 teleconnection with ECVs

Figure 42 and Figure 43 introduce precipitation and mean temperature links with the ATL3 index in DJF. Generally, the relationship with ATL3 is weaker than with Niño3.4. However, the stronger signals remain in the same seasons as Niño3.4: DJF and SON for precipitation and DJF and MAM for mean temperature.

When looking at the lag-0 month, the four seasons show totally different spatial patterns. For instance, DJF precipitation shows a positive relationship with ATL3 across almost the entire domain while in SON, negative correlations are more widespread (although the positive relationship can be seen along the western coast of 0-25ºS). As for temperature (of lag-0 month too), a widespread positive

correlation is seen in DJF (and SON) while a weak-to-negative relationship for MAM and JJA. Again, the temperature maximum and minimum are basically like the mean temperature (not shown here).

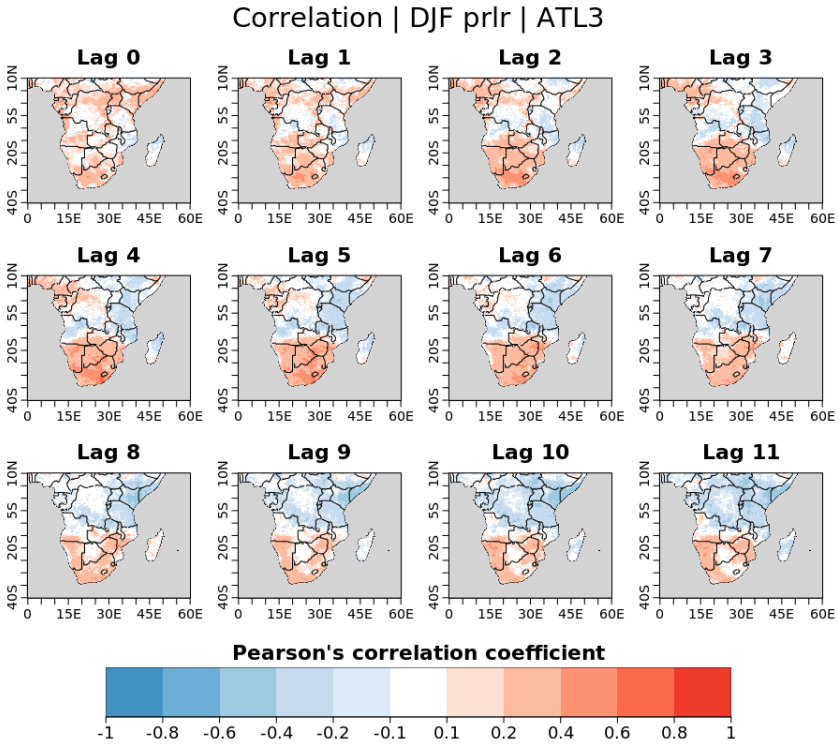

Figure 42: Same as Figure 40 but for the correlation with the ATL3 index.

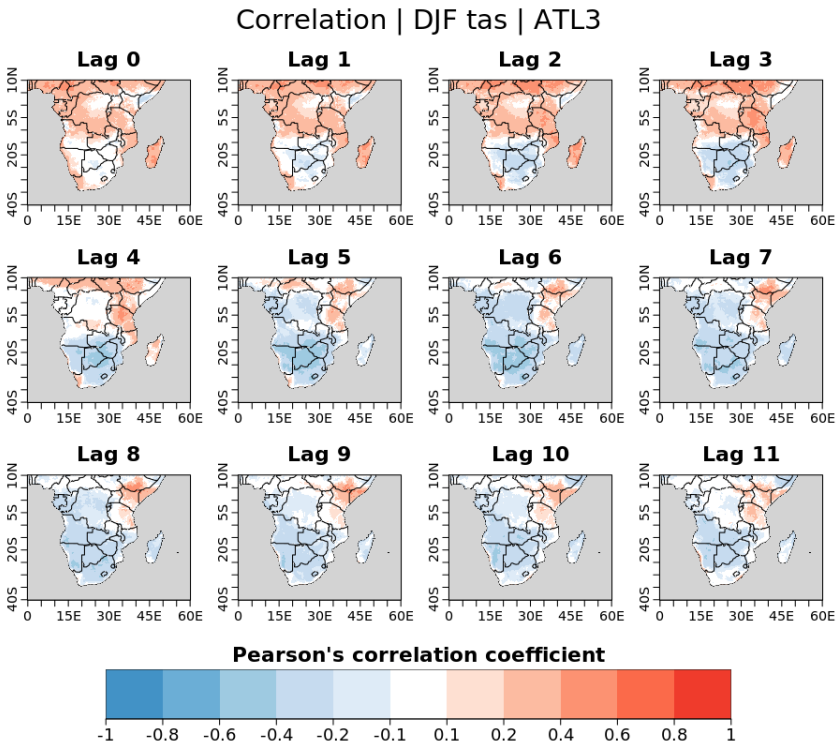

Figure 43: Same as Figure 41 but for the correlation with the ATL3 index.

Regarding the influence of the lagged ATL3 anomalies on the spatial pattern of correlation, DJF precipitation shows that the positive correlation in the region north to 15ºS progressively changes to negative while the southern areas remain positive. Negative (positive) correlations are seen in the northern areas in MAM and SON (JJA) although these relationships tend to weaken with lag month. On the other hand, for temperature, there is a switch of correlation over the northern half region in DJF (in MAM and SON too but only over the north-eastern area in JJA), changing from positive values to a weak-or-negative signal. Lastly, the temperature maximum and minimum are overall analogous to the mean temperature.

Predictability enhancement

The enhancement of seasonal predictability using linear regression models based on teleconnection indices comes from the hypothesis that, sometimes, these large circulation connections are poorly modelled by seasonal prediction systems over some areas (Lledó et al., 2020 and 2022). Hence, to better assess the amount of regional improvement we could get through this statistical approach, the numbers of grid points with an increase in the skill metrics have been calculated for each season/month and for each index (only over the land area within the SADC region). Here, the word 'improvement' means positive changes of correlations (or FRPSS) from bias corrected SEAS5 predictions to index-derived predictions which, simultaneously, must also have to be above zero. Hereafter, the improvement of correlation and FRPSS for seasonal precipitation and mean temperature are shown and discussed as examples. Moreover, the spatial pattern of the improvement is depicted with one season (DJF). Regarding the monthly ECVs, the percentages of the grid point with increased values of both skill metrics across all the months were, on average: below 10% (5%) for correlation of precipitation (the three types of temperature); and below 3% for FRPSS in all ECVs.

Precipitation : Figure 44 (Figure 45) shows the proportion of grid points with higher correlation (FRPSS) for the index-derived seasonal precipitation. Each column represents one of the 12 seasons from DJF to JFM and the indices are row-wise.

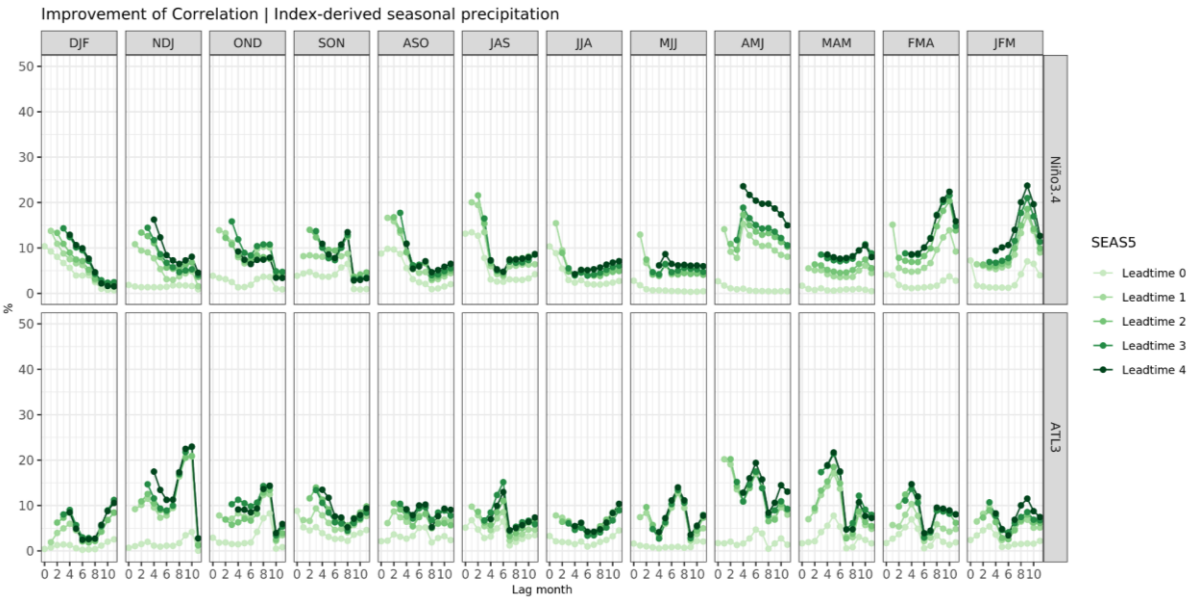

Figure 44: Percentage of the grid points in the land areas of the SADC region (y-axis) with increased correlation coefficients of the index-derived seasonal precipitation when compared to the bias corrected SEAS5 predictions of lead time up to four months (see the legend). The x-axis ranges from zero to eleven representing the lag months between the target season of ECV (see the column title) and the initialization month of the used index (see the row title on the right, top for Niño3.4 and bottom for ATL3). Each panel is composed of five curves depicting the SEAS5 lead times zero to four months (light to dark green). To

fairly compare the index-derived estimates with the SEAS5 predictions, each lead time of the latter was compared with the lag months of the former up to the same initialization date. For instance, the SEAS5 DJF precipitation prediction of lead time four was initialized in August, so the first four points of the lag months (zero to three) were removed because their initialization months, from December to September, came after August. This removal was applied to all the lead times (except for zero).

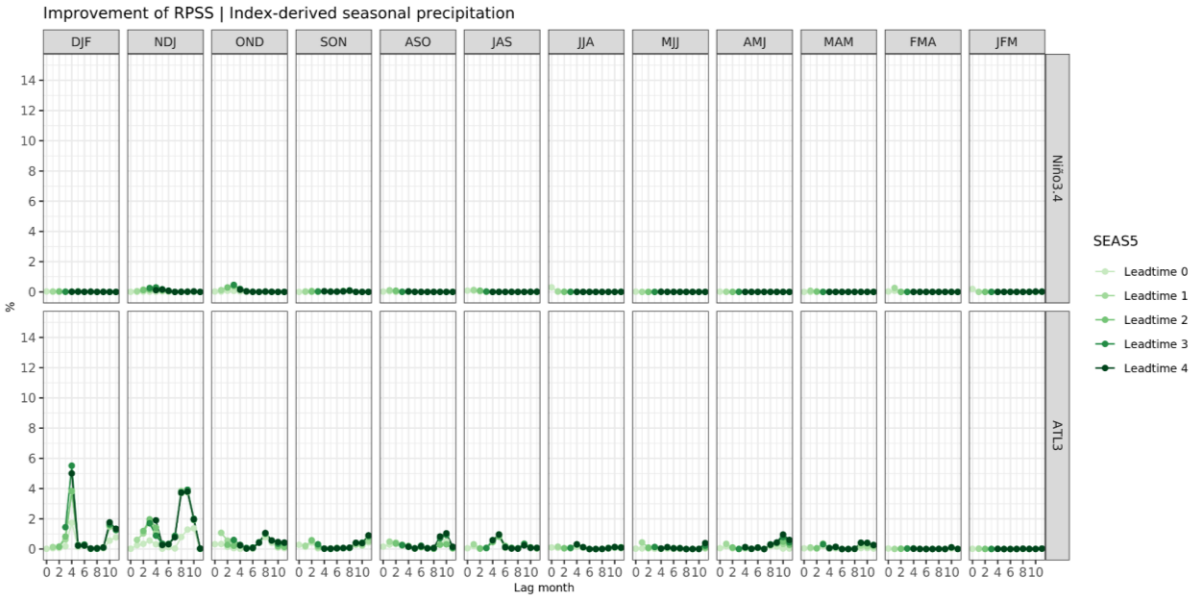

Figure 45: Same as Figure 44 but for FRPSS

The correlation of the seasonal precipitation prediction derived from the teleconnection indices has been higher than that of SEAS5 prediction in up to 25% of the entire domain. Since the forecasting skill of the SEAS5 prediction is decreased with lead time, it is expected to see the highest improvement when compared to lead time four SEAS5 predictions (i.e., the darkest green curve). In terms of the seasons with better improvement for each index (when compared to lead time 4), Niño3.4 could attain values up to 20-25% in AMJ, FMA and JFM whereas ATL3 enhancement ranged the same proportion but in NDJ, AMJ and MAM. As for the variability of improvement with the lag time of the index, Niño3.4 peaked in the earlier lag months in most seasons (except for MAM, FMA and JFM). For ATL3, on the other hand, this behaviour has been a little different, because not all the months tend to peak in the earlier lags. Regarding the comparison between the indices, Niño3.4 had more grid points with improved correlation than ATL3 in all seasons except for NDJ and MAM.

In terms of FRPSS as shown in Figure 45, only up to 5% of the grid points were improved by ATL3 (only in DJF and NDJ) while there was almost no addition for Niño3.4. Besides, the lag months with the biggest enhancement for ATL3 were also different depending on the season (lag four for DJF and lag nine for NDJ).

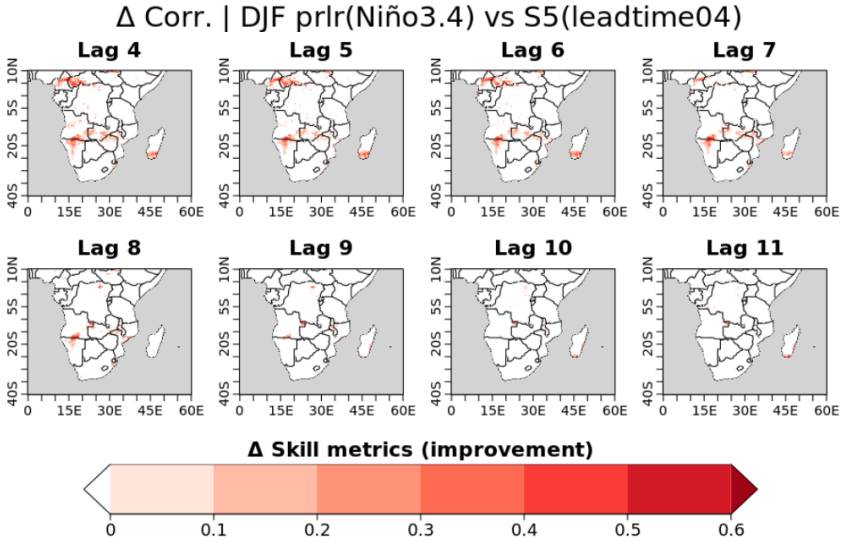

Figure 46: Spatial distribution of the increases in correlation for DJF precipitation estimates derived from the Niño3.4 index of 8 lag months (from four to eleven, see the subtitles) when compared with SEAS5 lead time four prediction. The first three lag months are removed because the initialization date of the used Niño3.4 (from December to September) is later than the initialization date of SEAS5 lead time four prediction (August).

To showcase an example of the spatial distribution of this improvement, DJF precipitation is selected for illustrative purposes. Actually, Figure 46 shows a marked increase in correlation over the north-western areas, a band between 15-20ºS and, also, in southern Madagascar. Although those improvements decrease with the lag month, they can still be found when a Niño3.4 index of 8 months ahead is used as a predictor. The improvement basically comes from locations where the SEAS5 prediction skills are low and the coupling with the index remains sufficiently strong.

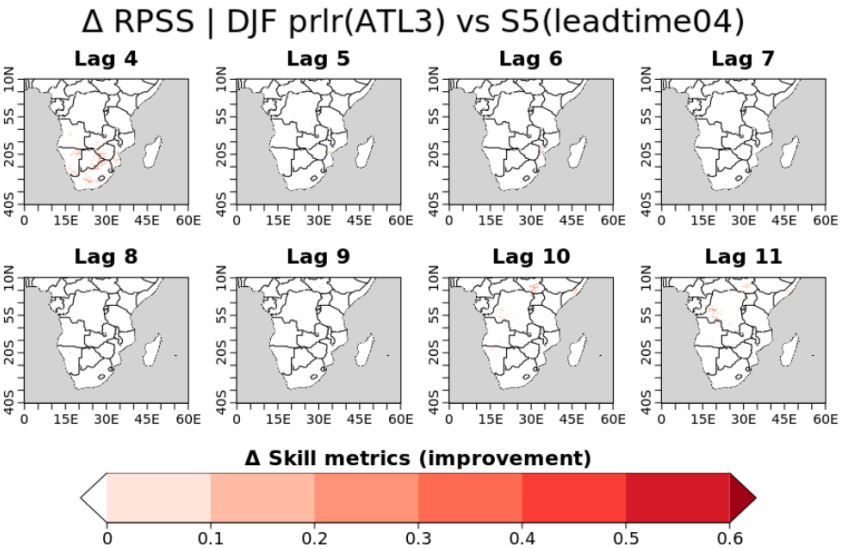

Figure 47: Spatial distribution of the increases in FRPSS for DJF precipitation estimates derived from the ATL3 index of eight lag months (from four to eleven, see the subtitles) when compared with SEAS5 lead time four prediction. The first three lag months are removed because the initialization date of the used ATL3 (from December to September) comes later than the initialization date of the lead time four SEAS5 prediction (August).

As for the FRPSS, higher values could only be found in lag month four in the southern areas of the continent. Afterwards, there was no enhancement in FRPSS until the lag months ten and eleven in which very limited improvement could be seen in South Sudan and the western Democratic Republic

of the Congo, respectively. When looking at the skills of SEAS5 prediction and the ATL3-derived estimate, the latter explains what is shown in Figure 47: the improvement only exists at lag month four due to the lack of teleconnection linkage from lag month five onwards.

Temperature : Figure 48 and Figure 49 show the improvement of correlation and FRPSS for seasonal mean temperature. Overall, the increases in correlation (FRPSS) for temperature are somewhat lower (higher) than precipitation. Furthermore, Niño3.4 tends to have more influence on the temperature than ATL3 because of very limited improvement in both skill metrics seen for the latter in most seasons. Moreover, the discrepancies of the improvement among the five lead times are much smaller than that of precipitation partially due to the relatively higher skills of the SEAS5 temperature predictions. For Niño3.4, the highest three seasons with improved correlation and FRPSS are FMA, MAM and DJF. 25-30% of the grid points with higher correlation could be found in MAM and FMA, and even 14% showed an improved FRPSS in FMA.

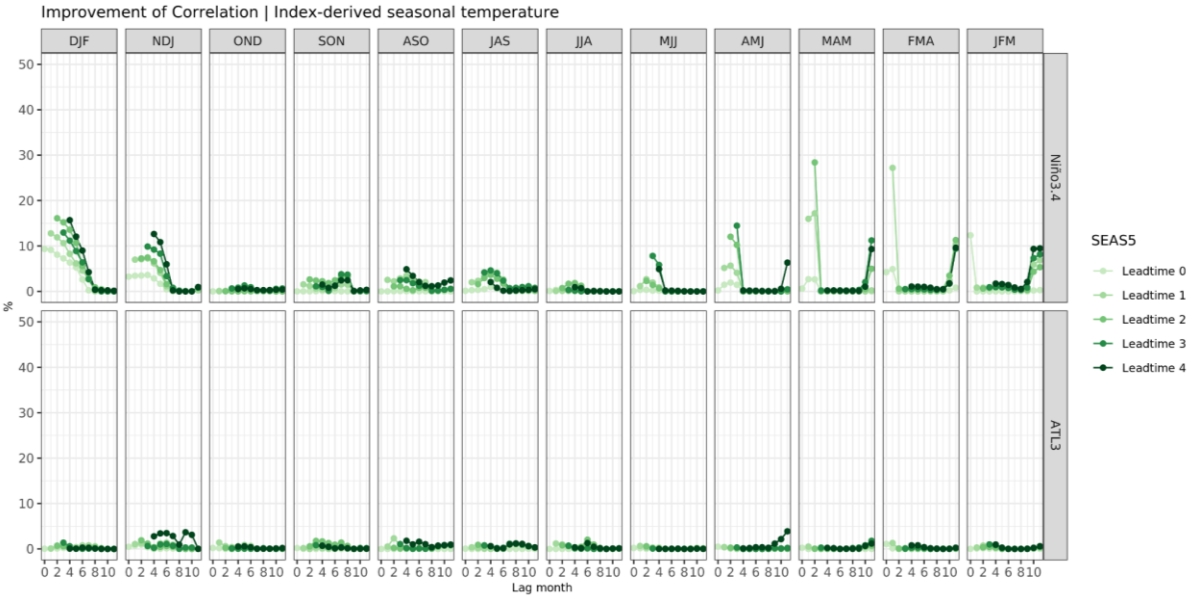

Figure 48: Same as Figure 44 but for seasonal mean temperature

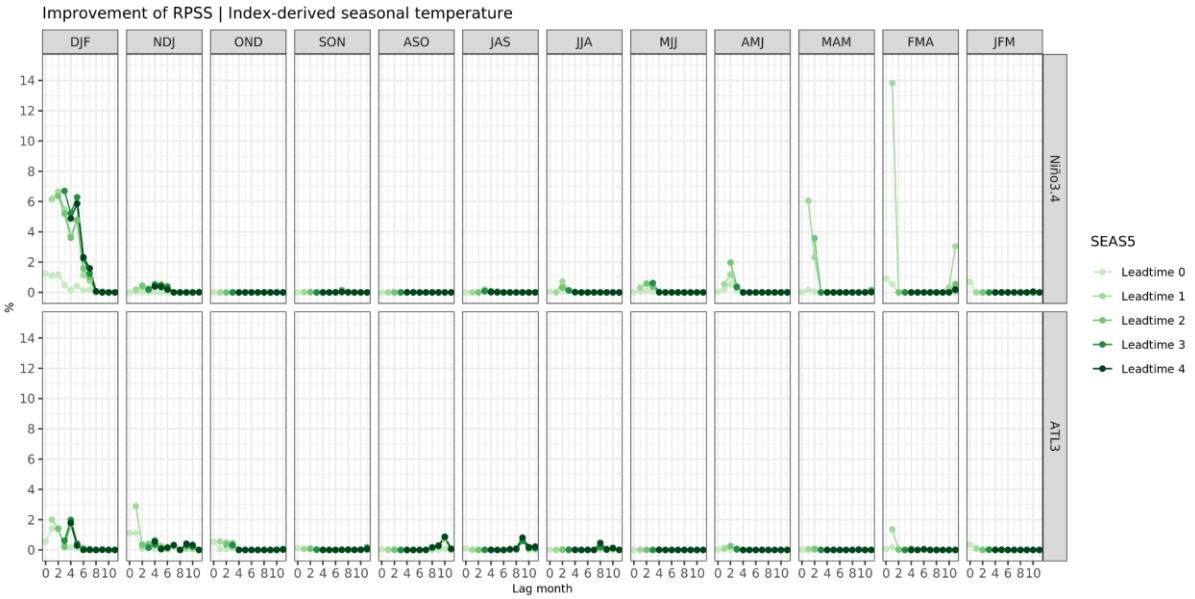

Figure 49: Same as Figure 45 but for FRPSS

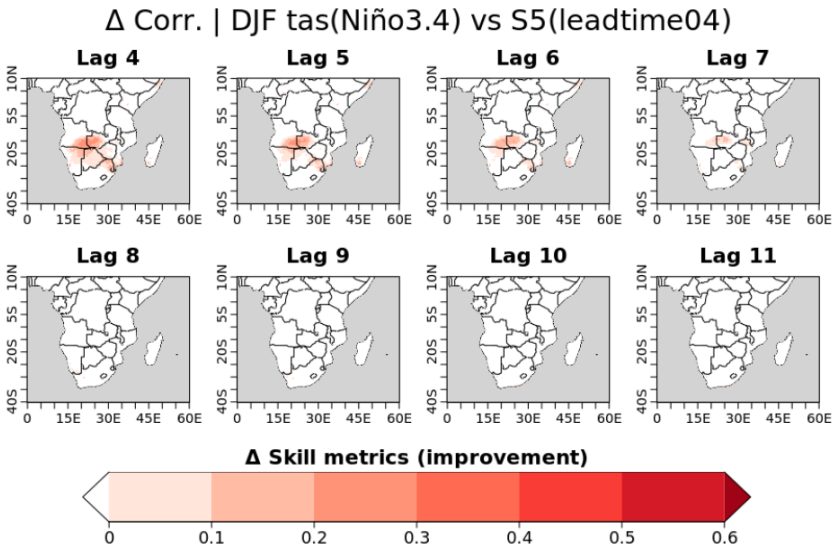

Figure 50: Spatial distribution of the increases in correlation for DJF mean temperature estimates derived from the Niño3.4 index of eight lag months (see the subtitles) when compared with lead time four SEAS5 prediction.

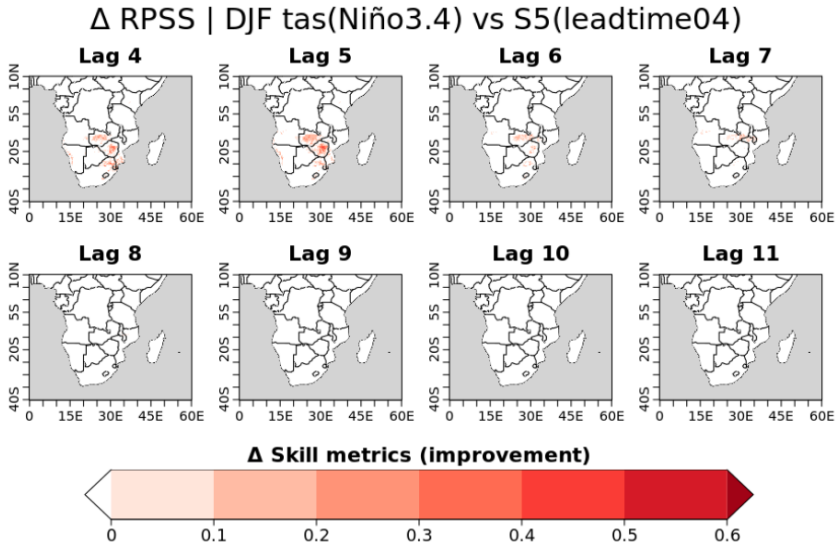

Figure 51: Spatial distribution of the increases in FRPSS for DJF mean temperature estimates derived from the Niño3.4 index of eight lag months (from four to eleven, see the subtitles) when compared with lead time four SEAS5 predictions.

Hereafter, DFJ is also analysed for illustrative purposes. In Figure 50, an increase in correlation by up to 0.3 could be found for the lag months four to six in the areas between 15-25ºS (namely western Zambia, eastern Angola and northern Namibia and Botswana). However, the improvement vanished from lag month eight onwards partially due to the decrease in correlation in lag month nine. Regarding FRPSS shown in Figure 51, most improvements were seen in western Zambia and Zimbabwe in the lag months four to six mainly because these three lag months have better teleconnection linkages. Besides, the maximum and minimum temperature basically show analogous patterns as the ones already discussed for mean temperature.

Summary

First, in terms of the relationship of ECVs with both indices over the SADC region, precipitation has a stronger signal in DJF and SON while temperature tends to correlate more in DJF and MAM. The fact that the stronger signals appear in the same seasons for both indices could hint that a window of opportunity may exist to improve the predictability of precipitation and temperature using either one of these indices in these seasons. Additionally, this association could be related to the link between Pacific and Atlantic Niño through the atmospheric circulation (Jia et al., 2019; Hounsou-Gbo et al., 2020). However, the characterization of the teleconnection depends on the index and ECV. For instance, precipitation manifests a mixture of positive and negative correlations with Niño3.4 while temperature displays mainly positive correlations. ATL3, on the other hand, shows a mixture of positive and negative correlations with all ECVs in most of the months/seasons. In addition, the spatial patterns of the correlation of the ECVs also change with the index. Taking DJF precipitation as an example, for the Niño3.4 negative correlations exist at the southern half of the SADC and positive values at the north, whereas the opposite pattern is found for ATL3. Finally, the correlation changes its sign with the lag month of the index too (depending on the location). For example, the DJF and MAM temperature show a positive relationship with ATL3 at the zero-to-three lag months that changes to negative afterwards (up to eleven lag months).

Regarding the improvement added by the teleconnection approach, there are more chances to see an enhancement for precipitation than temperature and correlations usually display a higher improvement than FRPSS. For example, when compared to SEAS5 lead four predictions, the increases in the correlation of the index-derived estimates of precipitation are seen in 10-25% of the entire domain in all seasons, but only five out of twelve seasons for temperature. As for FRPSS, only 4-6% of the region could see an improved FRPSS of precipitation when using ATL3 as a predictor (almost none for Niño3.4). On the contrary, FMA (DJF and MAM) temperature has higher FRPSSs in 14% (6-7%) of the area for Niño3.4 while only 2-3% for ATL3 (in DJF and NDJ only). The spatial distribution of the improvement highly depends on the seasons and variables, and it also changes with the lag month of the index and with the SEAS5 lead time comparison.

As per the analysis discussed above, it has been shown that a seasonal prediction with higher skills could be generated in certain locations of the SADC area by using estimates from the teleconnection indices (although the results depend on varying factors). This is especially apparent when comparing the longer SEAS5 lead times with the use of concurrent or past observations of the indices in the linear regression models. In that sense, these regression models provide a way to increase the horizon of the predictions beyond the conventional seasonal forecasting horizons.

5.2 ITCZ Teleconnection characterisation

Background

The seasonality of precipitation over most of Africa is arguable linked to the migration of the Tropical Rain Band (TRB) that is closely linked to large scale processes such as the Hadley circulation, through the Intertropical Convergence Zone (ITCZ)(Nicholson, 2009). Rainfall seasonality in Africa is subject to large interannual, decadal and multi-decadal variability that is responsible for the occurrence of regional droughts (Masih et al., 2014).

Methodology

The variability of the TRB over Africa can be estimated by three indexes related to the position (P), the intensity (I) and the spread (S). These can be calculated on a meridional cross-section of monthly mean precipitation averaged over 20°–30°E and then by fitting a Gaussian function the cross-section (Nikulin and Hewitson, 2019).

Crop production analysis

Precipitation during the austral summer (DJF) is closely related to the TRB Intensity in Mozambique and Zambia, and to the TRB position and spread over South Africa and Botswana (Nikulin and Hewitson, 2019). The TRB can be therefore considered a main feature that is relevant Southern Africa water availability, which is increasingly at risk because of climate change (Figure 52).

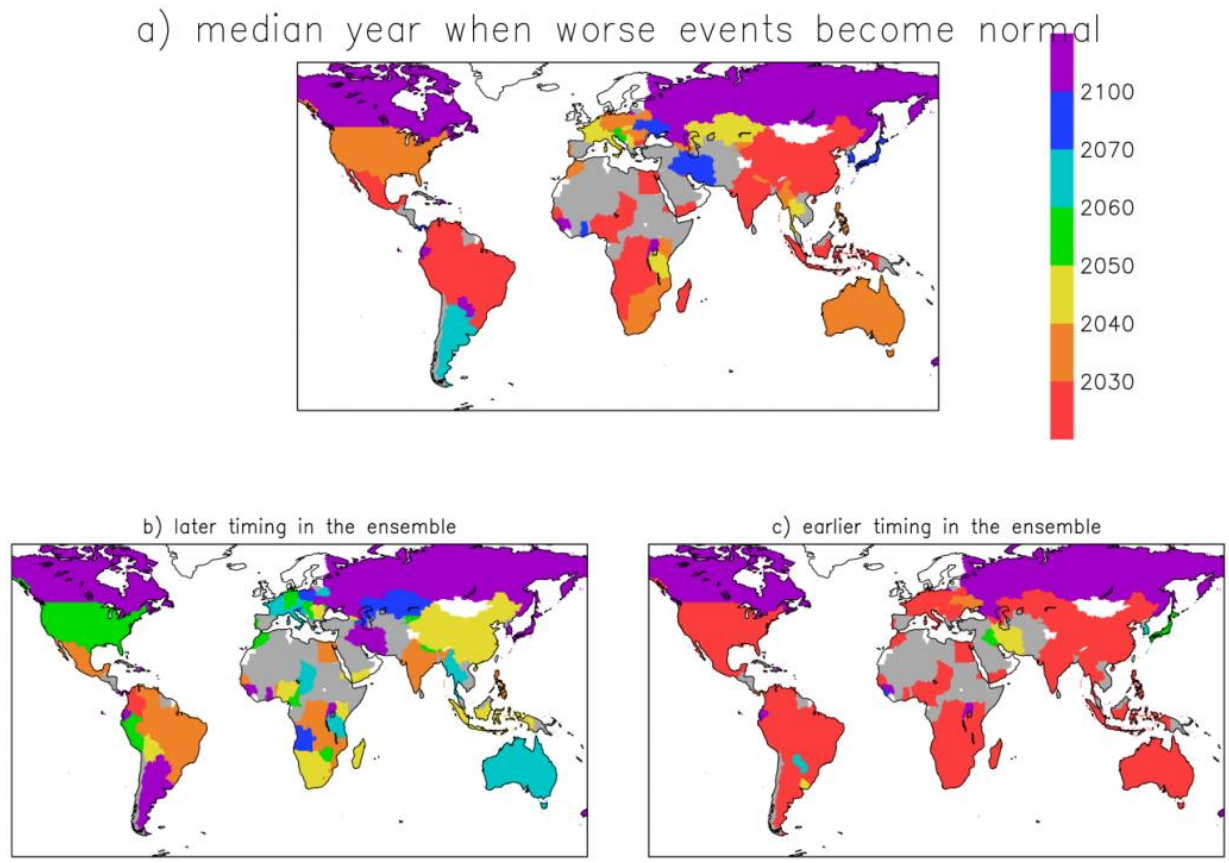

Figure 52: Global estimation of the future decade when the worst climate events causing large maize losses in the past are becoming normal (Zampieri et al., 2019) under RCP8.5 scenario. Panel a show a median estimation, panel b shows the most optimistic one, panel c the most pessimistic.

Over the Southern African countries, a large risk for maize crop is estimated with high confidence and very low uncertainty already soon (Figure 52). Over Southern Africa, a large increase of frequency of extreme events damaging maize is predicted before 2050 at last, more probably earlier. The analysis presented in Figure 52 strongly calls for action on adaptation because maize is a crop of paramount importance for food, feed, and labour in African countries (Figure 53).

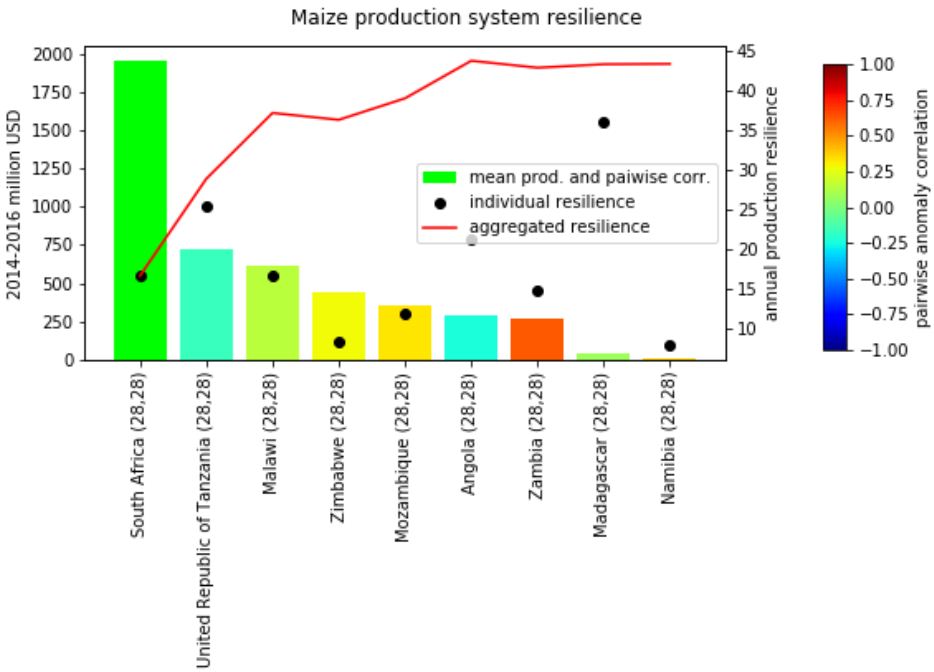

Figure 53: Integrated stability analysis for maize production by the main SADC producers. The histogram shows the reference value of agricultural production related to maize in the recent decades (FAOSTAT data, www.fao.org/faostat/en/). The dots indicate the production stabilities of the individual countries computed by the annual production resilience indicator (Zampieri et al., 2020). The red line represents the stability increase when the productions of the countries are progressively considered. The colours of the bars indicate the correlation of each country production with the sum of the previous, sorted in decreasing order. The plot is produced with an open source software called ResiPy (Zampieri et al., 2021).

Maize production over the Southern Africa Development Countries (SADC) and actually of overall Africa is dominated by South Africa, which is actually a producer of global importance (Zampieri et al., 2019). Measured by the value of production (a FAOSTAT indicator), Tanzanian and Malawi maize productions are about one third of the Southern African one. However, being statistically independent, they largely contribute to the increase of the total stability of the maize SADC production. Mozambique and the other countries contribute less to the total resilience, but with a significant quantity anyway.

Southern African agriculture, albeit not fully developed in terms of inputs such as fertilizers, pesticide and level of management compared to other countries in the middle latitude it is notably much more diversified (Figure 54).

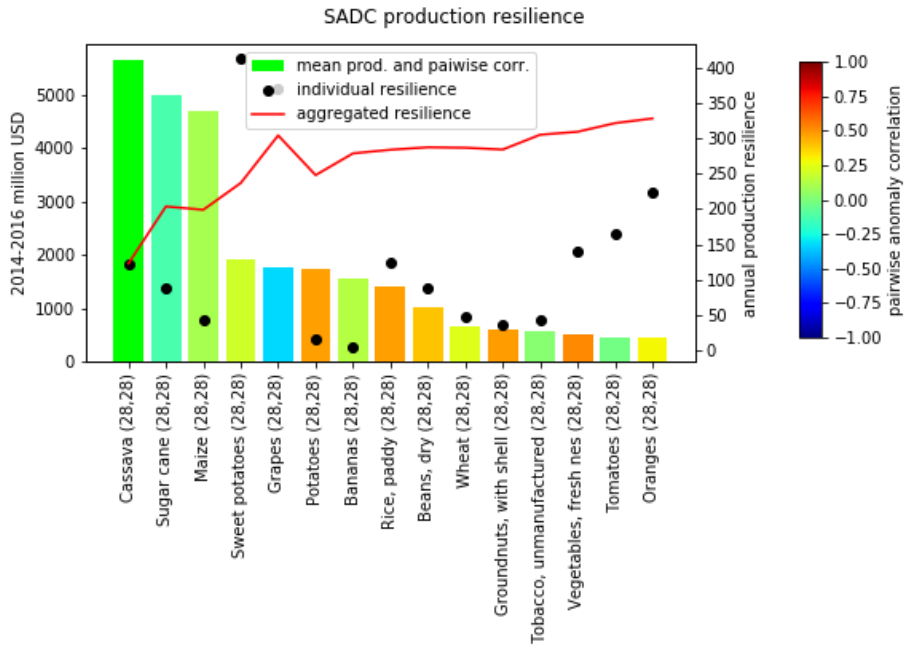

Figure 54: ResiPy analysis like Figure 53, but conducted for the sum of SADC production of different crops, ranked in decreasing order of economic importance.

Cassava and sugar cane production are of similar importance compared to maize (Figure 54). Indeed, in terms of economic output they surpass that of maize, and they are significantly more stable, i.e. they are characterized by comparatively smaller year-to-year variations. Potatoes, grapes, and other crops and fruits are present in more moderate entities, but they also contribute to raising the total stability of the system.

The importance of large-scale features such as the TRB in determining the local water availability and, ultimately, drought for African crops is demonstrated by the correlation with the crop yield reported by the FAO (www.fao.org/faostat/en/) and represented in Figure 55.

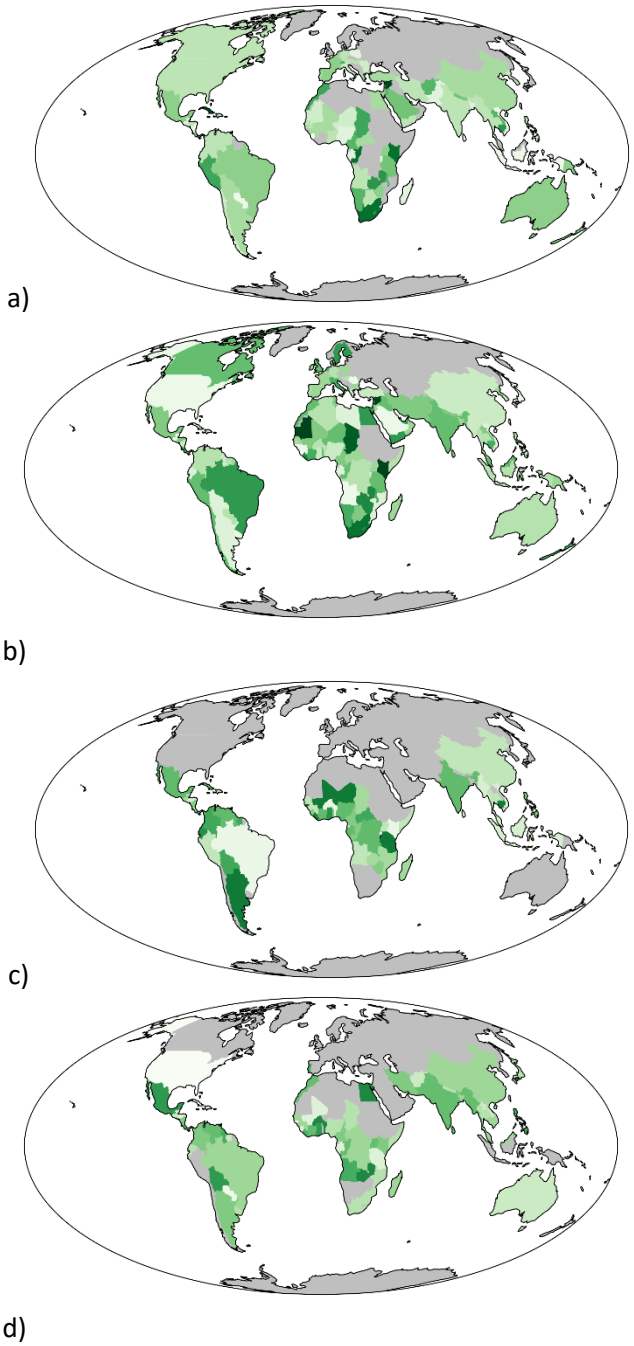

Figure 55: Number of monthly TRB related indicators (position, intensity and spread) that are significantly correlated with the yearly variations in national maize (a), total cereals (b), cassava (c) and sugar cane (d). The TRB is here computed using ERA5 monthly precipitation

Albeit the TRB indicators are computed over Africa only, they can be significantly correlated, to a certain level, also to national crop production of non-African countries. This is because of the link of the TRB to the ITCZ, which is a global climate feature. Nevertheless, higher levels of correlation are found over Africa. These are quantified through the number of TRB indicators computed at the monthly scale that are significantly correlated with the annual crop production (Figure 55). For generality, for each production year, the analysis presented in Figure 55 considers a total of 3 indicators (position, intensity and spread) for each month and for two consecutive years, because crop production could be recorded the year after in the FAOSTAT dataset and because the growing season in southern Africa happens at the end of the calendar year. A large number of significant matches for the SADC are found for maize (Figure 55a), which is known to be highly sensitive to climate variations

(Zampieri et al., 2019). The same holds for the sum of all cereals. Cassava and sugar cane are significantly linked to climate in a lesser number of countries. However, cassava shows a very strong climate (and therefore a greater climate related risk) sensitivity in Tanzania. Sugar cane shows a very strong sensitivity in Zambia. It is worth noticing that these rare lower estimates limited by the data quality. As discussed in other studies, the real links between crop production and climate variability could actually be stronger than those computed here (Zampieri et al., 2017).

TRB seasonal forecasts

Having demonstrated the importance of the water availability determined by the TRB position, intensity, and spread for the crops produced by the SADC, we computed a preliminary estimation of the skill of the seasonal forecasts provided by Copernicus in prediction the TRB position, intensity and spread (Figure 56, Figure 57, Figure 58).

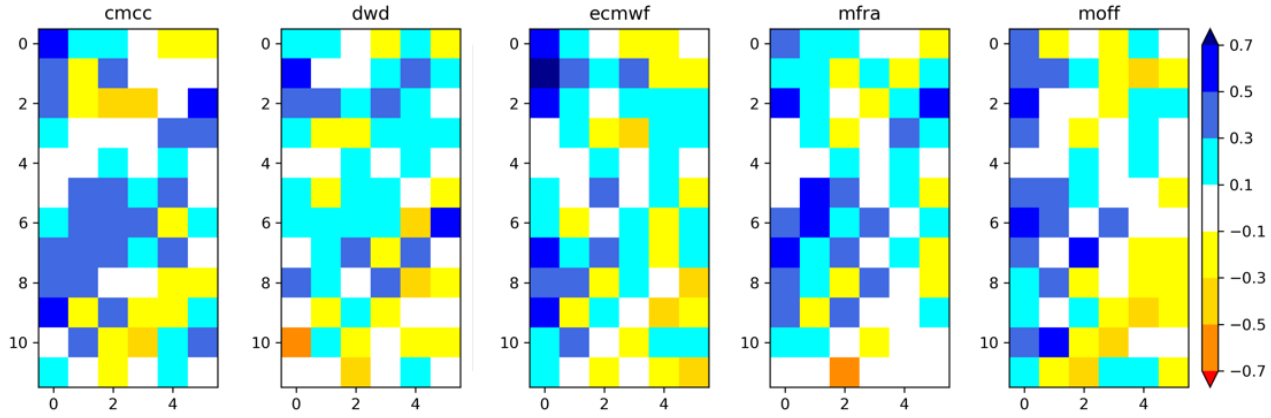

Figure 56: Ensemble mean linear correlation between the observed TRB intensity and that computed on the Copernicus seasonal forecast models (CMCC, DWD, ECMWF, Meteo France and Met Office) at different starting months (0=January, 11= December) and at different lead times. The reference observational dataset is the Rainfall Estimates from Rain Gauge and Satellite Observations (CHIRPS, Funk et al. 2016).

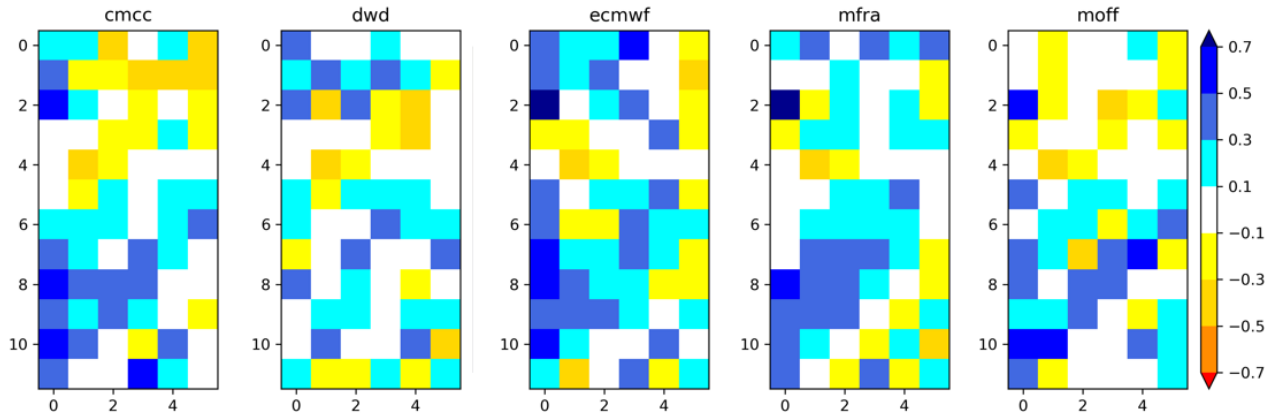

Figure 57: Same as Figure 56 but for the TRB position.

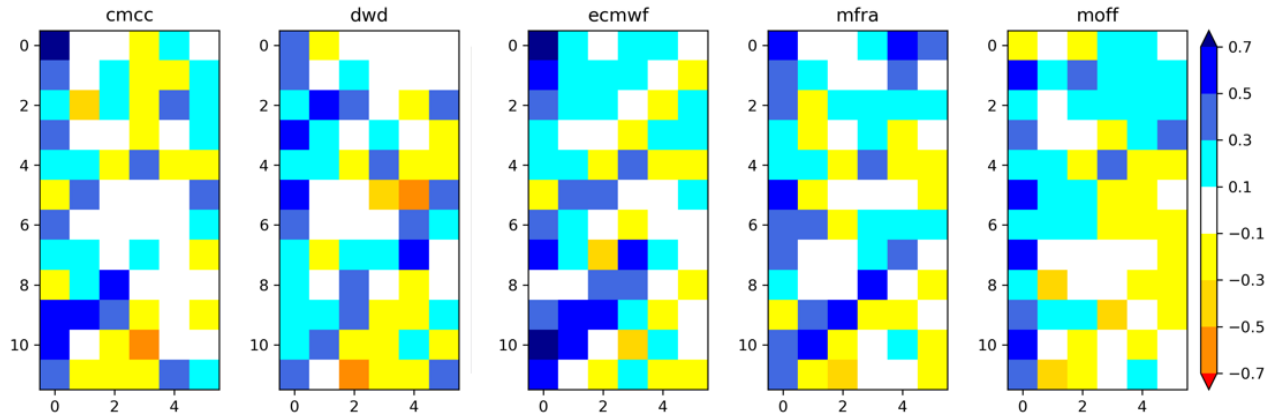

Figure 58: Same as Figure 56, but for the TRB spread.

The Copernicus seasonal forecast models available in the Climate Data Store (CDS) at the time this investigation was perform show some potential in predicting the main features of variability of the tropical rain band over Africa in key periods of the year well in advance. The determining skill will probably increase by considering all models at the same time. The probabilistic skill of the Copernicus models in predicting the monthly precipitation at the grid scale is also computed and is already available online together with operational seasonal forecast in the ASAP platform (ASAP - Seasonal Forecast (europa.eu)).

5.3 A show case for Mozambique

Background

Mozambique is one of the African countries most exposed to climate-related risks (Mavume et al., 2021), which is and will be exacerbated even more by climate change. Mozambique's agricultural production is characterized by moderately low productivity of a wide selection of staple crops, a diverse variety of annual and perennial horticultural products, and cash crops (Silva and Matyas, 2014). Rainfed agriculture, practiced by smallholder farmers, accounts for the vast majority of the cropped area, akin to other countries in the region. Maize and rice are the most widely grown crops in Mozambique and as of 2019 they account to more than 90% of the total cereal production (FAOSTAT, 2021). Climate variability and extremes have a profound influence on agricultural systems. Understanding their effects represents a necessary step to assess the resilience of agricultural systems to changing climate conditions as well as to develop adequate adaptation measures (Moore and Lobell, 2014). Large-scale atmospheric dynamics have a prominent role in driving the year-to-year variability in crop production by influencing the parameters that impact crop production. Thus, quantifying yield loss anomalies at large spatial scales and understanding their climatic drivers is a prerequisite to assess vulnerabilities and design adaptation measures to increase the resilience of food systems.

Numerous studies have investigated the link between climate change and crop yields (e.g. Ceglar et al., 2016, 2017; Guimarães, et al, 2019; Salinger et al, 2020; Lesk, et al, 2021). Even though the relationship between large-scale patterns and crop yields has been widely studied in the past and highlighted connections between indices of climate variability and common atmospheric variables, few have addressed the role of large-scale atmospheric drivers on the variability of agricultural production, particularly on Africa. A more thorough understanding of the net country-level impact of recent large-scale climate trends would help to anticipate impacts of future climate changes, as well as to assess more accurately the recent, technologically driven, progresses in crop yields.

This is the reason why here we characterize influential large-scale climate drivers on crop production and investigate the impact of those drivers by exploring the relationship between large-scale indices of climatic drivers and cereal yield.

Methodology and data

Country level annual crop yields for maize and rice were obtained from the Food and Agriculture Organization (FAO) of the United Nations (FAOSTAT, 2021). Data from 1981 – 2019 has been used in this study. Daily gridded weather dataset from the AgERA5 data set, consisting of maximum air temperature, minimum air temperature, rainfall, and vapour pressure, were obtained from the European Copernicus Program (AgERA5, 2021). AgERA5 makes the ERA5 data available to users in the agricultural sector. The atmospheric and oceanic parameters, mean sea level pressure (MSLP), 850mb level meridional (u850) and zonal (v850) wind were obtained from ERA5, the fifth generation of the ECMWF reanalysis for the global climate and weather for the past 4 to 7 decades (Hersbach et al., 2001).

To properly identify climate effects on crop yield requires that "noise" from other factors to be removed. In general, correlating two trending variables often leads to correlations that are not causal. Hence the model estimates for climate effects rely on year-to-year variations in climate and yields, and not on common trends (Lobell et al., 2011). A simple linear regression model has been applied to de-trend the crop yield time series (Junyu Lu et al., 2017).

Within the area of interest (latitude from 40°S to 40°N, and longitude from 5°W to 80°W), the Pearson product moment correlation analysis was used to explore the relationship between large-scale meteorological drivers and country-level crop yield variations. The target region within large-scale atmospheric circulation fields that drive the Mozambique's inter-annual yield variation was determined by computing the simultaneous correlation with respect to fields of de-trended crop yields and November-to-March average MSLP, 850 hPa meridional winds and zonal winds. Over the geographical area of interest, regions of significant influence, defined as the ones with an anomaly correlation coefficient greater than 20% with a 90% confidence level (i.e. p<0.1), were identified from the point-to-field correlation map. Points with a correlation lower than 20% were masked.

To investigate the relationship and linkage between the time series for yield and climatic drivers and quantify the climate impact, we used a multiple linear regression model with crop yield as the response variable, and climate drivers as predictor variables.

$$Yield \sim MSLP + U_{wind} + V_{wind} + Rain + T_{avg}$$

While an empirical study cannot attribute directions of causality, it is certainly assumed that climate variations caused yield changes, and not vice versa (Kukal et al, 2018). The multiple linear regression (MLR) model was used to estimate the role of climate in recent yield trends. Assuming the observed trend in the climate fields is attributed to the anthropogenic effect (due to climate change), two yield estimations was performed using the MLR model, one using the actual observed climate fields ($Y_{factual}$) as predictors and a second one using the detrended climate fields ($Y_{counterfactual}$) as predictors. Then, the climate impact on crop yield is estimated by comparing the factual and counterfactual yield estimations:

$$\Delta Y_{c,t} = \frac{\left(Y_{factual,c,t} - Y_{counterfactual,c,t}\right)}{\sum_{1981}^{2019} Y_{factual,c,1981:2019}}$$

where suffix t and c indicate the year and crop type, ΔY is the estimated yield impact $Y_{factual}$ is the estimated yield under the factual climate condition, $Y_{counterfactual}$ is the estimated yield under the

counterfactual climate condition and $Y_{factual,1981:2019}$ is the estimated average yield over the historical period estimated using factual climate data.

This approach was followed to identify the proportion of changes in yields due to climate trends relative to the historical average yield, and to assess whether the climate impact on yield was positive or negative. While an MLR model does not attempt to capture details of plant physiology or crop management, they do capture the net effect of the entire range of processes by which climate affects yields, including the effects of poorly modelled processes. Thus, such estimates of climate impacts can be viewed as an upper bound on the impacts of recent trends (Lobell and Field, 2007).

Analysis of the cropping season

The rainfall season in Mozambique lasts from October to May, though most rainfall is concentrated between November to April. The rainfed cropping season for major cereals covers November to May, since it depends on the rainy season. Results indicate a decreasing tendency of monthly rainfall totals during November (planting month) and February (reproductive stage for the cereals) since 1981. The decreasing trend of the November rainfall totals may cause frequent erratic onset of the rainy season over time, which creates unfavourable conditions for sowing during the planting window. Results also indicate that the January rainfall totals have been increasing significantly during the last 40 years (Figure 59). In addition, during January, the number of very heavy rain days are increasing throughout Mozambique whereas light to medium rain days is decreasing. As a result of these observed trends, the rainy season has been becoming shorter, with an increased frequency of extreme events.

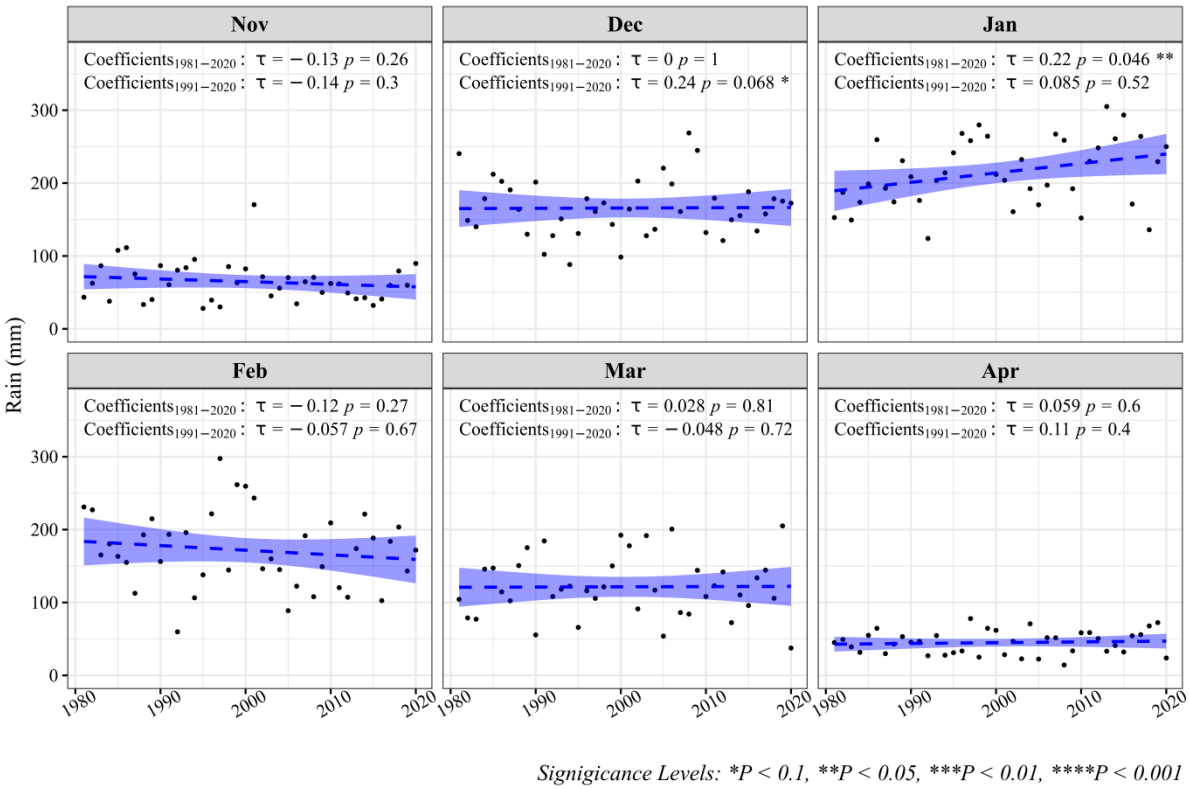

Figure 59: Linear trend (1981 - 2020) of Mozambique averaged monthly rainfall totals (mm per year).

The temperature anomaly during the crop season (Figure 60) shows a clear warming trend, which becomes more evident after 2002. It is also worth to notice, at some extent, a quasi-decadal variability in the growing season temperature that can be detected in the 5-year centred running average (black

line: for each year Y, the line shows the mean between Y-2 and Y+2 years), with lower relative values in 1989, 2003, and 2012.

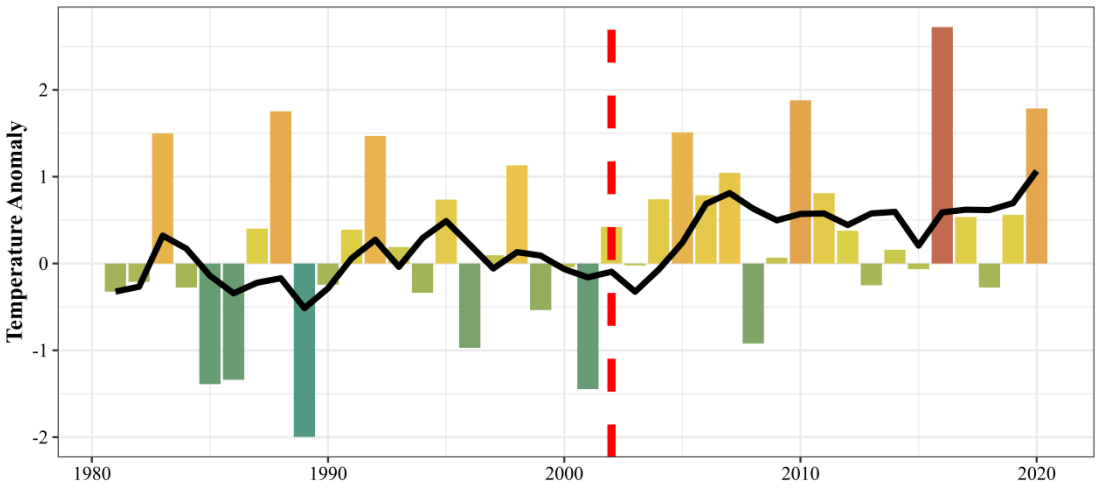

*The bold black line is 5-year moving averages

Figure 60: Standardized daily average temperature anomaly relative to 1981 - 2000: average over November to March. The black line shows the 5-year running mean.

Large scale climatic drivers

Mozambique's rainfall climatology is determined mainly by seasonal changes in large-scale circulation, part of which involves a series of variations:

- Southward migration of the Inter-Tropical Convergence Zone (ITCZ),
- Variation in the strength of Angola Low (AL),
- Changes in the Mozambique Channel Trough (MCT), characterized by a low-pressure area over the central and southern Mozambique Channel, and
- Variations in position and intensity of the Mascarene High (MH) pressure systems and perturbations in the associated southern hemisphere mid-latitude westerly circulation.

Large-scale climatic drivers of Mozambique were analysed by simultaneous correlation with respect to de-trended fields of MSLP, 850mb meridional and zonal wind and linkage with country level yield was investigated for the November to March cropping period. The correlation map between country-level yield and atmospheric variables (Figure 61) illustrates the features anticipating links between large-scale climatic drivers and yield. There is a negative MSLP signal in the northern Indian ocean including the Arabian Peninsula *(10° N to 30° N, 50° E to 70° E; MSLP-index),* an area dominated by Arabian high-pressure system which intensifies in strength and extent during this time of the year. There is a positive meridional wind signal over southern part of Africa *(10° S to 18° S, 10° E to 20° E; u850-index).* This region is dominated by Angola low which intensifies during this period (Crétat et al, 2019; Barimalala et al. , 2020). There is a distinct negative surface zonal wind correlation in the region located south of Madagascar *(30° S to 38° S, 23° E to 37° E; v850-index).*

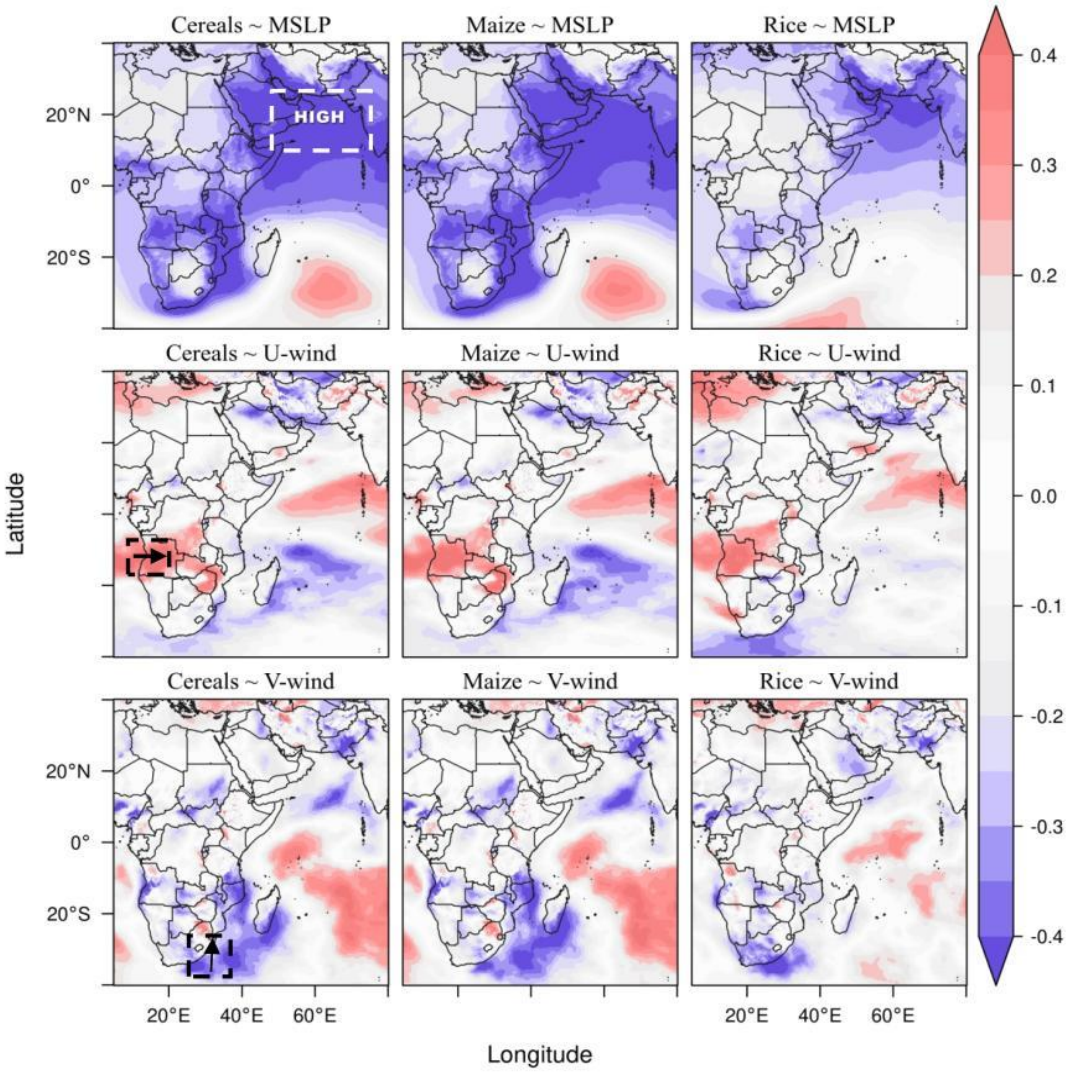

Figure 61: Correlation of continuous Mozambique yield anomalies: (1st column) Cereals, (2nd column) maize, (3rd column) rice, with simultaneous synoptic-scale meteorological drivers: (1st row) MSLP, (2nd row) U-wind @850 hPa, (3rd row) V-wind @850 hPa.Target area and key features are highlighted.

The country level climate indices (Rain, Tavg and VPD), together with identified atmospheric indices (MSLP-index, u850-index, and v850-index) from the influence area that drives the Mozambique cereal yield was used to describe the influences of large-scale atmospheric drivers on year-to-year variations of country-level yield progress. There is a strong association between climatic drivers and Mozambique's crop yield. An intensification of the high-pressure system over the Arabian subcontinent *(as indicated, e.g., by the MSLP-index)* leads to reduced crop yield. On the other hand, enhanced meridional winds over southern Africa *(as indicated by the u850-index)* and high seasonal rainfall totals tend to be associated with increased cereal yield values. Higher values of daily mean temperature, which leads to larger values of Vapour Pressure Deficit and weaker zonal wind over south of Madagascar *(v850-index)* result a reduced cereal yield gains (Figure 62).

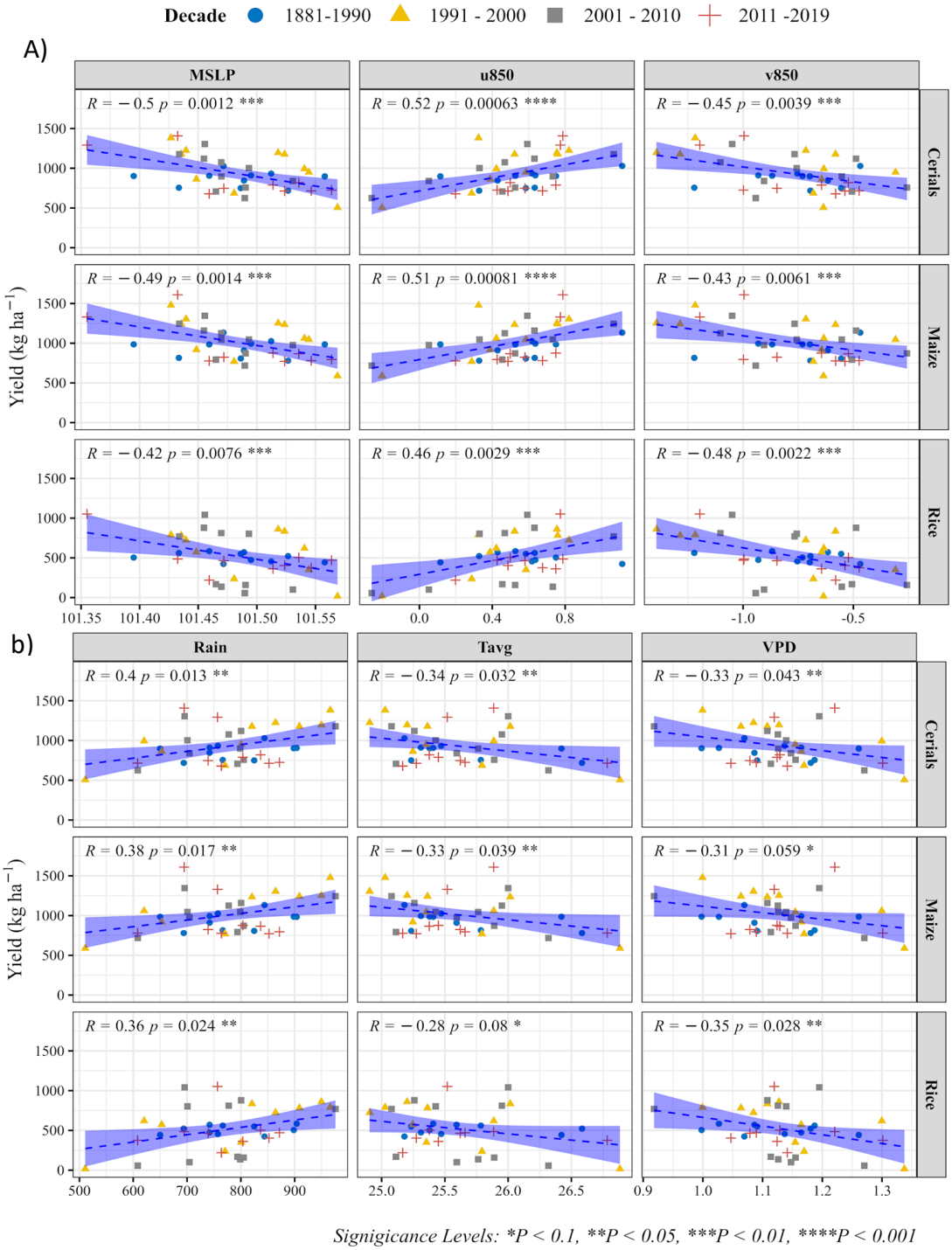

Figure 62: Relationship between crop yield (kg ha^{-1}) and climatic drivers. Each decade is shown with a different colour and shape, indicating that the relationships do not appear to change through time.

Maize and rice are widely grown crops in Mozambique. Based on the 2019 statistic from FAOSTAT (https://www.fao.org/faostat/en/#data/QCL), the two crops make up more than 90% of the total cereal production. Yields of total cereals and grain maize *(S-3)* have increased in the last 40 year, whereas rice yields are reduced, although a levelling off can be observed after 2015 and from 1981 to 1986. Following the method described by Lobell et al. (2007, 2011) and Iizumi et al. (2018), the role of

large-scale drivers in recent yield trends was investigated. We used a multiple linear regression model with crop yield as the response variable, and climate drivers as predictor variables to quantify the climate impact. The estimated impacts of climatic drivers on yield trends were statistically significant for cereal crops since 1981. These inferred impacts reflect only the influences of large-scale climatic drivers that were captured by the MLR models. Negative yield impacts since 2001 indicate that recent climate trends have suppressed Mozambique's cereal yield progress and need to be addressed through adaptation measures. The estimated average yield impacts in the historical period (1981 – 2019) due to historical climate change, relative to a counterfactual climate condition, observed to be negative for all major crops (Figure 63). rice appears to be more affected by climate change than maize. The MLR model estimates average yield loss of 20% for rice, 8% for maize and 9% for major cereals over the historical period.

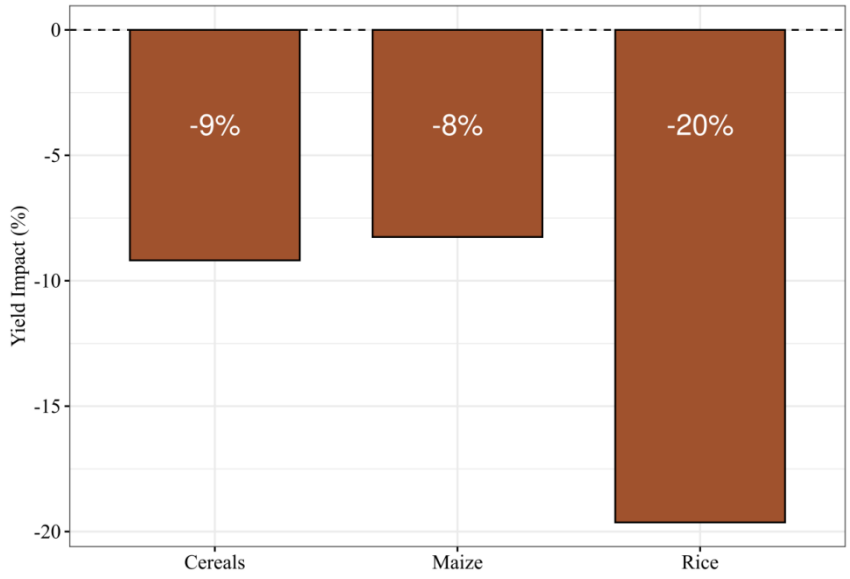

Figure 63: Estimated impacts of large-scale climate drivers on average yields for 1981–2019. Positive values indicate that the climate has increased the yields, and negative values indicate that climate has decreased the yields relative to what would have occurred without the anthropogenic effect.

Summary

Rainfall totals during the beginning and end of the season (November, February and March) have been decreasing since 1981, while rainfall totals during December and January are increasing. In other words, the rainfall season has been shortening, with more extreme precipitation events concentrated in Dec-Jan. The seasonal average temperature of the crop season has also been warming significantly from 1981 to 2020. The warming has been more pronounced and consistent after 2002.

Interannual yield anomalies are often linked to variations in the large-scale systems that control the regional climate with quasi-periodic fluctuations. The results suggest that recent large-scale climate trends, attribute to human activity, have a negative impact on the countries yield progress. The impact is significant since 2002. On average, since 1981, yield of maize and rice is reduced by 20% and rice 8% due to climate change alone.

The estimated climate impact in this study is limited to simulate yield responses effectively, when cropping areas shift and when change in agricultural policies are affecting the cultural cropping practice at large scale. Those changes will introduce an artificial temporary trend to the crop production progress and bias the regression estimator used to detrend yield to remove non-climatic factors. However, one can be confident that, the historical large-scale climate drivers and cereal yield relationships indicate that, at country scale, warming from 2002 very likely offset some of the cereal yield gains from technological advances. One of the most effective ways to overcome this anthropogenic warming effect will likely come from biology (Raza et al., 2019; Gomez-Zavaglia, et al., 2020). Plant breeding and genetic engineering may lead to different crops and crop varieties that produce higher yields and are more resilient to extreme temperature and moisture stress. More specifically, effective adaptation strategies for the agriculture sector in areas affected by climate change, such as Mozambique, could be developed by combining studies like this one, assessing how climate variability has been affecting crop yields, with studies that identify which crop varieties can adapt better to the ongoing and project climate change and with climate change projections (IPCC 2021).

6 Conclusion

With the deployment of operational centres around the globe and continued advances in climate modelling, in combination with user demand for climate services, predictions of the near-term climate have become more robust. Decadal prediction systems have shown levels of skill that are comparable to predictions in operational seasonal forecasting particularly for surface air temperature and to precipitation. In addition to these, predictions at this timescale also provide skilful information for the frequency of extreme events such as heatwaves and tropical storms. Of course, the main difference between the seasonal and decadal predictions is in the temporal resolution which would influence the applicability of such products depending on the needs of different sectors. As the skill levels of near-term climate predictions indicate, there is considerable potential for several sectors to benefit from such predictions.

In the context of SADC, SARCOF and SWIOCOF are using a series of predictors over the region for seasonal forecasting from different data sources and models. Over the years, ENSO, IOD, SIOD, Benguela Nino have been demonstrated to drive rainfall variability across southern Africa. Current statistical tools have useful predictability usually limited to years with strong ENSO signal. Statistical tools available carry quite well the ENSO signal and perform better in the ENSO years.

The evaluations of skill in the AMIP-simulations of inter-annual variability in the Southern Hemisphere confirm the results from operational seasonal forecasting, namely that a pronounced seasonal cycle in predictive skill exists over the Southern Hemisphere continents in the subtropics, with peak skill in summer in association with ENSO forcing. However, the seasonal prediction of winter rainfall and underpinning circulation anomalies need to focus on improved systems of initialisation and data assimilation, rather on sources of predictability, since for these regions the latter is insignificant compared to the dominating role of internal variability.

In SADC, drought is a multi-faceted phenomenon that occurs across a range of temporal and spatial scales and is experienced across a range of societal sectors that are dependent on climate and water resources. We investigated the observed interannual to multi-decadal variability and changes of droughts and other environmental conditions that directly affect rainfall, streamflow, and river discharges across the Orange River basin as it is the largest river system in southern Africa. This showed that the interannual and multi-decadal drought variability over the Orange River basins is largely explained by the natural variability throughout the 20th Century. However, the worsening of water stress due to loss from surface water, drainage systems, and other covers is likely associated

with temperature amplification. The impact of climate change on the future moisture budget and surface water resources may arise from the continental scale loss of water due to potential evapotranspiration and the shift of rainfall bearing systems, which seemingly tends to affect mostly the southern Africa region. However, the impact of climate change on rainfall is complex and nonlinear in nature and its signature is likely felt with a drastic shift on rainfall bearing systems.

We then focused on the analysis of the ability of seasonal forecasts to describe energy transfer in the atmosphere, applying spectral analysis to study the winter atmospheric variability at the mid-latitudes of the Southern Hemisphere from 1993 to 2020. This showed that this winter variability in the southern hemisphere can be explained mainly by the eastward propagation of the baroclinic waves. Therefore, the problems of seasonal forecasting in correctly predicting baroclinic activity may be directly related to the low skill values of precipitation predictions observed in the seasonal forecast demonstrating the importance of baroclinic activity in understanding the role of rainfall and temperature variability in seasonal forecast data. FOCUS-Africa case studies can thus directly benefit from the application of this approach to better understand how seasonal forecast precipitation and temperature fields can be corrected to account for this observed variability.

In a show case, we also investigated the linkage between low-level moisture fluxes and rainfall variability over the Lake Malawi catchment, towards potential implications to rainfall predictability at seasonal time scales. The analyses indicate that low level moisture transport plays an important role in rainfall over the Lake Malawi catchment, and its dynamics are linked to seasonal and interannual rainfall variability. The strength of the Malawi Low Level Jet is, however, inversely proportional to rainfall over the Lake Malawi catchment during the core of the rainy season but the relationship is inverse during the rest of the year. These relationships clearly indicate the importance of the dynamics of the low-level moisture fluxes, and, of the interactions between conditions facilitating westerly and easterly moisture flux, on the rainfall dynamics over the Lake Malawi catchment.

Concerning the exploration of large-scale processes, we investigated the prospects of improving seasonal predictions of ECVs in SADC by means of the characterization of teleconnection links with large scale patterns like El Niño Southern Oscillation (ENSO). First, in terms of the relationship of ECVs with both indices over the SADC region, precipitation has a stronger signal in DJF and SON while temperature tends to correlate more in DJF and MAM. The fact that the stronger signals appear in the same seasons for both indices could hint that a window of opportunity may exist to improve the predictability of precipitation and temperature using either one of these indices in these seasons. Therefore, a seasonal prediction with higher skills could be generated in certain locations of the SADC area by using estimates from the teleconnection indices, especially for precipitation using linear regression models. In that sense, these models provide a way to even increase the predictions range beyond the conventional seasonal forecasting horizons.

Furthermore, the seasonality of precipitation over most of Africa is arguable linked to the migration of the Tropical Rain Band that is closely linked to large scale processes such as the Hadley circulation through the ITCZ. We demonstrated that the importance of the water availability is determined by the TRB position, intensity, and spread for the crops. We also showed that the Copernicus seasonal forecast models show some potential in predicting the main features of variability of this tropical rain band over Africa in key periods of the year well in advance.

In another showcase, we characterized the influential large-scale climate drivers on crop production in Mozambique and investigated the impact of those drivers by exploring the relationship between large-scale indices of climatic drivers and cereal yield. This shows that the rainfall season has been shortening with totals in November, February and March decreasing since 1981 and totals during December and January increasing. The seasonal average temperature of the crop season has also been warming significantly from 1981 to 2020. The warming has been more pronounced and consistent after 2002. Interannual yield anomalies are often linked to variations in the large-scale systems that

control the regional climate with quasi-periodic fluctuations. The results suggest that recent large-scale climate trends, attribute to human activity, have a negative impact on the countries yield progress. The impact is significant since 2002. On average, since 1981, yield of maize and rice is reduced by 20% and rice 8% due to climate change alone.

Bibliography

Adana and S. J. Colucci (2005). Southern Hemisphere Blocking Onsets Associated with Upper-Tropospheric Divergence Anomalies, Journal of the Atmospheric Sciences, Vol. 62(5): 1614-1625

AgERA5 (2021). Copernicus Climate Change Service (C3S), Fifth generation of ECMWF atmospheric reanalysis of the global climate for agriculture and ago-ecological studies. Copernicus Climate Change Service Climate Data Store (CDS), July-2021.

Barimalala, R., Blamey, R. C., Desbiolles, F., & Reason, C. J. C. (2021). The influence of southeastern African river valley jets on regional rainfall. *Climate Dynamics*, *57*(9–10), 2905–2920. https://doi.org/10.1007/S00382-021-05846-1/FIGURES/9

Barimalala R, Blamey RC, Desbiolles F, Reason CJC (2020). Variability in the Mozambique Channel Trough and impacts on Southeast African Rainfall. J. Clim. 33:749–765.

Beraki, A. (2019). *Green Book – The Impact of Climate Change on Drought.* Technical report, Pretoria: CSIR

Berhane F. and Zaitchik B. (2014). Modulation of Daily Precipitation over East Africa by the Madden–Julian Oscillation. *Journal of Climate* **27** 6016-6034.

Blackmon (1976). A climatological spectral study of the 500 mb geopotential height of the Northern Hemisphere, Journal of the Atmospheric Sciences, Vol. 33: 1607–1623

Cambray, J.A., Davies B.R., Ashton P.J., Agnew J.D., De Moor F.C., Skelton P.H. (1986). The Orange-Vaal River system. In: Davies B.R., Walker K.F. (eds) The Ecology of River Systems. Monographiae Biologicae, vol 60. Springer, Dordrecht. https://doi.org/10.1007/978-94-017-3290-1_4

Caron, L.-P., Hermanson, L., Dobbin, A., Imbers, J., Lledó, L., & Vecchi, G. A. (2018). How Skillful are the Multiannual Forecasts of Atlantic Hurricane Activity? *Bulletin of the American Meteorological Society, 99*(2), 403-413. doi:10.1175/bams-d-17-0025.1

Ceglar A, Toreti A, Lecerf R, Van der Velde M and Dentener F (2016). Impact of meteorological drivers on regional inter-annual crop yield variability in France Agric. Forest Meteorol. 216 58–67

Ceglar A, Marco Turco, Andrea Toreti, Francisco J. Doblas-Reyes (2017). Linking crop yield anomalies to large-scale atmospheric circulation in Europe, Agricultural and Forest Meteorology, Volumes 240–241, Pages 35-45, ISSN 0168-1923, https://doi.org/10.1016/j.agrformet.2017.03.019.

Chatzopoulos, T., Pérez Domínguez, I., Zampieri, M., & Toreti, A. (2020). Climate extremes and agricultural commodity markets: A global economic analysis of regionally simulated events. *Weather and Climate Extremes, 27*. doi:10.1016/j.wace.2019.100193

Conway, D., Dalin, C., Landman, W.A. et al. (2017). Hydropower plans in eastern and southern Africa increase risk of concurrent climate-related electricity supply disruption. Nat Energy 2, 946–953. https://doi.org/10.1038/s41560-017-0037-4)

Cook K. H. (2001). A Southern Hemisphere Wave Response to ENSO with Implications for Southern Africa Precipitation. *Journal of the Atmospheric Sciences* **58** 2146-2162.

Crétat, J., Pohl, B., Dieppois, B. et al. (2019). The Angola Low: relationship with southern African rainfall and ENSO. Clim Dyn 52, 1783–1803. https://doi.org/10.1007/s00382-018-4222-3

Dell'Aquila, V. Lucarini, P. M. Ruti, S. Calmanti (2005). Hayashi spectra of the Northern Hemisphere mid-latitude atmospheric variability in the NCEP-NCAR and ECMWF reanalyses, Climate Dynamics, Vol. 25: 639–652

Dell'Aquila, P. M. Ruti, S. Calmanti, V. Lucarini (2007). Southern Hemisphere midlatitude atmospheric variability of the NCEP-NCAR and ECMWF reanalyses, Journal of Geophysical Research, Vol. 112

Dell'Aquila, P. M. Ruti, A. Sutera (2006). Effects of the baroclinic adjustment on the tropopause in the NCEP-NCAR reanalysis, Climate Dynamics, Vol. 28: 325–332

Dieppois, B., Pohl, B., Rouault, M., New, M., Lawler, D., & Keenlyside, N. (2016). Interannual to interdecadal variability of winter and summer southern African rainfall, and their teleconnections. *Journal of Geophysical Research: Atmospheres, 121*(11), 6215-6239. doi:10.1002/2015jd024576

Doblas-Reyes, F. J., R. Hagedorn, and T. N. Palmer (2005). The rationale behind the success of multi-model ensembles in seasonal forecasting—II. Calibration and combination. Tellus, 57A, 234–252, doi:10.3402/tellusa.v57i3.14658.

Doblas-Reyes, F. J., Andreu-Burillo, I., Chikamoto, Y., Garcia-Serrano, J., Guemas, V., Kimoto, M., van Oldenborgh, G. J. (2013). Initialized near-term regional climate change prediction. *Nat Commun, 4*, 1715. doi:10.1038/ncomms2704

Dore, M.H. (2005). Climate change and changes in global precipitation patterns: What do we know? Environ. Int. 31, 1167–1181.

Eade, R., Hamilton, E., Smith, D. M., Graham, R. J., & Scaife, A. A. (2012). Forecasting the number of extreme daily events out to a decade ahead. *Journal of Geophysical Research: Atmospheres, 117*(D21), n/a-n/a. doi:10.1029/2012jd018015

Ekine-Dzivenu, C.C., Mrode, R., Oyieng, E., Komwihangilo, D., Lyatuu, E., Msuta, G., Ojango, J.M.K., Okeyo, A.M. (2020). Evaluating the impact of heat stress as measured by temperature-humidity index (THI) on test-day milk yield of small holder dairy cattle in a sub-Sahara African climate. Livest. Sci. 242, 104314. doi:10.1016/j.livsci.2020.104314

Engelbrecht, F. and co-authors (2015). Projections of rapidly rising surface temperatures over Africa under low mitigation, *Environ. Res. Lett.*10, 085004.

Engelbrecht C.J., Phakula S., Landman W.A. and Engelbrecht F.A. (2021). Subseasonal deterministic prediction skill of low-level geopotential height affecting southern Africa. *Weather and Forecasting* **36** 3195-205. https://doi.org/10.1175/WAF-D-20-0008.1.

Engelbrecht F.A., McGregor J.L. and Engelbrecht C.J. (2009). Dynamics of the conformal-cubic atmospheric model projected climate-change signal over southern Africa. International Journal of Climatology **29** 1013-1033. https://doi.org/10.1002/joc.1742.

Engelbrecht F., Ndarana T., Landman W., Van der Merwe J., Ngwana I. and Muthige M. (2015). Radiative forcing of Southern African climate variability and change. No. 2163/1. WRC Report.

FAO (2004). *Drought impact mitigation and prevention in the Limpopo River Basin: A situation analysis.* Land and water Discussion Paper 4. Rome. http://www.fao.org/3/y5744e/y5744e00.htm#Contents (accessed 2021-02-28).

FAOSTAT (2021). Food and Agriculture Organization of the United Nations (FAO). FAOSTAT Database.

Ferro, C. A. T. (2014). Fair scores for ensemble forecasts. Quart. J. Roy. Meteor. Soc., 140, 1917–1923, https://doi.org/https://doi.org/10.1002/qj.2270.

Foltz, G., Brand, P., Richter, I., Rodríguez-Fonseca, B., Hernandez, F., Dengler, M., et al. (2019). The tropical Atlantic observing system.Frontiers in Marine Science,6, 206. https://doi.org/10.3389/fmars.2019.00206

Fraedrich and H. Bottger (1978). A wavenumber frequency analysis of the 500 mb geopotential at 50° N, Journal of the Atmospheric Science, Vol 35: 745–750.

Fricker, T. E., C. A. T. Ferro, and D. B. Stephenson (2013) Three recommendations for evaluating climate predictions. Meteor. Appl., 20, 246–255, https://doi.org/https://doi.org/10.1002/met.1409.

Funk, C., Harrison, L., Shukla, S., Pomposi, C., Galu, G., Korecha, D., Verdin, J. (2018). Examining the role of unusually warm Indo-Pacific sea-surface temperatures in recent African droughts.

Quarterly Journal of the Royal Meteorological Society, 144, 360-383. https://doi.org/10.1002/qj.3266

Gillett N.P., Kell T.D. and Jones P.D. (2006). Regional climate impacts of the Southern Annular Mode. Geophysical Research Letters 33 L23704.

Gomez-Zavaglia, J.C. Mejuto, J. Simal-Gandara (2020). Mitigation of emerging implications of climate change on food production systems, Food Research International, Volume 134, 2020, 109256, ISSN 0963-9969, https://doi.org/10.1016/j.foodres.2020.109256.

Gordon, HB, O'Farrell SP (2002). Transient Climate Change in the CSIRO Coupled Model with Dynamic Sea Ice. Mon Weather Rev. https://doi.org/10.1175/1520-0493(1997)125<0875:tccitc>2.0.co;2

Guimarães Nobre, G., Hunink, J.E., Baruth, B. et al. (2019). Translating large-scale climate variability into crop production forecast in Europe. Sci Rep 9, 1277. https://doi.org/10.1038/s41598-018-38091-4

Harris, I., Osborn, T.J., Jones, P. *et al.* (2020). Version 4 of the CRU TS monthly high-resolution gridded multivariate climate dataset. *Sci Data* **7,** 109. https://doi.org/10.1038/s41597-020-0453-3

Hayashi (1971). A generalized method of resolving disturbances into progressive and retrogressive waves by space Fourier and time cross-spectral analyses, Journal of the Meteorological Society in Japan, Vol. 49 No. 2

Hayashi (1979), *A generalized method of resolving transient disturbances into standing and traveling waves by space-time spectral analysis*, Journal of the Atmospheric Sciences, Vol. 36

Hermanson, L. et al, WMO Global Annual to Decadal Climate Update: A prediction for 2021-2025, Bull. Amer. Met. Soc., in press (2022)

Hersbach, H., Bell, B., Berrisford, P., Biavati, G., Horányi, A., Muñoz Sabater, J., Nicolas, J., Peubey, C., Radu, R., Rozum, I., Schepers, D., Simmons, A., Soci, C., Dee, D., Thépaut, J-N. (2018): ERA5 hourly data on pressure levels from 1979 to present. Copernicus Climate Change Service (C3S) Climate Data Store (CDS)

Hersbach, H, Bell, B, Berrisford, P, et al. (2020). The ERA5 global reanalysis. Q J R Meteorol Soc.; 146: 1999– 2049. https://doi.org/10.1002/qj.3803

Hobday, A. J., Hartog, J. R., Manderson, J. P., Mills, K. E., Oliver, M. J., Pershing, A. J., . . . Browman, H. (2019). Ethical considerations and unanticipated consequences associated with ecological forecasting for marine resources. *ICES Journal of Marine Science*. doi:10.1093/icesjms/fsy210

Hounsou-Gbo, A., Servain, J., Junior, F.D.C.V., Martins, E.S.P. and Araújo, M. (2020) Summer and winter Atlantic Niño: connections with ENSO and implications. Climate Dynamics, 55(11), pp.2939-2956. https://doi-org.recursos.biblioteca.upc.edu/10.1007/s00382-020-05424-x.

Huang, B., and Co-authors (2017). Extended Reconstructed Sea Surface Temperature version 5 (ERSSTv5), upgrades, validations, and intercomparisons. *J. Climate*, 30, 8179–8205.

Iizumi T, Shiogama H, Imada Y, Hanasaki N, Takikawa H, Nishimori M. (2018). Crop production losses associated with anthropogenic climate change for 1981–2010 compared with preindustrial levels. Int J Climatol. 2018;38:5405–5417. https://doi.org/10.1002/joc.5818

Indeje M., Semazzi F.H.M. and Ogallo L.J. (2000). ENSO signals in East African rainfall seasons. *International Journal of Climatology* **20** 19-46.

IPCC (2018). "Global Warming of 1.5 ºC"

IPCC (2021). Climate Change (2021). The Physical Science Basis. Contribution of Working Group I to the Sixth Assessment Report of the Intergovernmental Panel on Climate Change [Masson-Delmotte, V., P. Zhai, A. Pirani, S. L. Connors, C. Péan, S. Berger, N. Caud, Y. Chen, L. Goldfarb, M. I. Gomis, M. Huang, K. Leitzell, E. Lonnoy, J. B. R. Matthews, T. K. Maycock, T. Waterfield, O. Yelekçi, R. Yu and B. Zhou (eds.)]. Cambridge University Press. In Press.

Jia, F., Cai, W., Wu, L., Gan, B., Wang, G., Kucharski, F., Keenlyside, N. (2019). Weakening Atlantic Niño–Pacific connection under greenhouse warming. Science advances, 5(8), eaax4111. https://www.science.org/doi/10.1126/sciadv.abg9690.

Johnson, S. J., and Coauthors (2019). SEAS5: The new ECMWF seasonal forecast system. Geosci. Model Dev., 12, 1087–1117, https://doi.org/10.5194/gmd-12-1087-2019.

Johnston, P., A., Archer, E. R. M?Vogel, C., H. Reznidenhout C. N., Trennant W. J., Kushke R. (2004). Review of seasonal forecasting in South Africa: producer to end-user. Climate Research, vol. 28 No.1, pp 67-82.

Junyu Lu, Gregory J. Carbone, Peng Gao (2017). Detrending crop yield data for spatial visualization of drought impacts in the United States, 1895–2014, Agricultural and Forest Meteorology, Volumes 237–238, Pages 196-208, ISSN 0168-1923, https://doi.org/10.1016/j.agrformet.2017.02.001.

Jury, M. R., & Mwafulirwa, N. D. (2002). Climate variability in Malawi, part 1: dry summers, statistical associations and predictability. *International Journal of Climatology*, *22*(11), 1289–1302. https://doi.org/10.1002/JOC.771

Kolusu, S. R., Shamsudduha, M., Todd, M. C., Taylor, R. G., Seddon, D., Kashaigili, J. J., Ebrahim, G. Y., Cuthbert, M. O., Sorensen, J. P. R., Villholth, K. G., MacDonald, A. M., and MacLeod, D. A. (2019) The El Niño event of 2015–2016: climate anomalies and their impact on groundwater resources in East and Southern Africa, Hydrol. Earth Syst. Sci., 23, 1751–1762

Kukal, M.S., Irmak, S. (2018). Climate-Driven Crop Yield and Yield Variability and Climate Change Impacts on the U.S. Great Plains Agricultural Production. Sci Rep 8, 3450. https://doi.org/10.1038/s41598-018-21848-2

Kushnir, Y., Scaife, A. A., Arritt, R., Balsamo, G., Boer, G., Doblas-Reyes, F., Wu, B. (2019). Towards operational predictions of the near-term climate. *Nature Climate Change, 9*(2), 94-101. doi:10.1038/s41558-018-0359-7

Landman, W. A., Engelbrecht, F., Hewitson, B., Malherbe, J., & van der Merwe, J. (2017). Towards bridging the gap between climate change projections and maize producers in South Africa. *Theoretical and Applied Climatology, 132*(3-4), 1153-1163. doi:10.1007/s00704-017-2168-8

Landman W.A. and Beraki A. (2012). Multi-model forecast skill for mid-summer rainfall over southern Africa. *International Journal of Climatology* **32** 303 – 314.

Lesk, C., Coffel, E., Winter, J. et al. (2021) Stronger temperature–moisture couplings exacerbate the impact of climate warming on global crop yields. Nat Food 2, 683–691. https://doi.org/10.1038/s43016-021-00341-6.

Lim Kam Sian, K. T. C., Wang, J., Ayugi, B. O., Nooni, I. K., & Ongoma, V. (2021). Multi-Decadal Variability and Future Changes in Precipitation over Southern Africa. *Atmosphere, 12*(6). doi:10.3390/atmos12060742

Lledo, L., Cionni, I., Torralba, V., Bretonniere, P. A., & Samso, M. (2020). Seasonal prediction of Euro-Atlantic teleconnections from multiple systems. Environmental Research Letters, 15(7), 074009. https://doi.org/10.1088/1748-9326/ab87d2

Lledó, L., Ramon, J., Soret, A., & Doblas-Reyes, F. J. (2022). Seasonal prediction of renewable energy generation in Europe based on four teleconnection indices. Renewable Energy, 186, 420-430. https://doi.org/10.1016/j.renene.2021.12.130

Lobell, D.B. and Field, C.B. (2007). Global scale climate–crop yield relationships and the impacts of recent warming. Environmental Research Letters, 2, 014002. https://doi.org/10.1088/1748-9326/2/1/014002

Lobell, D.B., Schlenker, W. and Costa-Roberts, J. (2011). Climate trends and global crop production since 1980. Science, 333, 616–620. https://doi.org/10.1126/science.1204531

Lüdecke, H.-J., Müller-Plath, G., Wallace, M. G., & Lüning, S. (2021). Decadal and multidecadal natural variability of African rainfall. *Journal of Hydrology: Regional Studies, 34*. doi:10.1016/j.ejrh.2021.100795

Mahlalela P.T., Blamey R.C. and Reason, C.J.C (2019). Mechanisms behind early winter rainfall variability in the southwestern Cape, South Africa. *Clim Dyn* **53** 21–39. https://doi.org/10.1007/s00382-018-4571-y.

Malherbe J., Landman W.A. and Engelbrecht F.A. (2014). The bi-decadal rainfall cycle, Southern Annular Mode and tropical cyclones over the Limpopo River Basin, southern Africa. *Climate Dynamics* **42** 3121-3138. https://doi.org/10.1007/s00382-013-2027-y.

McGregor, JL, Dix MR (2008). An updated description of the conformal-cubic atmospheric model. In: High Resolution Numerical Modelling of the Atmosphere and Ocean. (pp. 51–75). Springer New York. https://doi.org/10.1007/978-0-387-49791-4_4

McKee, T.B., Doesken, N.J. and Kleist J., (1993). The relationship of drought frequency and duration ot time scales. Eighth Conference on Applied Climatology, American eteorological Society Jan 17-23, 1993, Anaheim CA, pp. 179-186.

McKee, T.B., Doesken N.J. and Kleist J., (1995). Drought monitoring with multiple time scales. Ninth Conference on Applied Climatology, American Meteorological Society Jan 15-20, 1995, Dallas TX, pp. 233-236.

Merryfield, W. J., Baehr, J., Batté, L., Becker, E. J., Butler, A. H., Coelho, C. A. S., . . . Yeager, S. (2020). Current and Emerging Developments in Subseasonal to Decadal Prediction. *Bulletin of the American Meteorological Society, 101*(6), E869-E896. doi:10.1175/bams-d-19-0037.1.

Mitchell, JFB, Davis RA, Ingram WJ, Senior CA (1995). On surface temperature, greenhouse gases, and aerosols: models and observations. J Clim. https://doi.org/10.1175/1520-0442(1995)008<2364:OSTGGA>2.0.CO;2

Morioka, Y., Engelbrecht, F., & Behera, S. K. (2015). Potential Sources of Decadal Climate Variability over Southern Africa. *Journal of Climate, 28*(22), 8695-8709. doi:10.1175/jcli-d-15-0201.1

Mabhaudhi, T., Simpson, G., Badenhorst, J., Senzanje, A., Jewitt, G.P.W., Chimonyo, V.G.P., Mpandeli, S., Nhamo, L., (2021). Developing a Framework for the Water-Energy-Food Nexus in South Africa, in: Climate Change and Water Resources in Africa. Springer International Publishing, Cham, pp. 407–431. doi:10.1007/978-3-030-61225-2_18

Masih, I., Maskey, S., Mussá, F.E.F., Trambauer, P. (2014). A review of droughts on the African continent: a geospatial and long-term perspective. Hydrol. Earth Syst. Sci. 18, 3635–3649. https://doi.org/10.5194/hess-18-3635-2014

Mavume, A.F.; Banze, B.E.; Macie, O.A.; Queface, A.J. (2021). Analysis of Climate Change Projections for Mozambique under the Representative Concentration Pathways. Atmosphere, 12, 588. https://doi.org/10.3390/atmos12050588

Moore, F., Lobell, D. (2014). Adaptation potential of European agriculture in response to climate change. Nature Clim Change 4, 610–614. https://doi.org/10.1038/nclimate2228

Mpandeli, S. Naidoo D, Mabhaudhi T. Nhemachena C. Nhamo L. Liphadzi S. Hlahla S. Modi A.T. (2018). Climate Change Adaptation through the Water-Energy-Food Nexus in Southern Africa. Int J Environ Res Public Health. 15(10): 2306. doi: 10.3390/ijerph15102306

Munday, C., Washington, R., & Hart, N. (2021). African Low-Level Jets and Their Importance for Water Vapor Transport and Rainfall. *Geophysical Research Letters*, *48*(1), e2020GL090999. https://doi.org/10.1029/2020GL090999

NCL - The NCAR Command Language (Version 6.4.0) [Software] (2017). Boulder, Colorado: UCAR/NCAR/CISL/TDD. http://dx.doi.org/10.5065/D6WD3XH5

Nhemachena, C., Nhamo, L., Matchaya, G., Nhemachena, C.R., Muchara, B., Karuaihe, S.T., Mpandeli, S., (2020). Climate Change Impacts on Water and Agriculture Sectors in Southern Africa: Threats and Opportunities for Sustainable Development. Water 12, 2673. doi:10.3390/w12102673

Niang I., Ruppel O.C., Abdrabo M.A., Essel A., Lennard C., Padgham J., Urquhart P. (2014). Climate Change 2014: Impacts, Adaptation, and Vulnerability. Part B: Regional Aspects. Contribution of Working Group II to the Fifth Assessment Report of the Intergovernmental Panel on Climate Change. Cambridge University Press; Cambridge, UK: New York, NY, USA: pp. 199–1265.

Nicholson, S.E. (2009). A revised picture of the structure of the “monsoon” and land ITCZ over West Africa. Clim. Dyn. 32, 1155–1171. https://doi.org/10.1007/s00382-008-0514-3

Nikulin, G., Hewitson, B. (2019). A simple set of indices describing the Tropical Rain Belt over central and southern Africa. Atmos. Sci. Lett. 20, e946. https://doi.org/https://doi.org/10.1002/asl.946

Oettli P., Tozuka T., Izumo T., Engelbrecht F.A. and Yamagata T. (2014). The self-organizing map, a new approach to apprehend the Madden-Julian Oscillation influence on the intraseasonal variability of rainfall in the southern-African region. *Climate Dynamics* **43** 1557-1573. https://doi.org/10.1007/s00382-013-1985-4.

O'Neill, B. C. *et al.*, (2017). "The roads ahead: Narratives for shared socioeconomic pathways describing world futures in the 21st century," *Glob. Environ. Chang.* 42, 169–180.

Pequeno, N. L. D., Hernandez-Ochoa, I.M., Reynolds, M., Sonder, K., Molero-Milan, A., Robertson, R., da Silva Sabino Lopes, M., Xiong, W., Kropff, M., Asseng, S., (2021). Climate impact and adaptation to heat and drought stress of regional and global wheat production. Environ. Res. Lett. doi:10.1088/1748-9326/abd970

Philippon, N., Rouault, M., Richard, Y., & Favre, A. (2012). The influence of ENSO on winter rainfall in South Africa. International Journal of Climatology, 32(15), 2333-2347. https://doi.org/10.1002/joc.3403

Pratt (1976). The interpretation of space-time spectral quantities, Journal of the Atmospheric Science, Vol. 33: 1060– 1066.

Ramirez-Villegas J, Ghosh A, Craparo A, Thornton P, Manvatkar R, Bogart B, Läderach P . (2021). Climate change and its impacts in Southern Africa: A synthesis of existing evidence in support of the World Food Programme's 2021 Climate Change Position Paper CCAFS Working paper No. 358. CGIAR Research Program on Climate Change, Agriculture and Food Security (CCAFS).

Raza A, Razzaq A, Mehmood SS, et al. (2019). Impact of Climate Change on Crops Adaptation and Strategies to Tackle Its Outcome: A Review. Plants (Basel). 2019;8(2):34. Published 2019 Jan 30. doi:10.3390/plants8020034.

Reason C.J.C (2001). Subtropical Indian Ocean SST dipole events and southern African rainfall. JGR, vol 28, No.11, pp 2225-2227.

Reason, C. J. C., Landman, W., and Tennant, W. (2006). Seasonal to decadal prediction of southern African climate and its links with variability of the Atlantic Ocean. *Bull. Amer. Meteor. Soc*. 87, 941–955. doi: 10.1175/BAMS-87-7-941.

Riahi, K., Rao, S., Krey, V. *et al.* (2011). RCP 8.5—A scenario of comparatively high greenhouse gas emissions. *Climatic Change* **109,** 33. https://doi.org/10.1007/s10584-011-0149-y

Salinger MJ et al (2020). Linking crop yields in Tuscany, Italy, to large-scale atmospheric variability, circulation regimes and weather types. The Journal of Agricultural Science 158, 606–623.

Siderius, Christian, Seshagiri R. Kolusu, Martin C. Todd, Ajay Bhave, Andy J. Dougill, Chris JC Reason, David D. Mkwambisi et al. (2021). "Climate variability affects water-energy-food infrastructure performance in East Africa." One Earth 4, no. 3, 397-410

Slivinski L.C., Compo G.P., Whitaker J.S., Sardeshmukh P.D., Giese B.S., McColl C., Allan R., Yin X., Vose R., Titchner H. and Kennedy J. (2019). Towards a more reliable historical reanalysis: Improvements for version 3 of the Twentieth Century Reanalysis system. *Quarterly Journal of the Royal Meteorological Society* **145** 2876-2908.

Smith, T. M., R. W. Reynolds, T. C. Peterson, and J. Lawrimore (2008). Improvements to NOAA's historical merged land–ocean surface temperature analysis (1880–2006). *J. Climate*, 21, 2283–2296.

Smith, D. M., Eade, R., Scaife, A. A., Caron, L. P., Danabasoglu, G., DelSole, T. M., Yang, X. (2019). Robust skill of decadal climate predictions. *npj Climate and Atmospheric Science, 2*(1). doi:10.1038/s41612-019-0071-y.

Solaraju-Murali, B., Gonzalez-Reviriego, N., Caron, L.-P., Ceglar, A., Toreti, A., Zampieri, M., . . . Doblas-Reyes, F. J. (2021). Multi-annual prediction of drought and heat stress to support

decision making in the wheat sector. *npj Climate and Atmospheric Science, 4*(1). doi:10.1038/s41612-021-00189-4.

Thompson D.W., Solomon S., Kushner P.J., England M.H., Grise K.M. and Karoly D.J. (2011). Signatures of the Antarctic ozone hole in Southern Hemisphere surface climate change. *Nature geoscience* **4** 741-749.

Thomson, A.M., Calvin, K.V., Smith, S.J. *et al.* (2011). RCP4.5: a pathway for stabilization of radiative forcing by 2100. *Climatic Change* **109,** 77. https://doi.org/10.1007/s10584-011-0151-4.

Trenberth, K. E. (1997). The definition of El Niño. Bull. Amer. Meteor. Soc.,78, 2771–2777.

Trenberth, K. E., & Stepaniak, D. P. (2001). Indices of el Niño evolution. Journal of climate, 14(8), 1697-1701. https://doi.org/10.1175/1520-0442(2001)014<1697:LIOENO>2.0.CO;2.

Vicente-Serrano, S.M., Beguería S., López-Moreno J.I. (2010). A multi-scalar drought index sensitive to global warming: the standardized precipitation evapotranspiration index – SPEI. J. Clim. 23: 1696–1718.

von Storch, H., and F. W. Zwiers (2001). Statistical Analysis in Climate Research. Cambridge University Press, 496 pp.

von Storch, H. *et al*, (2012). "The Physical Sciences and Climate Politics," in *The Oxford Handbook of Climate Change and Society*, 2012.

Wilhite, D. A. (2000). Drought as a natural hazard: Concepts and definitions, in *Drought: A Global Assessment*, *Hazards Disasters Ser.*, vol. **I**, edited by D. A. Wilhite, pp. 3–18, Routledge, New York.

WMO (World Meteorological Organization), (2020). 2020 on track to be one of three warmest years on record. Press Release No. 02122020, Geneva.

Xiang B., Zhao M., Held I.M. and Golaz J.C. (2017). Predicting the severity of spurious "double ITCZ" problem in CMIP5 coupled models from AMIP simulations. *Geophysical Research Letters* **44** 1520-1527.

Zampieri, M., Ceglar, A., Dentener, F., Dosio, A., Naumann, G., van den Berg, M., Toreti, A. (2019). When Will Current Climate Extremes Affecting Maize Production Become the Norm? Earth's Futur. 7, 113–122. https://doi.org/10.1029/2018EF000995.

Zampieri, M., Ceglar, A., Dentener, F., Toreti, A. (2017). Wheat yield loss attributable to heat waves, drought and water excess at the global, national and subnational scales. Environ. Res. Lett. 12, 64008. https://doi.org/10.1088/1748-9326/aa723b.

Zampieri, M., Toreti, A., Ceglar, A., De Palma, P., Chatzopoulos, T., Michetti, M. (2021). Analysing the resilience of agricultural production systems with ResiPy, the Python production resilience estimation package. SoftwareX 15, 100738. https://doi.org/https://doi.org/10.1016/j.softx.2021.100738.

Zampieri, M., Weissteiner, C.J., Grizzetti, B., Toreti, A., van den Berg, M., Dentener, F. (2020). Estimating resilience of crop production systems: From theory to practice. Sci. Total Environ. 735, 139378. https://doi.org/https://doi.org/10.1016/j.scitotenv.2020.139378.